Spring 2012

Multi-Term Approximation to the Boltzmann Transport Equation for Electron Energy Distribution Functions in Nitrogen

Yue Feng
Old Dominion University

MULTI-TERM APPROXIMATION TO THE BOLTZMANN TRANSPORT EQUATION FOR ELECTRON ENERGY DISTRIBUTION FUNCTIONS IN NITROGEN

by

Yue Feng
B.S. June 2005, Jiangxi Normal University, China
M.S. June 2007, Huazhong University of Science and Technology, China

A Dissertation Submitted to the Faculty of
Old Dominion University in Partial Fulfillment of the
Requirements for the Degree of

DOCTOR OF PHILOSOPHY

ELECTRICAL AND COMPUTER ENGINEERING

OLD DOMINION UNIVERSITY
May 2012

Approved by:

Ravindra P. Joshi (Director)

Jürgen Kolb (Member)

Shu Xiao (Member)

Linda L. Vahala (Member)

ABSTRACT

MULTI-TERM APPROXIMATION TO THE BOLTZMANN TRANSPORT EQUATION FOR ELECTRON ENERGY DISTRIBUTION FUNCTIONS IN NITROGEN

Yue Feng
Old Dominion University, 2012
Director: Dr. Ravindra P. Joshi

Plasma is currently a hot topic and it has many significant applications due to its composition of both positively and negatively charged particles. The energy distribution function is important in plasma science since it characterizes the ability of the plasma to affect chemical reactions, affect physical outcomes, and drive various applications. The Boltzmann Transport Equation is an important kinetic equation that provides an accurate basis for characterizing the distribution function–both in energy and space.

This dissertation research proposes a multi-term approximation to solve the Boltzmann Transport Equation by treating the relaxation process using an expansion of the electron distribution function in Legendre polynomials. The elastic and 29 inelastic cross sections for electron collisions with nitrogen molecules (N_2) and singly ionized nitrogen molecules (N_2^+) have been used in this application of the Boltzmann Transport Equation.

Different numerical methods have been considered to compare the results. The numerical methods discussed in this thesis are the implicit time-independent method, the time-dependent Euler method, the time-dependent Runge-Kutta method, and finally the implicit time-dependent relaxation method by generating the 4-way grid with a matrix solver. The results show that the implicit time-dependent relaxation method is the most accurate and stable method for obtaining reliable results. The results were observed to match with the published experimental data rather well.

This thesis is dedicated to my parents, Hong Feng and Lujia Jiang,
my grandmother, Jufang Fu, and my grandfather, Shenglin Jiang,
my uncle, Hong Jiang, and my aunt, Weixin Jiang,
for all their unconditional love and support,
and for having faith in my abilities.

ACKNOWLEDGEMENTS

I would like to express my sincerest gratitude to my advisor Dr. Ravindra P. Joshi for his great patience in introducing me into this new field as well as continuous encouragement, support and guidance that gave me clear research direction and significant help when I became stuck in difficulties. I enjoyed every busy day working with Dr. Ravindra P. Joshi .

I would like to send my appreciation to Dr. Shu Xiao, Dr. Juergen Kolb, and Dr. Linda Vahala for serving as my committee members and for providing their valuable suggestions.

I would also like to thank our department chair, Dr. Shirshak K. Dhali, and Graduate Program Director, Dr. Oscar R. Gonzalez, for caring for my progress of research and encouraging me at all times.

TABLE OF CONTENTS

Chapter Page

LIST OF TABLES

LIST OF FIGURES

Figure Page

CHAPTER 1

INTRODUCTION

A plasma is often referred to as the fourth state of matter (after solids, liquids and gases). At low temperatures all matter exists in solid form. When heat is added, solid material melts into liquid; and if more heat is added, liquid material evaporates into a gas. If one adds even more heat to a gas, atoms and molecules are ionized and a plasma is formed [1].

Therefore, a plasma is an ionized gas consisting of positively and negatively charged particles with approximately equal charge densities. Plasmas are usually produced by heating an ordinary gas to such a high temperature that the random kinetic energy of the molecules exceeds the ionization energy [2]. Electrons can then be emitted (due to their highly energetic state) from the bound state within the atoms/molecules to leave behind positively charged ions. Collisions can also strip some of the electrons from the atoms. The net result is the formation of a mixture of electrons and ions [3].

Since there are both positively and negatively charged particles in a plasma, one can let the charged particles take part in the physical and chemical reactions as needed. This is possible when the physical conditions can create the desired electron densities to initiate and realize the physical or chemical reactions needed for those applications. At low densities, for example, while most of the same reactions can occur at high densities, the number of events may be inordinately low to have any discernible effect. Hence, much higher plasma densities may be required for many practical applications. Apart from the densities (i.e., number of ions), their energy distribution is another important consideration. For example, two separate plasmas can have the same number of ions present. However, one could contain primarily low energy ions, while the other could have a high fraction of very energetic ions. Under these conditions, quite clearly, the second plasma is more capable of initiating chemical reactions, or causing plasma driven interactions or damage (such as plasma initiated material removal from surface

treatments). Hence, trying to figure out what the relationship is between the initial physical conditions and later electron energy distribution functions as a function of time is quite important. Therefore, the details of a plasma and its characteristics (e.g., density, average energy, deviation in the energy distribution, etc.) are important drivers that need to be characterized and understood. This is precisely the central aim of this simulation-based plasma research–trying to figure out the energy distribution functions for the electrons from an important kinetic equation–the Boltzmann Transport Equation.

Furthermore, the simulation process can also combine a lot of other physical factors, including electrical field, gas pressure, gas flow rate, discharge tube length, discharge gap space, dielectric thickness and so on, that all influence the distribution function [4]. The output simulation result for the distribution function will show how those factors impact the number of electrons with different energies under each condition. This can be used to fulfill different application purposes, to set those parameters in advance to produce the results that are needed and desired. This also explains the purpose of plasma simulations. Plasma simulation is based upon a lot of inherent plasma physics and is based upon including appropriate models for these physical elements. The simulation would help in the analysis of the effect of each element in the process (e.g., applied voltage, surrounding gas pressure, temperature etc.) on the result, and to decide on parameter changes needed to optimize the output (or drive effects in certain desired direction).

The objectives for our simulation can be summarized as trying to use multi-term Boltzmann Transport Equation analysis to obtain the drift velocity values under different electrical field to gas density ratios (i.e. E/N values). A necessary task would also be to carry out a careful comparison with some of previous published experiment results to verify the present numerical methods and program implementations. Besides this, the Townsend's first ionization coefficients in nitrogen gas are also obtained under different electrical field to gas pressure ratios (i.e. E/p values) and compared with published experiment results as further validation for the methods and

implementations. Another related task would be to obtain the electron energy distribution functions under steady state conditions.

With respect to the present dissertation, Chapter 2 deals with background theory and summarizes plasma applications. It includes the basic concept behind and derivation of the Boltzmann Transport Equation. It also touches upon the Monte Carlo Simulation and discusses the concept of Cross Sections that will be applied in our numerical simulations. Chapter 3 introduces the "Multi-Term Approximation" to the Boltzmann Transport Equation (BTE) for energy distribution functions. It clearly gives the governing equations we need to solve. It also gives detailed step-by-step process of the numerical methods applied on the governing equations to obtain the distribution functions and drift velocity. Both advantages and disadvantages of each numerical method are considered. The reasons for the improvement of numerical methods are also discussed. Chapter 4 shows the simulation results corresponding to each numerical method and verify that our results are in good agreement with published experimental data. This proves and validates our numerical methods and code implementations as being correct and acceptable.

The primary contribution of this dissertation research can be summarized as: (1) At the most basic level, this is an important first step at developing plasma-simulation capability at Old Dominion University. (2) More importantly, four different numerical methods of solving the Boltzmann Transport Equation have been implemented and compared for accuracy and speed. (3) In terms of computational efficiency and accuracy, the Boltzmann Transport Equation is a much better alternative than other methods (such as the Monte Carlo Simulation) for probing high energy portions of the distribution function and resulting effects such as ionization. So this research provides an important step in the analysis of processes involving ion generation. (4) Although results focus on nitrogen, the methods developed and implemented are general. Hence, upon replacing the collision cross-sections for nitrogen by those for oxygen [5], a complete analysis for air-plasmas can be carried out. This should open the doorway to the analysis for plasma processing and plasma chemistry.

CHAPTER 2

PLASMA SCIENCE AND BOLTZMANN TRANSPORT EQUATION: BACKGROUND THEORY

2.1 Plasma Applications

There are wide applications of plasmas to a variety of fields nowadays [6]. Basically, there are mainly four categories of plasma applications. The first category is gas treatment, including ozone synthesis and pollution control. The second category is surface treatment, including surface cleaning, processing of plastics, plasma spraying of surface coatings for temperature and wear resistance. The third category is plasma-based light sources, including excimer and exciplex plasma lights. The fourth category encompasses plasma display technology, including plasma display televisions and electronics.

All the applications above involve a series of physical and chemical reactions. Almost all these physical and chemical reactions have requirements for threshold energy of electrons. For electrons below the threshold energy, a given process cannot be initiated. If one wants to improve the efficiency of those physical and chemical reactions, one needs to create more electrons with energies that surpass the threshold energy levels. However, for stability, one also requires that the number of electrons whose energies surpass the threshold do not reach very high values if one wants the reaction to proceed in a controlled, pre-determined manner. Next let's look at examples in each category to see how electron energy plays an important part in the physical and chemical reactions.

2.1.1 Ozone Synthesis

Ozone is typically synthesized by electrical discharge, particularly dielectric barrier discharge, which is a potential method for producing large amounts of ozone at high concentrations. The plasma conditions in the micro-discharges have to be optimized for exciting and dissociating oxygen and nitrogen molecules. Initially, the

major fraction of the energy gained by the electrons in the electrical field is deposited in creating excited atomic and molecular states.

Starting from electron impact on ground state O_2 molecules, two reaction paths leading to dissociation are available [7]: (i) excitation of the $A^3\Sigma_u^+$ state with an energy threshold of about 6 eV, and (ii) excitation of the $B^3\Sigma_u^+$ state starting at 8.4 eV. These mechanisms can be written as:

$$e + O_2 \rightarrow e + O_2(A^3\textstyle\sum_u^+) \rightarrow e + O(^3P) + O(^3P) \rightarrow O_2 + O(^3P) \rightarrow O_3 \quad at 6eV, \qquad (2.1)$$

$$e + O_2 \rightarrow e + O_2(B^3\textstyle\sum_u^+) \rightarrow e + O(^3P) + O(^3D) \rightarrow O_2 + O(^3P) \rightarrow O_3 \quad at 8.4eV. \qquad (2.2)$$

Ozone is then formed in a three-body reaction, involving O and O_2, leading to the formation of the O_3 molecule. Thus:

$$O + O_2 + M \rightarrow O_3^* + M \rightarrow O_3 + M. \qquad (2.3)$$

where M is a third collision partner: O_2, O_3^*, O (or, in the case of air, also N_2). O_3^* stands for a transient excited state in which the ozone molecule is initially formed after the reaction of an O atom with an O_2 molecule.

Therefore, 6 eV and 8.4 eV are two important electron energy thresholds in these two reactions. In order to facilitate the reactions, one needs to let the electrons have a proper distribution relative to these thresholds. In other words, for successful reaction rates, a relatively high number of electrons in the plasma swarm need to have energies above 8.4 eV. In this context then, one needs plasma simulations based on predictive models to be able to gauge and optimize the production of the desired ionic species.

2.1.2 Pollution Control

Air pollution control is one of the major environmental issues that many countries are trying to address at the present time. This is also an important field to which plasma science is applied. The essence of the de-pollution process is based on trying to dissociate gas molecules into corresponding atoms, and make electrons

obtained from micro-discharge processes react with those toxic compounds in order to covert them to non-hazardous or less hazardous substances. In this process, the electron energies play quite an important role. Research shows that a high electrical field produces higher energetic electrons, and in the pipe-cylinder reactor the average field is about 140 kV/cm resulting in an average electron energy of about 13 eV [8]. These energetic electrons collide with other background gas molecules, resulting in the generation of more excited species and ions. In this example category, again, the existence of an energy threshold (13 eV) is an important driver for the need to use simulations to predict the energy distributions.

2.1.3 Surface Treatment

With the advent of readily available and affordable plastic foils and other polymer materials since the 1960s, it soon became apparent that, for a number of applications, their surface properties required modification. One possibility to substantially increase the surface energy of different substrates is corona treatment in atmospheric-pressure air. It developed into a reliable surface treatment process that can match the production speed of foils. The key point in the process of surface treatment still hinges on the energy of electrons that decide which physical and chemical reactions take place, as well as the kind of substances from which the new surface is composed.

2.1.4 KrCl Excimer Lamp

Let's use the KrCl excimer lamp as an example of plasma-based light sources in the third category. The reaction kinetics for the formation of $KrCl^*$ excimer begin with collisional excitation, ionization or dissociative attachment of energetic electrons to krypton or chlorine [9]. In these processes, the energy of electrons plays an important role in deciding how many reactions below can take place. Only the high-energy electrons excite and ionize the krypton or chlorine atoms, or dissociate the chlorine molecules:

$$e^- + Kr \rightarrow Kr^* + e^-, \tag{2.4}$$

$$e^- + Kr \rightarrow Kr^+ + 2e^-, \tag{2.5}$$

and $$e^- + Cl_2 \rightarrow Cl + Cl^-. \tag{2.6}$$

$KrCl^*$ excimers are then created by a three-body recombination of Kr^+ and Cl^- ions or the harpooning reactions in which the excited Kr^* species transfers its loosely bound electron to the cholorine molecule, which leads to the formation of an electronically excited state of $KrCl^*$ as below:

$$Kr^+ + Cl^- + M \rightarrow KrCl^* + M, \tag{2.7}$$

where M is a collisional third partner, which in many cases can be an atom or molecule of the active species, or otherwise,

$$Kr^* + Cl_2 \rightarrow KrCl^* + Cl, \tag{2.8}$$

The $KrCl^*$ excimers are unstable and will decompose rapidly, giving up their excitation energy in the form of a UV photon. This is how excimer lamps radiate.

$$KrCl^* \rightarrow Kr + Cl + UV\ radiation. \tag{2.9}$$

Therefore, we can see that $KrCl^*$ is the direct chemical to produce UV photon and reactions (2.7)-(2.9) are three decisive steps in producing $KrCl^*$. Since the electron energy plays an important role in reactions (2.7)-(2.9), it is also important in the whole process to produce final UV radiation.

In this context, the relative densities of the various species are an important consideration, and a driver for the overall dynamics leading to efficient laser production.

2.1.5 Plasma Display Panel

Plasma display panels are composed of millions of tiny cells containing a mixture of noble gases and a small amount of mercury between two panels of glass. When the mercury is vaporized and a voltage is applied across the cell, the gas in the cells form a plasma. Some of the electrons strike mercury particles and thereby

increase the energy level of the mercury molecule until the excess energy is shed. The energy mercury sheds is dispersed as ultraviolet (UV) photons [10]. The UV photons then strike a phosphor that is painted on the inside of the cell, and produces visible light of different colors depending on the type of phosphor struck. In the whole process, the energy of initial electrons which strike mercury particles determines the energy level to which the mercury molecule increased, and the amount of excess energy that can be shed as ultraviolet photons for striking the phosphor later to produce visible light. Therefore, the energy of the initial electrons is a key factor and requires critical attention.

Since all the applications indicate the importance of electron energy, electron energy distribution function becomes an important parameter that needs to be obtained carefully.

2.2 Boltzmann Transport Equation

2.2.1 Maxwellian Distribution

The Maxwellian distribution is the unique distribution function that arises when a gas is in thermal equilibrium. In general the distribution of velocities for particles of type s is given by the Maxwellian distribution, which is:

$$f_s(v) = n_s\left(\frac{m_s}{2\pi\kappa T_s}\right)^{3/2} e^{-\frac{m_s v^2}{2\kappa T_s}}. \tag{2.10}$$

where $f_s(v)$ is the distribution function, v is the velocity, m_s is the mass of the particles, κ is Boltzmann's constant, and T_s is the temperature. The temperature of particles of type s is directly proportional to their average random kinetic energy.

The distribution function is normalized such that $f_s(v)$ integrated over all velocities gives the number density of particles of type s,

$$\int_{-\infty}^{\infty} f_s(v)dv_x dv_y dv_z = n_s, \tag{2.11}$$

$$C_s = \sqrt{\frac{\kappa T_s}{m_s}}. \tag{2.12}$$

where C_s will be referred to as the thermal speed. The average kinetic energy is given by

$$\left\langle \frac{1}{2} m_s v^2 \right\rangle = \frac{3}{2} \kappa T_s. \tag{2.13}$$

where the angle brackets indicate an average over the entire population. The equation shows that the temperature is directly proportional to the average kinetic energy of the particles.

2.2.2 Kinetic Theory

According to a general principle of statistical mechanics called the H-theorem [11], the Maxwellian distribution is the unique distribution function that arises when a gas is in thermal equilibrium. For a plasma in thermal equilibrium, not only should the distribution function for each species be a Maxwellian, but the temperature of all species must be equal. However, because collisions occur very infrequently in a tenuous plasma (especially if the gas pressure is not very high), the approach to thermal equilibrium is often very slow. Therefore, non-equilibrium effects are quite common in plasmas. Under these circumstances, the velocity distribution of the beam usually cannot be represented by a Maxwellian distribution but by equations of the kinetic theory [2].

For a system with a large number of particles, it is neither possible nor desirable to determine the motion of every particle. Instead, a statistical approach to compute the average motions of a large number of particles is introduced. This approach is called kinetic theory.

To carry out a statistical description of a plasma, it is convenient to introduce a six-dimensional space, called phase space, that consists of the position coordinates x, y, z and velocity coordinates v_x, v_y, v_z. For a system of many particles, the dynamical state of the entire system can then be represented by a collection of points in phase space, with one point for each particle. If the number of particles is very large, it is meaningful to define the average number density of particles in a small volume

element of phase space. This density is called the distribution function $f(r,v,t)$ and is defined such that:

$$dN = f(r,v,t)d^3xd^3v, \tag{2.14}$$

where dN is the number of particles in the phase-space volume element at time t.

$$d^3xd^3v = dxdydzdv_xdv_ydv_z. \tag{2.15}$$

We shall assume that the number of particles is sufficiently large that $f(r,v,t)$ can be regarded as a continuous function of r and v. The total number of particles, N, in the system is obtained by integrating $f(r,v,t)$ over all of phase space:

$$N = \int_{-\infty}^{\infty} f(r,v,t)d^3xd^3v. \tag{2.16}$$

Having defined the distribution function, we can then use the standard rules of statistics for computing various macroscopic averages. The average (expectation) value of any dynamical quantity $g(r,v)$ in a region R of phase space is given by [12,13]:

$$\langle g(r,v)\rangle = \frac{1}{N}\int_R g(r,v)f(r,v,t)d^3xd^3v. \tag{2.17}$$

Since several species may be present in a plasma, it is necessary to define a distribution function $f_s(r,v,t)$ for each particle species s in the plasma. Some of the most commonly used averages are the following:

Number density, $n_s = \int_V f_s(r,v,t)d^3v,$ (2.18)

Average velocity, $U_s = \frac{1}{n_s}\int_V vf_s(r,v,t)d^3v,$ (2.19)

Kinetic energy density, $W_s = \int_V \frac{1}{2}m_sv^2f_s(r,v,t)d^3v,$ (2.20)

Pressure tensor, $\overleftrightarrow{P}_s = \int_V m_s(v-U_s)(v-U_s)f_s(r,v,t)d^3v.$ (2.21)

where the integrations are over velocity space, V. The number density, n_s, is the average number of particles of type s. The velocity, U_s, is the average velocity of particles of type s. The kinetic energy density, W_s, is the average kinetic energy, of

particles of type s per unit volume. The pressure tensor, $\overleftrightarrow{P}_s = [P_{ij}]$ is the average rate at which momentum is transported in the *i*-direction across surface j in a frame of reference moving at the average velocity U_s.

2.2.3 Derivation for the Boltzmann Transport Equation

The forces acting on the particles can be classified into two types: long-range and short-range. Forces that are the same for all particles in a given phase-space volume element are long-range forces. These originate from the collective effects of a large number of particles acting over relatively long distances. Short-range forces originate from a small number of particles acting over relatively short distances. Short-range forces correspond to what are commonly called collisions. Collisions produce large, nearly instantaneous changes in the velocities of the interacting particles.

Detailed discussion for the derivation process is available in the literature [2] and some key steps are cited here. To derive the Boltzmann Transport Equation, we first assume that there are no short-range forces (i.e., no collisions). All particles in an infinitesimal volume of phase space, d^3xd^3v, then experience the same long-range force F and start with the zero velocity. Since the force on a representative particle in phase space is given by Newton's Law $F = m\frac{dv}{dt}$, it follows that the particle trajectories can never intersect. Therefore, if we follow the evolution of a volume element that moves with the particles, then all of the particles within the volume element d^3xd^3v at time t is the same as corresponding volume element $d^3x'd^3v'$ at time $t' = t + dt$. Since the number of particles in the phase-space volume element is conserved, we can write

$$f(r,v,t)d^3xd^3v = f'(r',v',t')d^3x'd^3v', \tag{2.22}$$

where f is the distribution function at time t, and f' is the distribution function at time t'. The equations of motion for the particles in phase space are given by $x_r' = x_r + v_r dt$ and $v_r' = v_r + \frac{F_r}{m}dt$ where we use index notation $r = (1,2,3)$ to

represent $x_r = (x, y, z)$ and $v_r = (v_x, v_y, v_z)$. These equations can be viewed as simply a transformation from phase-space coordinates (r, v) to new phase-space coordinates (r', v'). The infinitesimal volume elements involved in this transformation are determined by $d^3x'd^3v' = Jd^3xd^3v$ where J is the Jacobian of the transformation. Jacobian is given by the 6×6 determinant

$$J = \begin{vmatrix} \frac{\partial x'}{\partial x} & \frac{\partial x'}{\partial y} & \cdots & \cdots \\ \frac{\partial y'}{\partial x} & \frac{\partial y'}{\partial y} & \cdots & \cdots \\ \vdots & & \vdots & \\ \vdots & & \vdots & \frac{\partial v_z'}{\partial v_z} \end{vmatrix}, \tag{2.23}$$

After computing the appropriate derivatives and sorting out the lowest order terms in dt, the equation can be written in the form

$$d^3x'd^3v' = [1 + \sum_r \frac{\partial v_r}{\partial x_r} dt + \sum_r \frac{\partial}{\partial v_r}\left(\frac{F_r}{m}\right) dt] d^3x d^3v. \tag{2.24}$$

where the summation extends over r=1,2,and 3 (i.e., x, y and z). To complete the derivation of the function f' using the chain rule, with $v_r = dx_r / dt$ and $dv_r / dt = F_r / m$, we obtain:

$$df = f' - f = \frac{\partial f}{\partial t} dt + \sum_r v_r \frac{\partial f}{\partial x_r} dt + \sum_r \left(\frac{F_r}{m}\right) \frac{\partial f}{\partial v_r} dt, \tag{2.25}$$

That is, $$f' = f + \frac{\partial f}{\partial t} dt + \sum_r v_r \frac{\partial f}{\partial x_r} dt + \sum_r \left(\frac{F_r}{m}\right) \frac{\partial f}{\partial v_r} dt. \tag{2.26}$$

Substituting $d^3x'd^3v'$ from Equation (2.24) and f' from Equation (2.26) to equation (2.22) and ignore lowest order terms in dt, we get:

$$f = f + \frac{\partial f}{\partial t} dt + \sum_r v_r \frac{\partial f}{\partial x_r} dt + \sum_r \left(\frac{F_r}{m}\right) \frac{\partial f}{\partial v_r} dt + \sum_r f \frac{\partial v_r}{\partial x_r} dt + \sum_r f \frac{\partial}{\partial v_r}\left(\frac{F_r}{m}\right) dt, \tag{2.27}$$

which simplifies to the following first-order partial differential equation:

$$\frac{\partial f}{\partial t}+\sum_r \frac{\partial}{\partial x_r}(v_r f)+\sum_r \frac{\partial}{\partial v_r}(\frac{F_r}{m} f)=0, \tag{2.28}$$

Since v_r and x_r are independent variables, $\partial v_r/\partial x_r$ is zero. Since mass m is independent of velocity, the term $(\partial/\partial v_r)(F_r/m)$ is zero. These two simplifications imply that the Jacobian is $J=1$. Then above equation reduces to

$$\frac{\partial f}{\partial t}+\sum_r v_r \frac{\partial f}{\partial x_r}+\sum_r \frac{F_r}{m}\frac{\partial f}{\partial v_r}=0, \tag{2.29}$$

or in vector notation: $$\frac{\partial f}{\partial t}+v\cdot\nabla f+\frac{F}{m}\cdot\nabla_v f=0. \tag{2.30}$$

where ∇_v is the gradient operator in velocity space, $\nabla_v=\partial x/\partial v_x+\partial y/\partial v_y+\partial z/\partial v_z$.

All the discussion is based upon the long-range forces. That is based upon the realistic case when collective forces are much more important than collisional forces. Under this condition, the collision term can be ignored, i.e. $\delta_c f/\delta t=0$. If we apply Lorentz force into the equation, $F=q[E+v\times B]$, then the equation turns to

$$\frac{\partial f}{\partial t}+v\cdot\nabla f+\frac{q}{m}[E+v\times B]\cdot\nabla_v f=0, \tag{2.31}$$

This equation is called the Vlasov equation, after Vlasov who first applied this equation to the study of plasma. The Vlasov equation is based upon the collisions between plasmas is ignored to be zero.

However, if we consider the effect of short-range forces (i.e., collisions) and this is usually the actual case, the right hand side cannot be always zero. Because short-range forces are not the same for all particles in a volume element, collisions act to scatter particles into and out of the phase-space volume element. The main effect of short-range interactions is to introduce a nearly discontinuous change in the particle velocity. Changes to the distribution function due to collisions as the phase-space volume element evolves from time t to time $t+dt$ are taken into account by adding a collision operator, $\delta_c f/\delta t$, to the right hand side of Vlasov equation, that is:

$$\frac{\partial f}{\partial t}+v\cdot\nabla f+\frac{F}{m}\cdot\nabla_v f=\frac{\delta_c f}{\delta t}, \tag{2.32}$$

This equation is called the Boltzmann Transport Equation (BTE), after Boltzmann who first used this equation to analyze particle transport phenomena in ordinary gases. The left-hand side of the Boltzmann equation describes the response of the particles to long-range collective forces, and the right-hand side describes the response to short-range collisional forces.

To be specific, if we put Lorentz Force into the Boltzmann Equation and write it for each species i as well as specify the collision terms, we can write Boltzmann Equation as:

$$\frac{\partial f_i}{\partial t} + v \cdot \nabla f_i + \frac{q_i}{m_i}[E + v \times B] \cdot \nabla_v f_i = -J(f_i, F_0) - \sum_{i'} J(f_i, f_{i'}), \tag{2.33}$$

where $J(f_i, F_0)$ and $J(f_i, f_{i'})$ denote the collision terms for charged particle-neutral molecule collisions and charged particle-charged particle interactions respectively and F_0 is the neutral velocity distribution. $J(f_i, f_{i'})$ describes interaction between charged particles via the Coulomb force [14,15].

If we categorize the collision terms into elastic and inelastic collisions, the right hand side will include both elastic and inelastic collision operators, respectively. The Boltzmann equation can also be written as

$$\frac{\partial f_i}{\partial t} + v \cdot \nabla f_i + \frac{q_i}{m_i}[E + v \times B] \cdot \nabla_v f_i = (J_{el} + J_{in}) f. \tag{2.34}$$

2.3 Monte Carlo Simulation

In contrast to the simulations monitoring each particle's motion with a fixed assumed equation–Boltzmann Transport Equation, Monte Carlo Simulation is another simulation method to obtain the particle's distribution functions by tracking each particle's actual movement. Detailed discussion of Monte Carlo Simulation can be found in Venkata's thesis [16] at Old Dominion University. In addition to a number of published reports in the literature [17-20], some relevant and important points are summarized here.

2.3.1 Initial Distribution

Monte Carlo Simulation also starts with a specification of the initial locations and velocities(and hence, the energies) of the particles following Maxwellian distribution. The initial free energy distribution of the i th electron is generated randomly using the formula:

$$E(i) = -K_B T \ln[r_a(i)], \tag{2.35}$$

where K_B is the Boltzmann Constant, T is the temperature and $r_a(i)$ represents a random number generated for the i th electron. The energy associated with the particle is purely kinetic and is given by:

$$E = \frac{1}{2}mv^2, \tag{2.36}$$

where m is the mass of the electron and v is the velocity of the particle.

The momentum p of the particle is given by:

$$p = mv, \tag{2.37}$$

The wave vector k is related to particle wavelength λ by:

$$k = \frac{2\pi}{\lambda}, \tag{2.38}$$

We can also express wavelength λ in terms of the Plank constant h and momentum p as:

$$\lambda = \frac{h}{p}, \tag{2.39}$$

Combining Equations (2.37), (2.38) and (2.39), we have:

$$p = mv = \bar{h}k, \tag{2.40}$$

where $\bar{h} = h/2\pi$ is the reduced Plank's Constant.

Combining Equations (2.36) and (2.40), we get:

$$k = \sqrt{\frac{2Em}{\bar{h}^2}}, \tag{2.41}$$

$$\text{and,} \quad v = \frac{\bar{h}k}{m}. \tag{2.42}$$

2.3.2 Mean Free Path During Electron Flight Between Collisions

We define the effective cross section σ for two colliding particles in terms of the radius of two colliding particles r_1, r_2 by the following equation:

$$\sigma = \pi r^2 = \pi(r_1 + r_2)^2, \tag{2.43}$$

Consider a gas layer of thickness dx at a distance x from the origin. If N is the density of the gas molecules per volume (m^3), the effective cross section in a unit area is given by $N\sigma dx$. Let $n(0)$ be the number of particles per unit area at $x=0$ and $n(x)$ be the number of remaining particles at any distance x, the number of particles scattered in the layer of thickness dx is $dn = -nN\sigma dx$. (2.44)

That is, $\frac{1}{n}dn = -N\sigma dx$. Integrating both sides yields

$$n(x) = n(0)e^{-N\sigma x}. \tag{2.45}$$

The mean free path can then be obtained as:

$$\overline{\lambda} = \langle x \rangle = \frac{\int_0^\infty x n(x)dx}{\int_0^\infty n(x)dx} = \frac{1}{N\sigma}. \tag{2.46}$$

2.3.3 Collision Frequency and Collision Time

The transit time is given by:

$$\tau = \langle t \rangle = \left\langle \frac{x}{v} \right\rangle = \frac{1}{N\sigma v}. \tag{2.47}$$

The collision frequency f is given by:

$$f = \frac{1}{\tau} = N\sigma v. \tag{2.48}$$

According to Equation (2.45),

$$x = -\frac{1}{N\sigma}\ln\frac{n(x)}{n(0)}, \tag{2.49}$$

where $\frac{n(x)}{n(0)}$ varies between 0 and 1. This fraction is referred to be collisional probability p_c. Therefore, combining equation (2.47-2.49), one gets:

$$t = \frac{x}{v} = -\frac{\ln(p_c)}{N\sigma v} = -\frac{\ln(p_c)}{f}. \tag{2.50}$$

2.3.4 Null Collisions

Monte Carlo Simulation starts with the "null collision method" which was first introduced by Skullerud [21,22]. A more computationally efficient method was proposed later by Lin and Bardsley [21,23]. The basic idea is as: if one sets $\sigma = 1/v$, the collision frequency f becomes constant. Equation (2.50) yields:

$$t = -\frac{1}{N(\sigma v)_{\max}}\ln(p_c). \tag{2.51}$$

Experiments show that the virtual cross section is greater than the actual one for any energy. In order to distinguish the collisions between real and null collisions, a random number generator is used. The decision function $f(v)$ for such collisions can be defined by the equation

$$f(v) = \frac{N\sigma(v)v}{f} = \frac{\sigma(v)v}{(\sigma(v)v)_{\max}}, \tag{2.52}$$

where $f(v)$ is in the range (0,1). Since $(\sigma(v)v)_{\max}$ is the maximum value in all the $(\sigma(v)v)$ among real collisions and null collisions, for each v, the cross section value of null collision is larger than real collision, we can generate a random number R to determine the type of collision. If the value of R is less than $f(v)$, a real collision occurred; otherwise, a "null collision" occurred. That is:

If $R < f(v) \Rightarrow$ Real collision

$R > f(v) \Rightarrow$ Null collision

If a particle undergoes a null collision, its velocity and direction are unchanged, and it simply keeps going by another random collision until a real collision occurs. When a real collision occurs, the specific kind of collision is determined by using the relative frequencies of each collision type as:

$$r(j) = \sum_{i=1}^{N} \frac{v\sigma_j}{(v\sigma_t)_{\max}}, \tag{2.53}$$

where j is the type of collision to be chosen, N is the number of all the particles, σ_j is the particular cross section, and σ_t is the total cross section. If the cumulative scattering ratio falls in the range of $r(j)$ to $r(j+1)$, the jth type of collision is chosen. There are three types of collisions which can take place. Following the value of $r(j)$ from the maximum to minimum, there can either be null collisions, elastic collisions, or inelastic collisions taking place. The inelastic collisions include ionization, excitation, rotational, emission and vibrational scatterings. The threshold (i.e., index j of $r(j)$) for ionization scattering is larger than excitation, rotational, emission and vibrational scatterings.

2.3.5 Calculation of new Energy, Drift Velocity and Direction After Collisions

After determining the type of collision, the two parameters, energy and direction of the electron, must be updated. The new particle energy is calculated based on the type of collision undergone by the entity. If an elastic collision occurs, the energy loss is to be zero. So the particle energy remains unchanged.

$$E_n = E_i. \tag{2.54}$$

There are two kinds of inelastic collisions. If excitation, rotational, emission and vibrational scattering occur, the new energy is calculated as the difference between the initial energy and threshold energy of respective process. Thus:

$$E_n = E_i - E_{th}, \tag{2.55}$$

where E_n, E_i and E_{th} are the new, initial and threshold energies of the processes, respectively. If the process is ionization, two electrons exist after the collision. Therefore, the new energy is equally divided between the two particles. E_n becomes

$$E_n = \frac{E_i - E_{th\_ion}}{2}. \tag{2.56}$$

The direction of the scattered electron is assumed to be isotropic (i.e., to be between -180° to 180° in the azimuthal direction and between 0° to 360° along the polar plane). In case of such isotropic scattering, a uniform angular distribution is used along with the random number to yield the assigned angle.

The new energies of the particles with new velocity and the new direction are the initial condition for next collision. The whole process of changes in energy and angle is continually repeated until the end of the designated simulation time. By counting the number of occurrences of each type of collision and keeping track of the total time of the simulation, the distances traveled by particles, their drift velocities, average energy, position and collision frequency can all be calculated.

2.3.6 Flowchart of Monte Carlo Simulation

The basic flowchart of Monte Carlo simulations can be summarized as follows:

1. Start with a specification of the initial locations and velocities (and hence, the energies) of the particles following a Maxwellian distribution.
2. Initialize electric field E, total simulation time t_{sim} and time step Δt.

   Initialize cross section σ_j, pressure p_j, velocity v_j and position z_j for each particle.
3. Start with $i = 0$. $i = i + 1$, $t_{count} = i \times \Delta t$.
4. Applying the algorithm proposed by Skullerud [18] to generate collision time t.
5. Calculate v_j, z_j and E_j at time t of collision. Store the energy E_j.

6. Applying Equation (2.52) to decide if it is real collision. If not, go back to step 3.
7. If it is real collision, generate new direction for particle and use equation (2.53) to generate $r(j)$ for collision decision.
8. Using the value of $r(j)$ to decide which type of collision occurs.
9. Depending on the type of collision, use Equations (2.54-2.56) to compute the new energies of the particles.
10. Store the new energies and directions of the particles for next collision.
11. Check if $t_{count} \geq t_{sim}$. If not, go back to step 3.
12. If it reaches the end of simulation, calculate average energies, drift velocity values, positions for all particles after the collision.

2.3.7 Comparison of Monte Carlo Simulation and Boltzmann Transport Equation

There are both advantages and disadvantages for either the Boltzmann Transport Equation or the Monte Carlo Simulation method. As we know, one does not need to monitor the motion of every particle with the Boltzmann Transport Equation. Hence, the Boltzmann Transport Equation solution is always quick and does not consume much computer memory. Furthermore, since it solves the distribution functions with partial differential equations and numerical methods, it always yields smooth distribution functions. However, when we use multi-term solution to solve Boltzmann Transport Equation, we assume the form of the distribution function to be Legendre Polynomials and try to fit to this form by adding a number of distribution functions. This will result the obtained distribution functions are on the basis of an assumed form. This can be a more serious drawback when solving transient cases where quasi-equilibrium has not been reached because the shape of the distribution function is unknown and can deviate substantially from assumed form. It is also not good for low density cases when there may not be too many collisions to shape the distribution into an "expected" form.

In contrast to Boltzmann Transport Equation, Monte Carlo simulation is based upon each particle's actual motion to obtain distribution function. There is no assumed function form such as the Legendre Polynomials that are implicit in some solutions of the BTE. However, its accuracy is based upon the use of a large number of particles to avoid the corresponding statistical noise. This does, unfortunately, make the computations more intensive which take longer time and occupy more computer memory. Another reason to take longer time is that time steps have to be set as short as the inter-collision times. Finally, Monte Carlo simulation cannot either correctly simulate ionizations or avalanche multiplication due to increases in particle numbers since finite-sized arrays have to be used in the numerical implementations.

2.4 Electronic Cross Sections in Atmospheric Nitrogen

The cross sections applied in later numerical simulations for Boltzmann Transport Equation in this dissertation research are for processes of electron collisions with both nitrogen molecules (N_2) and singly ionized nitrogen molecules (N_2^+). These are important in studying low-temperature plasmas in nature and industrial techniques of gaseous electronics and plasma processing. Since nitrogen is the most abundant gas in the atmosphere, calculations involving nitrogen is a useful starting point. Not only can N_2 be used, other gases such as O_2, Ne, Ar can also be used in applications. So the solution to Boltzmann Transport Equation can easily be extended to other gas cross sections rather than nitrogen molecules (N_2) and the singly ionized nitrogen molecules (N_2^+) discussed in this work. Experimental results among different gases can be compared to see how the cross sections play a part in the electron distribution function.

There are mainly seven cross section equations with nitrogen molecules (N_2) and singly ionized nitrogen molecules (N_2^+), and these seven equations follow three basic equations as below:

$$f_1(x;c_1,c_2) = \sigma_0 c_1 (x/E_R)^{c_2}, \tag{2.57}$$

$$f_2(x;c_1,c_2,c_3,c_4) = f_1(x;c_1,c_2)/[1+(x/c_3)^{c_2+c_4}], \tag{2.58}$$

$$f_3(x;c_1,c_2,c_3,c_4,c_5,c_6) = f_1(x;c_1,c_2)/[1+(x/c_3)^{c_2+c_4}+(x/c_5)^{c_2+c_6}], \tag{2.59}$$

with $\sigma_0 = 1\times10^{-16} cm^2$ and $E_R = 1.361\times10^{-2} keV$. The symbols x and $c_i (i = 1,2,3,\ldots,6)$ denote dummy parameters. The cross sections with nitrogen molecules (N_2) and singly ionized nitrogen molecules (N_2^+) are expressed by one of the following forms involving the combination of the above functions:

$$\sigma = f_2(E_1;a_1,a_2,a_3,a_4), \tag{2.60}$$

$$\sigma = f_2(E_1;a_1,a_2,a_3,a_4) + f_2(E_1;a_5,a_6,a_7,a_4), \tag{2.61}$$

$$\sigma = f_2(E_1;a_1,a_2,a_3,a_4) + f_2(E_1;a_5,a_6,a_7,a_8), \tag{2.62}$$

$$\sigma = f_2(E_1;a_1,a_2,a_3,a_4) + f_2(E_1;a_5,a_6,a_7,a_8) + f_2(E_1;a_9,a_{10},a_{11},a_{12}), \tag{2.63}$$

$$\sigma = f_3(E_1;a_1,a_2,a_3,a_4,a_5,a_6), \tag{2.64}$$

$$\sigma = f_3(E_1;a_1,a_2,a_3,a_4,a_5,a_6) + f_2(E_1;a_7,a_8,a_9,a_{10}), \tag{2.65}$$

$$\sigma = \sigma_0 a_1 (\ln(E/E_{th}) + a_2)/[E_{th} E(1+a_3/E_1)^{a_4}], \tag{2.66}$$

where $E_1 = E - E_{th}$ with E the incident electron energy in keV and E_{th} the threshold energy of reaction in keV. Depending on the formula chosen from Equations (2.60) to (2.66) above, a_1, a_2, etc., are substituted for c_1, c_2, etc.

Tables 1 and 2 from the literature [24] give the values of the fitting parameters $(a_1, a_2, \ldots)$, which have been determined by least-squares fits to the collected data. Some of the plots for elastic and inelastic scatterings cross-sections versus energy that will be applied in later numerical simulations for Boltzmann Transport Equation are given below. Because of the space, only nine plots for excitational scattering processes are given below. In our numerical simulations, rotational scattering, vibrational scattering, ionization scattering and excitation1~excitation26 scatterings

are included as the inelastic scatterings. All the other excitational scattering plots besides those given here can be found in the literature [24].

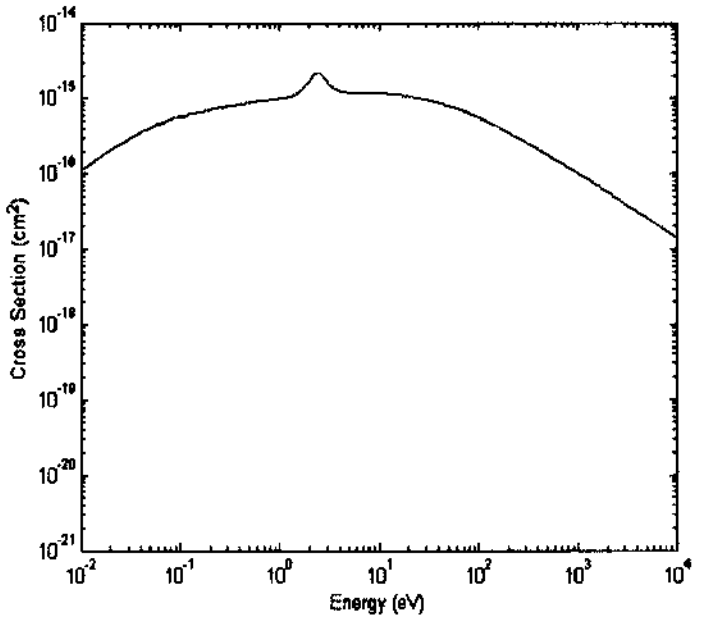

(a) Elastic Scattering/ N_2.

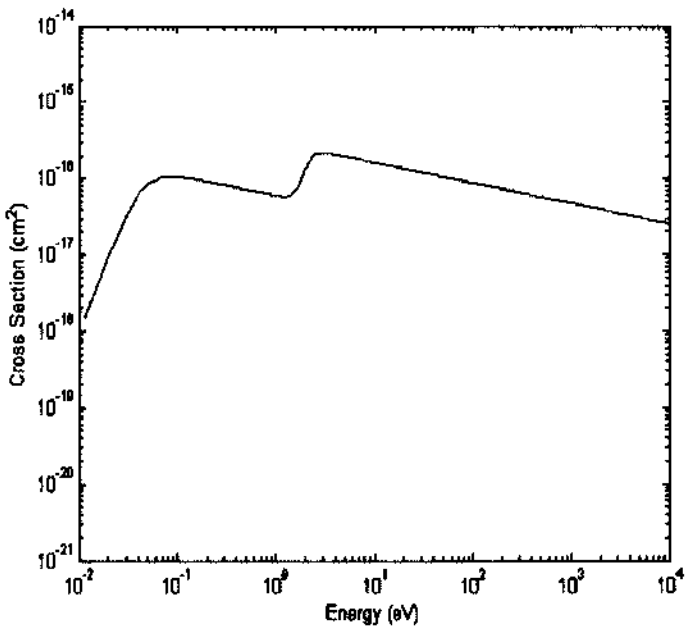

(b) Rotational Excitation $(J = 0 \rightarrow 2)/N_2$.

Figure 2.1 Cross Sections for Electrons in Collisions with Nitrogen Molecules (N_2) and Singly Ionized Nitrogen Molecules (N_2^+).

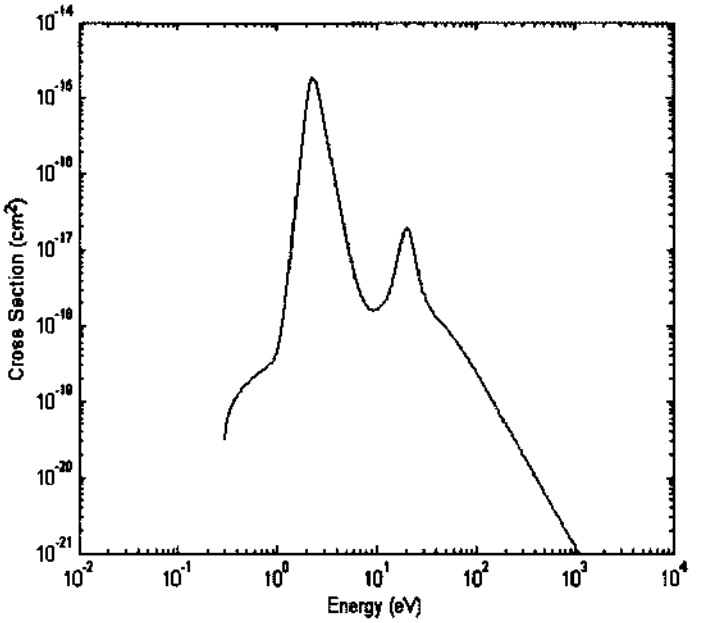

(c) Total Vibrational Excitation/ N_2.

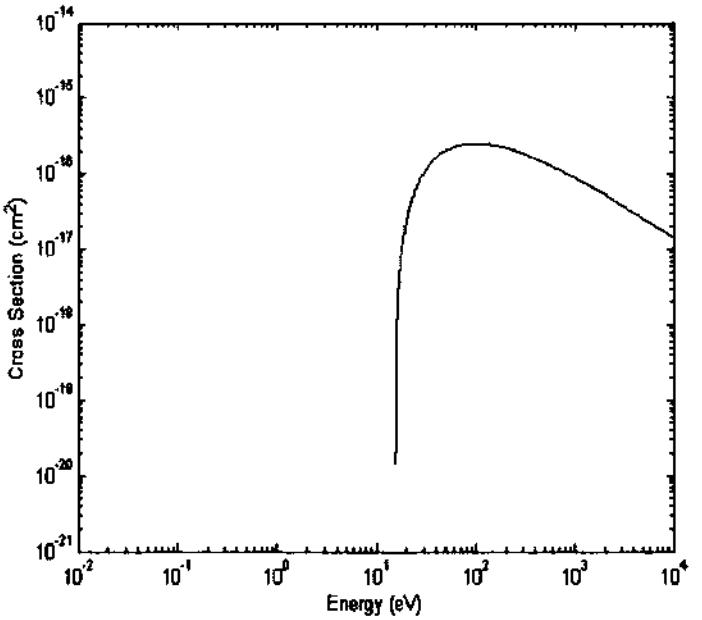

(d) Total Ionization/ N_2.

Figure 2.1 (Continued)

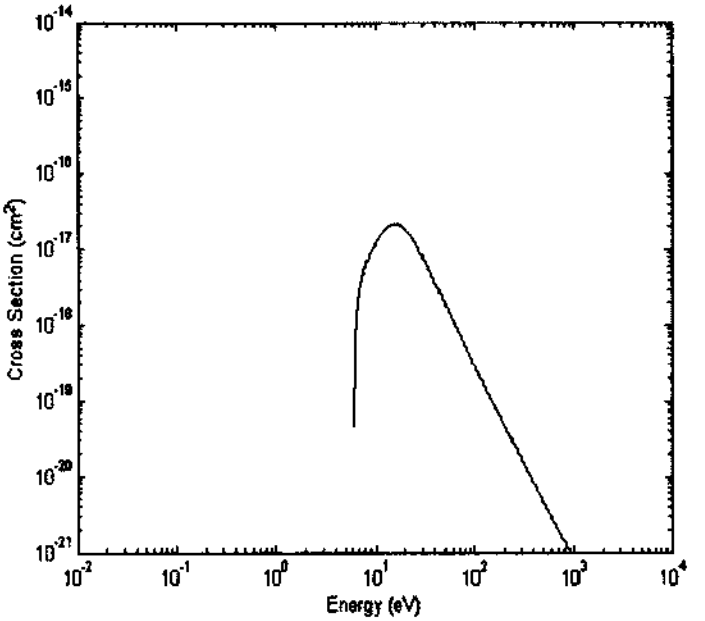

(e) Excitation to $(A\ ^3\Sigma_u^+)/N_2$.

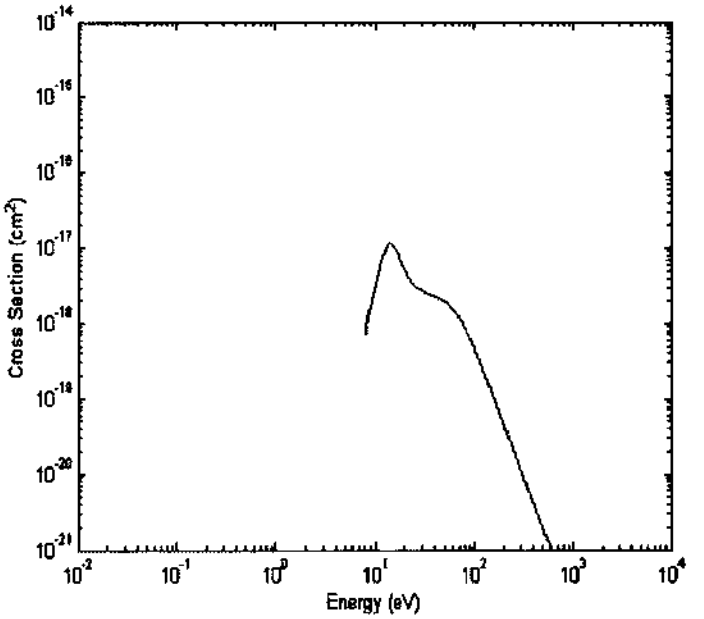

(f) Excitation to $(B'\ ^3\Sigma_u^+)/N_2$.

Figure 2.1 (Continued)

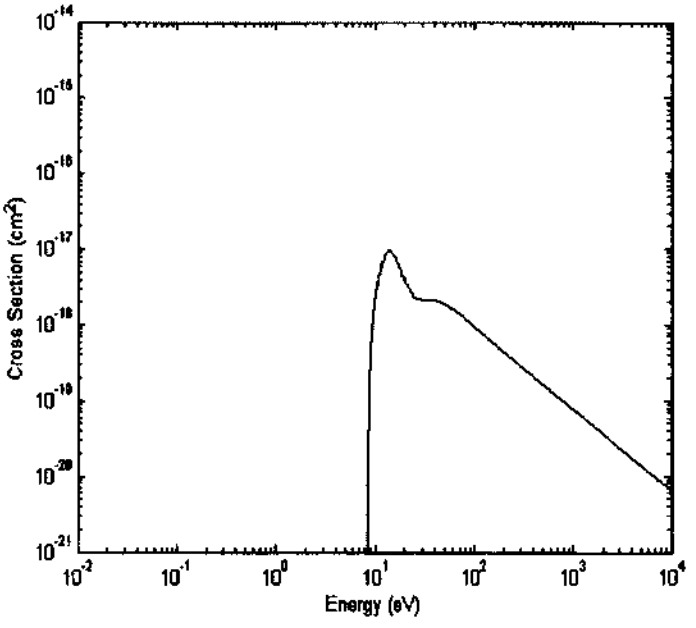

(g) Excitation to $(a'\ ^1\Sigma_u^-)/N_2$.

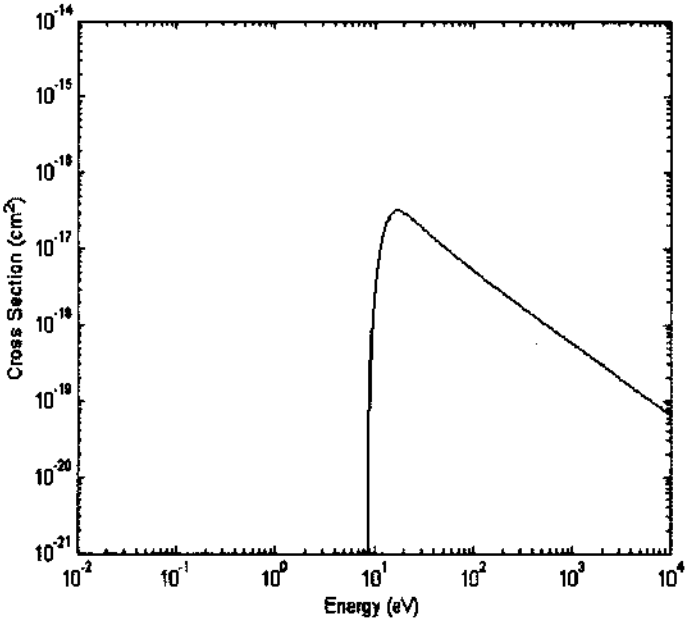

(h) Excitation to $(a\ ^1\Pi_g)/N_2$.

Figure 2.1 (Continued)

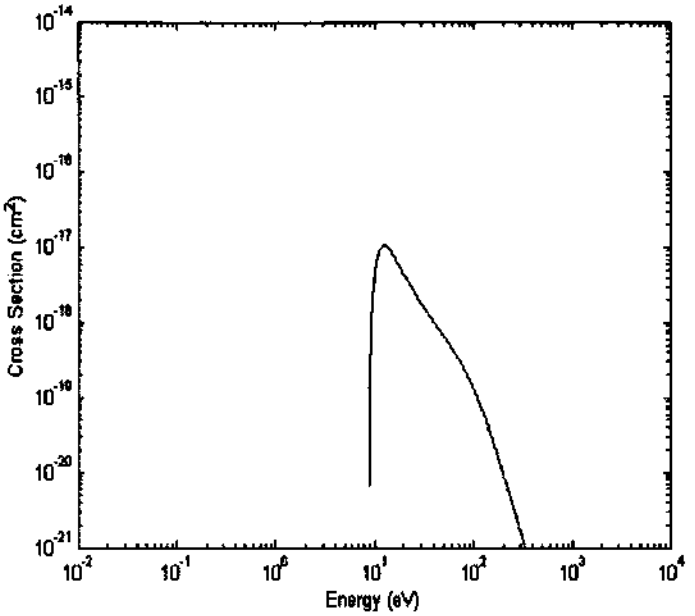

(i) Excitation to $(w\ ^1\Delta_u)/N_2$.

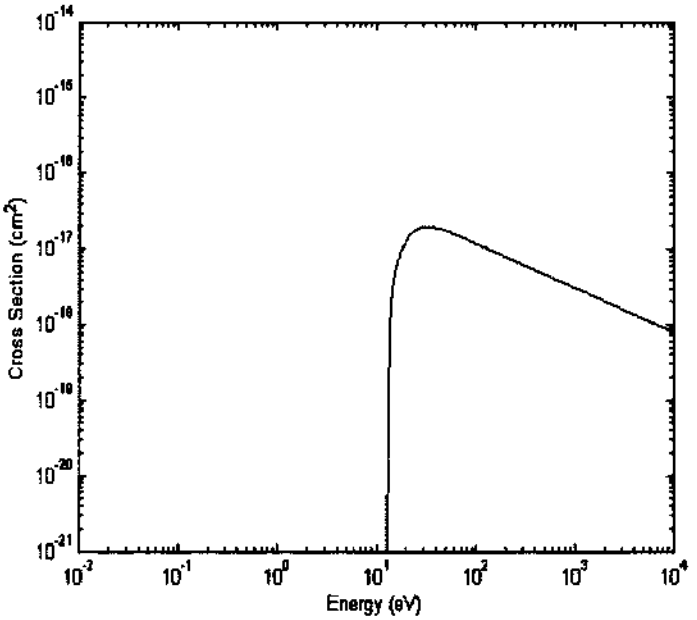

(j) Excitation to $(b\ ^1\Pi_u)/N_2$.

Figure 2.1 (Continued)

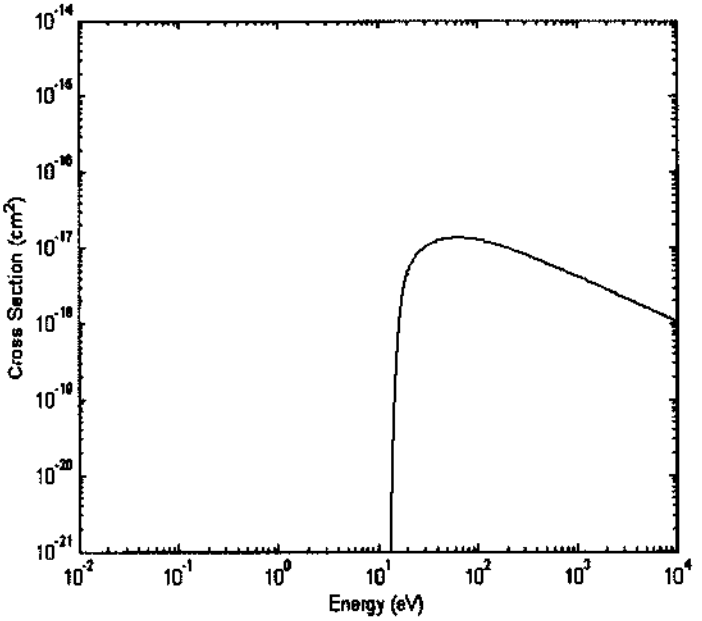

(k) Excitation to $(b'\ ^1\Sigma_u^+)/N_2$.

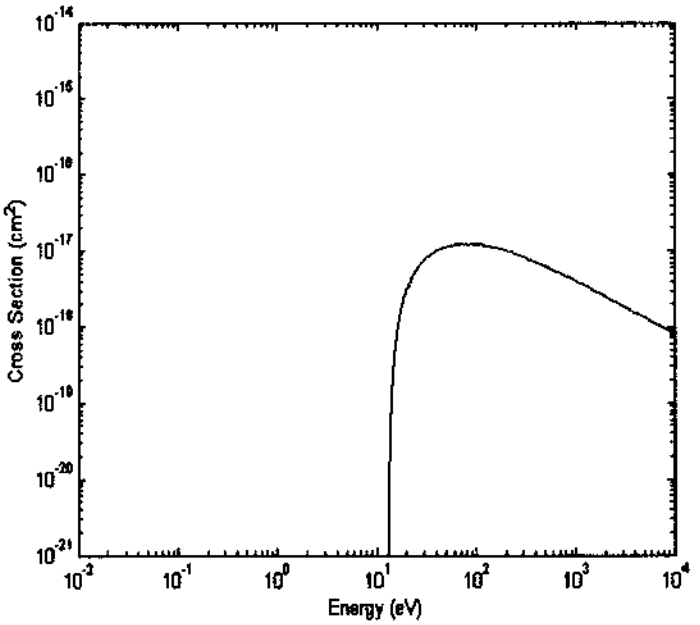

(l) Excitation to $(c'_4\ ^1\Sigma_u^+)/N_2$.

Figure 2.1 (Continued)

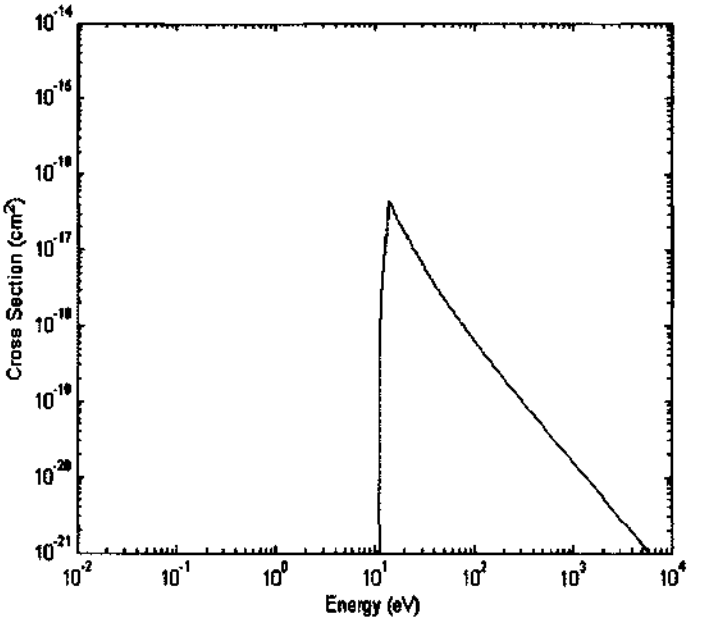

(m) Excitation to $(c\ ^3\Pi_u)/N_2$.

Figure 2.1 (Continued)

CHAPTER 3

MULTI-TERM APPROXIMATION TO THE BOLTZMANN TRANSPORT EQUATION FOR ELECTRON ENERGY DISTRIBUTION FUNCTIONS

3.1 Introduction

In order to solve the time-dependent and time-independent behavior of charged particle swarms in an unbounded neutral gas, we propose a multi-term approximation for Boltzmann Transport Equation. The multi-term approximation is based on using an expansion of the electron velocity distribution function in Legendre Polynomials [25]. This method improves the accuracy of the time-dependent treatment of the electron kinetics and efficiently solves the extended time-dependent equation system relevant to the isotropic part and the various anisotropic components of the expansion of the velocity distribution.

3.2 Multi-Term Approximation

Multi-term Approximation means the representation of the distribution function in directions of velocity space through an expansion in spherical harmonics, $Y_m^l(\theta)$.

$$f_i(r,v,t) = \sum_{l=0}^{\infty} \sum_{m=-l}^{l} f_{i,m}^l(r,v,t) Y_m^l(\theta), \tag{3.1}$$

where θ is the angle between the field and velocity vectors [26,27]. This reduces to an expansion in terms of Legendre polynomials $P_l(\cos\theta)$ under circumstances of high symmetry (e.g., under azimuthal symmetry) [28]. In any practical calculation the infinite expansion above must be truncated to finite size by imposing an upper limit $l_{\max}$.

$$f_i(r,v,t) = \sum_{l=0}^{l_{\max}} \sum_{m=-l}^{l} f_{i,m}^l(r,v,t) Y_m^l(\theta). \tag{3.2}$$

For light particles, such as electrons undergoing predominantly elastic collisions, one can approximately choose $l_{max}=1$. This is called a two-term approximation. It formed the basis for the "classical theory" of electron transport properties. However, it is entirely inappropriate when the distribution function deviates substantially from isotropy in velocity space when inelastic collisions are significant. This could happen under conditions of high electrical fields or large pressures. Energy transfer is no longer relatively small and collisions no longer merely have the effect of randomizing the direction of electron motion while largely preserving their speeds. In these circumstances, a multi-term approximation is required, in which $l_{max}>1$ must be varied incrementally until some convergence/accuracy criterion is attained. Usually it requires $l_{max}\geq 5$ to obtain transport coefficients accuracy better than 1%, even for electrons.

Using the multi-term approximation, the homogeneous Boltzmann Transport Equation is transformed essentially into a system of partial differential equations [29]. The key point is to improve the accuracy of the treatment of the homogeneous kinetic equation of the electrons and to analyze the impact of the higher order terms on both of the electron velocity distribution function and the relevant macroscopic quantities of the electrons.

3.3 Governing Equations

These are partial differential equations to obtain the distribution function $f_0 \sim f_{l-1}$ [30,31].

$$\frac{\partial}{\partial t}f_0+\frac{qE}{3}\left(\frac{2}{mU}\right)^{\frac{l}{2}}\frac{\partial}{\partial U}(Uf_1)-\frac{1}{U^{1/2}}\frac{\partial}{\partial U}\left(U^{\frac{3}{2}}2\frac{m}{M}\nu_{el}(U)f_0\right)+\sum_l \nu_{in}^l(U)f_0- \sum_l\left(\frac{U+U_{in}^l}{U}\right)^{\frac{l}{2}}\times\nu_{in}^l(U+U_{in}^l)f_0(U+U_{in}^l,t)=0, \tag{3.3}$$

$$\frac{\partial}{\partial t}f_n - \frac{n}{2n-1}\left(\frac{2}{m}\right)^{\frac{1}{2}}qE\times\left[U^{\frac{1}{2}}\frac{\partial}{\partial U}f_{n-1} - \frac{n-1}{2}\left(\frac{1}{U}\right)^{\frac{1}{2}}f_{n-1}\right] - \frac{n+1}{2n+3}\left(\frac{2}{m}\right)^{\frac{1}{2}}qE$$
$$\times\left[U^{\frac{1}{2}}\frac{\partial}{\partial U}f_{n+1} + \frac{n+2}{2}\left(\frac{1}{U}\right)^{\frac{1}{2}}f_{n+1}\right] + \left(\nu_{el}(U) + \sum_l \nu_{in}^l(U)\right)f_n = 0 \quad 1 \le n \le total-2, \tag{3.4}$$

$$\frac{\partial}{\partial t}f_{total-1} - \frac{total-1}{2total-3}\left(\frac{2}{m}\right)^{\frac{1}{2}}qE\times\left[U^{\frac{1}{2}}\frac{\partial}{\partial U}f_{total-2} - \frac{total-2}{2}\left(\frac{1}{U}\right)^{\frac{1}{2}}f_{total-2}\right]$$
$$+\left(\nu_{el}(U) + \sum_l \nu_{in}^l(U)\right)f_{total-1} = 0. \tag{3.5}$$

Here q is the quantity of electricity for electron, E is the electrical field value, m is the electron masse, M is the gas particle masse, $U = mv^2/2$ is the instantaneous electron energy. U_{in}^l denotes the energy loss in the l^{th} inelastic collision process. *total* is the index of the last energy distribution function we will consider. The quantities

$$\nu_{el}^l(U) = \left(\frac{2}{m}\right)^{\frac{1}{2}}U^{\frac{1}{2}}n\sigma_{el}(U), \tag{3.6}$$

and $$\nu_{in}^l(U) = \left(\frac{2}{m}\right)^{\frac{1}{2}}U^{\frac{1}{2}}n\sigma_{in}^l(U), \tag{3.7}$$

are the electron-energy-dependent collision frequencies for elastic and inelastic collisions, where σ_{el} and σ_{in}^l denote the total cross sections for elastic and the l th inelastic collision process, and n is the gas density.

To be specific, if we put Equation (3.6) and (3.7) back to the original governing Equations (3.3)-(3.5) and only leave the derivative term of distribution function to time in the left hand side as well as move all the other terms to the right hand side, we can obtain the time-dependent Boltzmann Transport Equations for distributions f_0 to f_6 as below.

$$\frac{\partial f_0}{\partial t} = -\frac{qE}{3}\sqrt{\frac{2}{mU}} f_1(U) - \frac{qE}{3}\sqrt{\frac{2U}{m}}\frac{\partial f_1(U)}{\partial U} - \sum_l n\sqrt{\frac{2U}{m}}\sigma_{in}^l(U) f_0(U) \tag{3.8}$$

$$+\sum_l \sqrt{\frac{U+U_{in}^l}{U}} n\sqrt{\frac{2(U+U_{in}^l)}{m}}\sigma_{in}^l(U+U_{in}^l) f_0(U+U_{in}^l) + 2n\frac{m}{M}\sqrt{\frac{2}{mU}}\frac{\partial}{\partial U}(U^2\sigma_{el}(U) f_0(U)),$$

$$\frac{\partial f_1}{\partial t} = -qE\sqrt{\frac{2U}{m}}\frac{\partial f_0(U)}{\partial U} - n\sqrt{\frac{2U}{m}}(\sigma_m(U) + \sum_l \sigma_{in}^l(U)) f_1(U) - \frac{2}{5}qE\sqrt{\frac{2U}{m}}$$

$$(\frac{\partial f_2(U)}{\partial U} + \frac{3}{2U} f_2), \tag{3.9}$$

$$\frac{\partial f_2}{\partial t} = -\frac{2}{3}qE\sqrt{\frac{2U}{m}}\frac{\partial f_1(U)}{\partial U} + \frac{1}{3}qE\sqrt{\frac{2}{mU}} f_1 - \frac{3}{7}qE\sqrt{\frac{2U}{m}}(\frac{\partial f_3}{\partial U} + \frac{2}{U} f_3) - n\sqrt{\frac{2U}{m}}(\sigma_m(U) +$$

$$\sum_l \sigma_{in}^l(U)) f_2(U), \tag{3.10}$$

$$\frac{\partial f_3}{\partial t} = -\frac{3}{5}qE\sqrt{\frac{2U}{m}}\frac{\partial f_2(U)}{\partial U} + \frac{3}{5}qE\sqrt{\frac{2}{mU}} f_2 - \frac{4}{9}qE\sqrt{\frac{2U}{m}}(\frac{\partial f_4}{\partial U} + \frac{5}{2U} f_4) - n\sqrt{\frac{2U}{m}}(\sigma_m(U) +$$

$$\sum_l \sigma_{in}^l(U)) f_3(U), \tag{3.11}$$

$$\frac{\partial f_4}{\partial t} = -\frac{4}{7}qE\sqrt{\frac{2U}{m}}\frac{\partial f_3(U)}{\partial U} + \frac{6}{7}qE\sqrt{\frac{2}{mU}} f_3 - \frac{5}{11}qE\sqrt{\frac{2U}{m}}(\frac{\partial f_5}{\partial U} + \frac{3}{U} f_5) - n\sqrt{\frac{2U}{m}}(\sigma_m(U) +$$

$$\sum_l \sigma_{in}^l(U)) f_4(U), \tag{3.12}$$

$$\frac{\partial f_5}{\partial t} = -\frac{5}{9}qE\sqrt{\frac{2U}{m}}\frac{\partial f_4(U)}{\partial U} + \frac{10}{9}qE\sqrt{\frac{2}{mU}} f_4 - \frac{6}{13}qE\sqrt{\frac{2U}{m}}(\frac{\partial f_6}{\partial U} + \frac{7}{2U} f_6) - n\sqrt{\frac{2U}{m}}(\sigma_m(U) +$$

$$\sum_l \sigma_{in}^l(U)) f_5(U), \tag{3.13}$$

$$\frac{\partial f_6}{\partial t} = -\frac{6}{11}qE\sqrt{\frac{2U}{m}}\frac{\partial f_5(U)}{\partial U} + \frac{15}{11}qE\sqrt{\frac{2}{mU}} f_5 - n\sqrt{\frac{2U}{m}}(\sigma_m(U) + \sum_l \sigma_{in}^l(U)) f_6(U). \tag{3.14}$$

We only focus on f_0 and f_1 at the moment. So the governing equations will be:

$$\frac{\partial f_0}{\partial t} = -\frac{qE}{3}\sqrt{\frac{2}{mU}} f_1(U) - \frac{qE}{3}\sqrt{\frac{2U}{m}}\frac{\partial f_1(U)}{\partial U} - \sum_l n\sqrt{\frac{2U}{m}}\sigma_{in}^l(U) f_0(U) \tag{3.8}$$

$$+\sum_l \sqrt{\frac{U+U_{in}^l}{U}} n\sqrt{\frac{2(U+U_{in}^l)}{m}}\sigma_{in}^l(U+U_{in}^l) f_0(U+U_{in}^l) + 2n\frac{m}{M}\sqrt{\frac{2}{mU}}\frac{\partial}{\partial U}(U^2\sigma_{el}(U) f_0(U)),$$

$$\frac{\partial f_1}{\partial t} = -qE\sqrt{\frac{2U}{m}}\frac{\partial f_0(U)}{\partial U} - n\sqrt{\frac{2U}{m}}(\sigma_{el}(U) + \sum_l \sigma_{in}^l(U)) f_1(U). \tag{3.15}$$

These two governing equations will occur as the governing equations for time-dependent Euler method and time-dependent Runge Kutta method discussed later. The governing equations for implicit time-independent method and implicit

time-dependent relaxation method will still base upon these two equations but with a few transformations. The details are given in each section.

In the next sections, different numerical methods will be applied to solve these partial differential equations (PDEs) and obtain the energy distribution functions f_0 and f_1 under steady state conditions. The important symbol for steady state is that drift velocity will not change any more. In addition a number of results will be obtained, such as the normal and semi-logarithmic plots for two-dimensional (2D) energy distribution functions at different moments for different E/N values, three-dimensional (3D) energy distribution function plots with 2D energy distribution function relevant with time for different E/N values, as well as drift velocity plots for different E/N values. In the end, plots will be presented which will show comparisons between our drift velocity results and experimental results published by other research groups, as well as our ionization coefficient results and those published in the literature. The comparisons will be observed to be in very good agreement. This will essentially validate the method and its numerical implementation.

The numerical methods introduced here are: the implicit time-independent relaxation method by solving the matrix equation, a time-dependent Euler method, the time-dependent Runge-Kutta method, and finally the implicit time-dependent relaxation method by generating the 4-way grid as well as solving the matrix equation.

The simulation process starts with including only one inelastic process and finally extends to include all the inelastic processes. The figures shown in Chapter 4 are results obtained with all the inelastic processes included.

3.4 Implicit Time-Independent Method

3.4.1 Introduction

We begin by introducing the implicit time-independent method. "Time-independent" here means all the electrons have already reached steady state and the distribution functions do not change with time any more. "Implicit" means

one couples f_0 and f_1 together in a vector, and solves them together by solving a coupled matrix equation rather than updating f_0 and f_1 sequentially with an explicit method. This is a realistic and simultaneous approach. Let's assign $\frac{\partial f_0}{\partial t}=0,\ \frac{\partial f_1}{\partial t}=0.$ in the governing equations and try to obtain the distribution functions under these coupled conditions. Then the distribution functions and the drift velocity obtained will be those for the steady state. This method omits all the updating steps relevant with each time step and estimates the distribution functions (as well as drift velocity) in a fast manner, although the results obtained do not yield any temporal development.

3.4.2 Method Description

Next this implicit time-independent method is explained step-by-step, including the relevance of creating a matrix and subsequently solving the resulting matrix equations.

Let's start by rewriting the various terms of the governing Equation (3.3). The second term can be simplified to Equation (3.16) as below:

$$\frac{qE}{3}\sqrt{\frac{2}{mU}}\frac{\partial}{\partial U}(Uf_1)=\frac{qE}{3}\sqrt{\frac{2}{mU}}f_1+\frac{qE}{3}\sqrt{\frac{2U}{m}}\frac{\partial f_1}{\partial U}, \tag{3.16}$$

The third term of Equation (3.3) can be re-written as:

$$\begin{aligned}&\frac{1}{U^{1/2}}\frac{\partial}{\partial U}\left(U^{\frac{3}{2}}2\frac{m}{M}v_{el}(U)f_0\right)=\frac{1}{U^{1/2}}\frac{\partial}{\partial U}\left(U^{\frac{3}{2}}2\frac{m}{M}\left(\frac{2}{m}\right)^{\frac{1}{2}}U^{\frac{1}{2}}n\sigma_{el}(U)f_0\right)\\&=\frac{1}{\sqrt{U}}2\frac{m}{M}\sqrt{\frac{2}{m}}n\frac{\partial}{\partial U}\left(U^2\sigma_{el}(U)f_0\right)=2\frac{m}{M}\sqrt{\frac{2U}{m}}n(2\sigma_{el}(U)f_0+U\frac{\partial\sigma_{el}(U)}{\partial U}f_0\\&+U\sigma_{el}(U)\frac{\partial f_0}{\partial U})=2\frac{m}{M}\sqrt{\frac{2U}{m}}n(2\sigma_{el}(U)f_0+U\frac{\sigma_{el}(U+dU)-\sigma_{el}(U-dU)}{2dU}f_0\\&+U\sigma_{el}(U)\cdot\frac{f_0(U+dU)-f_0(U-dU)}{2dU}),\end{aligned} \tag{3.17}$$

After replacing these two terms listed as given by Equations (3.16) and (3.17) into the governing Equations (3.3) and (3.4), these two coupled equations still need to be solved for the simple case of the two-term Legendre Polynomial expansion for

f_0 and f_1. With the simplifications given by Equations (3.16) and (3.17), the equivalent governing equations become:

$$\frac{\partial f_0}{\partial t} = -\frac{qE}{3}\sqrt{\frac{2}{mU}}f_1(U) - \frac{qE}{3}\sqrt{\frac{2U}{m}}\frac{f_1(U+dU)-f_1(U-dU)}{2dU} - \sum_i n\sqrt{\frac{2U}{m}}\sigma_{in}^i(U)f_0(U)$$
$$+\sum_i \sqrt{\frac{U+U_{in}}{U}}n\sqrt{\frac{2(U+U_{in})}{m}}\sigma_{in}^i(U+U_{in})f_0(U+U_{in})$$
$$+2n\frac{m}{M}\sqrt{\frac{2U}{m}}(2\sigma_{el}(U)f_0(U)+U\frac{\sigma_{el}(U+dU)-\sigma_{el}(U-dU)}{2dU}f_0(U)) \quad (3.18)$$
$$+\frac{2n\frac{m}{M}\sqrt{\frac{2U}{m}}U\sigma_{el}(U)}{2dU}f_0(U+dU) - \frac{2n\frac{m}{M}\sqrt{\frac{2U}{m}}U\sigma_{el}(U)}{2dU}f_0(U-dU),$$

$$\frac{\partial f_1}{\partial t} = -qE\sqrt{\frac{2U}{m}}\frac{f_0(U+dU)-f_0(U-dU)}{2dU} - n\sqrt{\frac{2U}{m}}(\sigma_{el}(U)+\sum_i \sigma_{in}^i(U))f_1(U). \quad (3.19)$$

Here we consider the steady state situation as a simplified sub-set of the overall solution. Thus, the drift velocity and all the distribution functions would be time invariant under this chosen temporal regime. Thus: $\frac{\partial f_0}{\partial t}=0, \frac{\partial f_1}{\partial t}=0$. The boundary conditions need to be taken into account as well for a complete solution. The process for updating f_0 and f_1 under this implicit scheme is as listed below.

Updating f_0:

For $i=1$, we follow the principle that

$$4\pi K\int v^2 f(v)dv = number\ of\ electrons \quad (3.20)$$

Expanding the Equation (3.20) we get

$$\frac{2\pi}{m^{\frac{3}{2}}}du[(U_1+U_2)^{\frac{1}{2}}(f_0(U_1)+f_0(U_2))+(U_2+U_3)^{\frac{1}{2}}(f_0(U_2)+f_0(U_3))+ \quad (3.21)$$
$$(U_3+U_4)^{\frac{1}{2}}(f_0(U_3)+f_0(U_4))+\cdots+(U_{num-1}+U_{num})^{\frac{1}{2}}(f_0(U_{num-1})+f_0(U_{num}))]$$
$$= n_{electron}.$$

In the above, $n_{electron}$ represents the electron density. For $1<i<num$, where num represents the number of grid points covering the energy-range, we make the left hand side of Equation (3.18) be zero in order to fulfill the time invariant situation. This yields:

$$
\begin{aligned}
&-\frac{qE}{3}\sqrt{\frac{2}{mU}}f_1(U)-\frac{qE}{3}\sqrt{\frac{2U}{m}}\frac{f_1(U+dU)-f_1(U-dU)}{2dU}-\sum_l n\sqrt{\frac{2U}{m}}\sigma_{in}^l(U)f_0(U)\\
&+\sum_l \sqrt{\frac{U+U_{in}}{U}}n\sqrt{\frac{2(U+U_{in})}{m}}\sigma_{in}^l(U+U_{in})f_0(U+U_{in})\\
&+2n\frac{m}{M}\sqrt{\frac{2U}{m}}(2\sigma_{el}(U)f_0(U)+U\frac{\sigma_{el}(U+dU)-\sigma_{el}(U-dU)}{2dU}f_0(U))\\
&+\frac{2n\frac{m}{M}\sqrt{\frac{2U}{m}}U\sigma_{el}(U)}{2dU}f_0(U+dU)-\frac{2n\frac{m}{M}\sqrt{\frac{2U}{m}}U\sigma_{el}(U)}{2dU}f_0(U-dU)=0.
\end{aligned}
\tag{3.22}
$$

For $i = num$, $f_0(U_{num}) = 0$. This simply represents an approximation of zero electron density at the highest energy.

For updating f_1, the procedure is given next.

For $i = 1$, $f_1(U_1) = 0$.

For $1 < i < num$, we will make the left hand side of Equation (3.19) be zero in order to fulfill the time invariant situation.

$$
\frac{qE}{n(\sigma_{el}(U)+\sum_l \sigma_{in}^l(U))}\frac{f_0(U+dU)-f_0(U-dU)}{2dU}+f_1(U)=0. \tag{3.23}
$$

For $i = num$, $f_1(U_{num}) = 0$.

The function f_0 and f_1 can be coupled together in a vector X as Equation (3.25) shows and we used coupling matrix G to solve f_0 and f_1 together rather than using Equation (3.22) and (3.23) alone to solve f_0 and f_1 separately.

The above discretized equation can be written in matrix form for convenience and compactness. The matrix we use here is as follows:

$$
G=\begin{pmatrix} A & B \\ C & D \end{pmatrix}_{2num*2num}, \tag{3.24}
$$

$$
X=\begin{pmatrix} f_0(1) \\ \vdots \\ f_0(num) \\ f_1(1) \\ \vdots \\ f_1(num) \end{pmatrix}_{2num\times 1}, \tag{3.25}
$$

$$E=\begin{pmatrix}1\\0\\\vdots\\0\\0\\\vdots\\0\end{pmatrix}_{2num*1}, \tag{3.26}$$

$$G\times X = E, \tag{3.27}$$

$$P = inv(G), \tag{3.28}$$

$$X = P\times E. \tag{3.29}$$

The desired energy distribution functions f_0 and f_1 are stored in the array X. In this manner, the energy distribution functions f_0 and f_1 are obtained. The non-zero elements in matrix G are as below:

$$A(1,1) = (U_1 + U_2)^{\frac{1}{2}}, \tag{3.30}$$

$$A(1,i) = (U_{i-1} + U_i)^{\frac{1}{2}} + (U_i + U_{i+1})^{\frac{1}{2}} \quad (1 < i < num), \tag{3.31}$$

$$A(1,num) = (U_{num-1} + U_{num})^{\frac{1}{2}}, \tag{3.32}$$

For $1 < i < num$,

$$A(i,i) = 2n\frac{m}{M}\sqrt{\frac{2U}{m}}(2\sigma_{el}(U) + U\frac{\sigma_{el}(U+dU) - \sigma_{el}(U-dU)}{2dU}) \tag{3.33}$$

$$-\sum_l n\sqrt{\frac{2U}{m}}\sigma_{in}^l(U),$$

$$A(i,i-1) = -\frac{2n\frac{m}{M}\sqrt{\frac{2U}{m}}U\sigma_{el}(U)}{2dU}, \tag{3.34}$$

$$A(i,i+1) = \frac{2n\frac{m}{M}\sqrt{\frac{2U}{m}}U\sigma_{el}(U)}{2dU}, \tag{3.35}$$

For $1 \le l \le in\_num$,

$$A(i,ihigh^l) = A(i,ihigh^l) + \sqrt{\frac{U+U_{in}^l}{U}} n \sqrt{\frac{2(U+U_{in}^l)}{m}} \sigma_{in}^l (U+U_{in}^l) \tag{3.36}$$

$$(ihigh^l = \frac{U+U_{in}^l}{dU}),$$

$$A(num,num) = 1, \tag{3.37}$$

The other elements of matrix A are 0.

For $1 < i < num$,

$$B(i,i) = -\frac{qE}{3}\sqrt{\frac{2}{mU}}, \tag{3.38}$$

$$B(i,i+1) = -\frac{qE}{3}\sqrt{\frac{2U}{m}}\frac{1}{2dU}, \tag{3.39}$$

$$B(i,i-1) = \frac{qE}{3}\sqrt{\frac{2U}{m}}\frac{1}{2dU}, \tag{3.40}$$

The other elements of matrix B are 0.

For $1 < i < num$,

$$C(i,i+1) = \frac{qE}{n(\sigma_{el}(U) + \sum_l \sigma_{in}^l(U))}\frac{1}{2dU}, \tag{3.41}$$

$$C(i,i-1) = \frac{-qE}{n(\sigma_{el}(U) + \sum_l \sigma_{in}^l(U))}\frac{1}{2dU}, \tag{3.42}$$

The other elements of matrix C are 0.

For $1 \le i \le num$,

$$D(i,i) = 1, \tag{3.43}$$

The other elements of matrix D are 0.

After obtaining the energy distribution function f_0 and f_1, the drift velocity can be obtained as:

$$< V >= \frac{1}{3}\sqrt{\frac{2}{m}}\frac{\int_0^{U_{max}} f_1(U) U\, dU}{\int_0^{U_{max}} f_0(U)\sqrt{U}\, dU}. \tag{3.44}$$

This formula (3.44) will also be applied to the various numerical methods discussed next as well. For each E/N value, there will be a corresponding drift velocity value that will be obtained.

3.4.3 Method Analysis

This implicit time-independent method obtains drift velocity as well as the energy distribution functions f_0 and f_1 without computing the updating values at each time step. Therefore, it is the fastest way to obtain the steady-state parameters. The energy distribution functions are obtained from an initial Maxwellian distribution and this method omits all the updates relevant to each time step. Therefore, it is only a quick solution for the final steady state, and does not provide the temporal development and dynamical details. Moreover, since it is a fast estimate method, it reaches a final solution without having to perform iterative calculations or intermediate steps. Moreover, since it is a fast estimate method, we do not apply many energy gaps in the program, that is, the energy distribution function f_0 and f_1 are obtained and shown with a large energy step. Here, this is brought out by the fact that the curves for f_0 and f_1 are not smooth. This is usually a symptom of inaccuracy. There is also another drawback for this method. Since the energy term U_i occurs in the denominator, this implementation does not apply the average of the first two successive energy values to avoid the case of $U_i = 0$. Instead, we treat the first point in a special and different manner. However, there are still error accumulations related with the integral equation: $4\pi K\int v^2 f(v)dv = number\ of\ electrons$. Therefore, if the electric field is set to a very large value, the integral over velocity can present a problem unless care is taken to provide for a large energy range. Overall this method can serve as a start method for estimating drift velocity values. If we want to proceed to obtain accurate energy distribution functions, we need to follow the time-dependent methods given next.

3.5 Time-Dependent Euler Method

3.5.1 Introduction

Since implicit time-independent method can only obtain the approximate drift velocity and distribution functions under the special case of a steady-state, to overcome these deficiencies, we need to proceed to time-dependent method to see if one can obtain better results. The Time-dependent Euler method is a fully explicit method and it is sequentially updating f_1 and f_0 with a time step Δt. However, this explicit method is easy to accumulate step error and is not stable in simulation with large E/N values either.

3.5.2 Method Description

As stated in Section 3.3, governing equations will remain unchanged. These will, therefore, still be:

$$\frac{\partial f_0}{\partial t} = -\frac{qE}{3}\sqrt{\frac{2}{mU}} f_1(U) - \frac{qE}{3}\sqrt{\frac{2U}{m}}\frac{\partial f_1(U)}{\partial U} - \sum_l n\sqrt{\frac{2U}{m}}\sigma_{in}^l(U) f_0(U) \tag{3.8}$$

$$+\sum_l \sqrt{\frac{U+U_{in}^l}{U}} n\sqrt{\frac{2(U+U_{in}^l)}{m}}\sigma_{in}^l(U+U_{in}^l) f_0(U+U_{in}^l) + 2n\frac{m}{M}\sqrt{\frac{2}{mU}}\frac{\partial}{\partial U}(U^2\sigma_{el}(U) f_0(U)),$$

$$\frac{\partial f_1}{\partial t} = -qE\sqrt{\frac{2U}{m}}\frac{\partial f_0(U)}{\partial U} - n\sqrt{\frac{2U}{m}}(\sigma_{el}(U) + \sum_l \sigma_{in}^l(U)) f_1(U). \tag{3.15}$$

In this method, the two time-dependent equations are treated with any self-consistency. Thus, first the distribution function f_1 is updated as follows:

$$f_1(U_1 = 0, t) = 0, \tag{3.45}$$

For $2 \le i \le num$,

$$f_1(U_i, t+\Delta t) = f_1(U_i, t) - \Delta t \cdot (qE\sqrt{\frac{2U_i}{m}}\frac{f_0(U_i, t) - f_0(U_i - \Delta U, t)}{\Delta U} - n\sqrt{\frac{2U_i}{m}}$$

$$(\sigma_{el}(U_i) + \sum_l \sigma_{in}^l(U_i)) f_1(U_i, t)), \tag{3.46}$$

Then, using the new updated values for f_1, the other distribution function f_0 is updated. Thus:

For $1 \le i \le num - 1$,

$$f_0(U_i,t+\Delta t)=f_0(U_i,t)-\Delta t\cdot\{\frac{qE}{3}\sqrt{\frac{2}{m(\frac{U_i+U_i+\Delta U}{2})}}f_1(U_i,t+\Delta t)$$
$$-\frac{qE}{3}\sqrt{\frac{2U_i}{m}}\frac{f_1(U_i+\Delta U,t+\Delta t)-f_1(U_i-\Delta U,t+\Delta t)}{2\Delta U}-\sum_l n\sqrt{\frac{2U_i}{m}}\sigma_{in}^l(U_i)f_0(U_i,t)$$
$$+\sum_l\sqrt{\frac{U_i+U_{in}^l}{(\frac{U_i+U_i+\Delta U}{2})}}n\sqrt{\frac{2(U_i+U_{in}^l)}{m}}\sigma_{in}^l(U_i+U_{in}^l)f_0(U_i+U_{in}^l,t)+2n\frac{m}{M} \qquad (3.47)$$
$$\sqrt{\frac{2}{m(\frac{U_i+U_i+\Delta U}{2})}}\frac{((U_i+\Delta U)^2\sigma_{el}(U_i+\Delta U)f_0(U_i+\Delta U,t)-U_i^2\sigma_{el}(U_i)f_0(U_i,t))}{\Delta U}\}.$$

By alternately continuing this procedure, values for f_1 and f_0 are progressively obtained at each time step.

3.5.3 Method Analysis

The Euler method is the simplest time-dependent numerical method. It is quite easy to develop equations for the updates. Although simple, this method has many disadvantages. As we notice, each update with time is based upon one time step *dt* directly which will cause large accumulation error when it runs a long period of time. Therefore, most of the drift velocities obtained with this method will be quite different from the actual values as have been reported in experimental research studies. Moreover, it is an explicit numerical method and the updating process always comes with updating f_1 first then f_0 later rather than updating both simultaneously. Therefore, this method is quite unstable as well. When it comes to running with large E/N values or a long period of time, particularly going to higher order distribution functions such as $f_2 \sim f_6$, the program will be mostly likely to overflow before it reaches the end and will likely produce unpredictable final results.

3.6 Time-Dependent Runge-Kutta Method

3.6.1 Introduction

As a substantial improvement over the previous time-dependent Euler method, the time-dependent Runge-Kutta method updates with a much smaller time step and

works to update both f_0 and f_1 self-consistently. Compared to time-dependent Euler method, this method is much more accurate and stable.

3.6.2 Method Description

As stated in Section 3.3, for this implementation, the governing equations will still be unchanged, and given as:

$$\frac{\partial f_0}{\partial t} = -\frac{qE}{3}\sqrt{\frac{2}{mU}} f_1(U) - \frac{qE}{3}\sqrt{\frac{2U}{m}}\frac{\partial f_1(U)}{\partial U} - \sum_l n\sqrt{\frac{2U}{m}}\sigma_{in}^l(U) f_0(U) \tag{3.8}$$

$$+\sum_l \sqrt{\frac{U+U_{in}^l}{U}} n\sqrt{\frac{2(U+U_{in}^l)}{m}}\sigma_{in}^l(U+U_{in}^l) f_0(U+U_{in}^l) + 2n\frac{m}{M}\sqrt{\frac{2}{mU}}\frac{\partial}{\partial U}(U^2\sigma_{el}(U) f_0(U)),$$

$$\frac{\partial f_1}{\partial t} = -qE\sqrt{\frac{2U}{m}}\frac{\partial f_0(U)}{\partial U} - n\sqrt{\frac{2U}{m}}(\sigma_{el}(U) + \sum_l \sigma_{in}^l(U)) f_1(U). \tag{3.15}$$

For i=1,

$$F(f_0, f_1) = -\frac{qE}{3}\sqrt{\frac{2}{m(\frac{U_i + U_i + \Delta U}{2})}} f_1(U_i) - \frac{qE}{3}\sqrt{\frac{2U_i}{m}}\frac{f_1(U_i+\Delta U) - f_1(U_i - \Delta U)}{2\Delta U}$$

$$-\sum_l n\sqrt{\frac{2U_i}{m}}\sigma_{in}^l(U_i) f_0(U_i) + 2n\frac{m}{M}\sqrt{\frac{2}{m(\frac{U_i + U_i + \Delta U}{2})}} \tag{3.48}$$

$$\cdot\frac{((U_i+\Delta U)^2\sigma_{el}(U_i+\Delta U) f_0(U_i+\Delta U) - U_i^2\sigma_{el}(U_i) f_0(U_i))}{\Delta U},$$

$$G(f_0, f_1) = 0, \tag{3.49}$$

For $2 \le i \le num - 1$, one has

$$F(f_0, f_1) = -\frac{qE}{3}\sqrt{\frac{2}{m(\frac{U_i + U_i + \Delta U}{2})}} f_1(U_i) - \frac{qE}{3}\sqrt{\frac{2U_i}{m}}\frac{f_1(U_i+\Delta U) - f_1(U_i - \Delta U)}{2\Delta U}$$

$$-\sum_l n\sqrt{\frac{2U_i}{m}}\sigma_{in}^l(U_i) f_0(U_i) + \sum_l \sqrt{\frac{U_i + U_{in}^l}{U_i}} n\sqrt{\frac{2(U_i+U_{in}^l)}{m}}\sigma_{in}^l(U_i+U_{in}^l) f_0(U_i+U_{in}^l)$$

$$+2n\frac{m}{M}\sqrt{\frac{2}{m(\frac{U_i + U_i + \Delta U}{2})}}\frac{((U_i+\Delta U)^2\sigma_{el}(U_i+\Delta U) f_0(U_i+\Delta U) - U_i^2\sigma_{el}(U_i) f_0(U_i))}{\Delta U},$$

(3.50)

$$G(f_0, f_1) = -qE\sqrt{\frac{2U_i}{m}}\frac{f_0(U_i) - f_0(U_i - \Delta U)}{\Delta U} - n\sqrt{\frac{2U_i}{m}}(\sigma_{el}(U_i) + \sum_i \sigma_{in}^i(U_i))f_1(U_i). \tag{3.51}$$

For $1 \le i \le num - 1$, one gets

$$f_0(U_i, t + \Delta t) = f_0(U_i, t) + \frac{\Delta t}{6} \times (k_1 + 2k_2 + 2k_3 + k_4), \tag{3.52}$$

$$f_1(U_i, t + \Delta t) = f_1(U_i, t) + \frac{\Delta t}{6} \times (l_1 + 2l_2 + 2l_3 + l_4), \tag{3.53}$$

where,

$$k_1 = F(f_0, f_1), \tag{3.54}$$

$$l_1 = G(f_0, f_1), \tag{3.55}$$

$$k_2 = F(f_0 + \frac{\Delta t}{2}k_1, f_1 + \frac{\Delta t}{2}l_1), \tag{3.56}$$

$$l_2 = G(f_0 + \frac{\Delta t}{2}k_1, f_1 + \frac{\Delta t}{2}l_1), \tag{3.57}$$

$$k_3 = F(f_0 + \frac{\Delta t}{2}k_2, f_1 + \frac{\Delta t}{2}l_2), \tag{3.58}$$

$$l_3 = G(f_0 + \frac{\Delta t}{2}k_2, f_1 + \frac{\Delta t}{2}l_2), \tag{3.59}$$

$$k_4 = F(f_0 + \Delta t \cdot k_3, f_1 + \Delta t \cdot l_3), \tag{3.60}$$

and $l_4 = G(f_0 + \Delta t \cdot k_3, f_1 + \Delta t \cdot l_3)$. (3.61)

For i=num,

$$f_0(U_i, t) = 0, \tag{3.62}$$

and $f_1(U_i, t) = 0$. (3.63)

3.6.3 Method Analysis

The Runge-Kutta method in a rough sense is a more sophisticated version of the Euler method. Its updating process changes from updating with each time step *dt* by having several refinements. This effectively implies that the updates are carried out at much smaller time steps, and in a stable manner. Furthermore, this method updates f_0 and f_1 simultaneously, making it more accurate and stable compared to

Euler method. All this can be seen from the results and figures presented in Chapter 4. Although the results still show some differences with respect to published experimental results, the error is much smaller compared to the Euler method. However, this method is still not the fully implicit method and is not fully stable. When it comes to higher order items of distribution functions such as $f_2 \sim f_6$, the program will overflow before it reaches the end and produce unpredictable final results.

3.7 Implicit Time-Dependent Relaxation Method

3.7.1 Introduction

Although time-dependent Runge-Kutta method is much more accurate and stable compared to time-dependent Euler method, it is still not the fully implicit method and is not unconditionally stable. In order to obtain more accurate and stable results, we need to proceed to fully implicit time-dependent method as discussed below. Again, "implicit" here means generating 4-way grid that couples each grid point to its four neighboring grid points in time and energy space. In addition, this scheme couples the distribution functions f_0 and f_1 together in a vector and solving them via a combined time-dependent matrix equation.

3.7.2 Method Description

The partial differential equations (PDEs) are discretized by taking centered differences. These are basically the points $(U_{i+1/2}, t_{k+1/2})$ with $1 \le i \le n_\infty$ and $k \ge 0$ in the mesh. Using a second-order-correct centered difference implementation as:

$$f^n_{i+\frac{1}{2},k+\frac{1}{2}} = \frac{1}{4}(f^n_{i+1,k+1} + f^n_{i,k+1} + f^n_{i+1,k} + f^n_{i,k}), \tag{3.64}$$

$$(\frac{\partial}{\partial t} f_n(U,t))_{i+\frac{1}{2},k+\frac{1}{2}} = \frac{1}{2\Delta t}(f^n_{i+1,k+1} - f^n_{i+1,k} + f^n_{i,k+1} - f^n_{i,k}), \tag{3.65}$$

$$(\frac{\partial}{\partial U} f_n(U,t))_{i+\frac{1}{2},k+\frac{1}{2}} = \frac{1}{2\Delta U}(f^n_{i+1,k+1} - f^n_{i,k+1} + f^n_{i+1,k} - f^n_{i,k}), \tag{3.66}$$

and,

$$U_i = (i-1)\Delta U \quad \Delta U = \frac{U_\infty}{n_\infty} \quad 1 \le i \le n_\infty + 1, \tag{3.67}$$

$$U_{i+1/2} = \frac{U_i + U_{i+1}}{2} = (\frac{i-1+i}{2})\Delta U = (i - \frac{1}{2})\Delta U, \tag{3.68}$$

$$t_k = k\Delta t \quad k \ge 0, \tag{3.69}$$

$$f_{i,k}^n = f_n(U_i, t_k) \quad 0 \le n \le l-1, \tag{3.70}$$

$$f_0(U \ge U_\infty, t) = 0, \tag{3.71}$$

$$f_n(U = 0, t) = 0 \quad \textit{for odd } n \ge 1, \tag{3.72}$$

and, $f_n(U = U_\infty, t) = 0 \quad \textit{for even } n \ge 2.$ (3.73)

The governing equations change to:

$$\left.\frac{\partial f_0}{\partial t}\right|_{i+\frac{1}{2},k+\frac{1}{2}} = \{-\frac{qE}{3}\sqrt{\frac{2}{mU}} f_1(U) - \frac{qE}{3}\sqrt{\frac{2U}{m}}\frac{\partial f_1(U)}{\partial U} - \sum_l n\sqrt{\frac{2U}{m}}\sigma_{in}^l(U) f_0(U) \tag{3.74}$$

$$+ \sum_l \sqrt{\frac{U+U_{in}^l}{U}} n\sqrt{\frac{2(U+U_{in}^l)}{m}}\sigma_{in}^l(U+U_{in}^l) f_0(U+U_{in}^l) + 2n\frac{m}{M}\sqrt{\frac{2}{mU}}$$

$$\cdot\frac{\partial}{\partial U}(U^2\sigma_{el}(U) f_0(U))\}\Big|_{i+\frac{1}{2},k+\frac{1}{2}},$$

$$\left.\frac{\partial f_1}{\partial t}\right|_{i+\frac{1}{2},k+\frac{1}{2}} = \{-qE\sqrt{\frac{2U}{m}}\frac{\partial f_0(U)}{\partial U} - n\sqrt{\frac{2U}{m}}(\sigma_{el}(U) + \sum_l \sigma_{in}^l(U)) f_1(U)\}\Big|_{i+\frac{1}{2},k+\frac{1}{2}}. \tag{3.75}$$

There is a term $f_0(U_{i+1/2} + U_{in}, t_{k+1/2})$ in the above equation. If $U_{i+1/2} + U_{in}$ is not an integer, we calculate this term by computing the mean value of two continuous moments. In this scheme, each moment value is calculated as the mean value of the previous integer and next integer with the coefficients as the distances between this float number and its previous integer as well as next integer. We apply:

$$p = ((i - \frac{1}{2})\Delta U + U_{in})/\Delta U, \tag{3.76}$$

$$p1 = floor(((i - \frac{1}{2})\Delta U + U_{in})/\Delta U), \tag{3.77}$$

$$p2 = ceil(((i - \frac{1}{2})\Delta U + U_{in})/\Delta U) = p1 + 1, \tag{3.78}$$

$$co1 = p - p1, \tag{3.79}$$

and, $co2 = p2 - p.$ (3.80)

For example, if:

$$U_{i+1/2}+U_{in}=18.7\Delta U,\ p=18.7,\ p1=18,\ p2=19,\ co1=0.7,\ co2=0.3,$$

$$f_0(U_{i+1/2}+U_{in},t_{k+1/2})=f_0(18.7\Delta U,t_{k+1/2})=\frac{0.7\cdot f^0_{19,k+1}+0.3\cdot f^0_{18,k+1}+0.7\cdot f^0_{19,k}+0.3\cdot f^0_{18,k}}{2}$$

$$=\frac{co1\cdot f^0_{p2,k+1}+co2\cdot f^0_{p1,k+1}+co1\cdot f^0_{p2,k}+co2\cdot f^0_{p1,k}}{2}. \tag{3.81}$$

According to the notations listed above, we can expand the governing equations to be:

$$\frac{1}{2\Delta t}(f^0_{i+1,k+1}-f^0_{i+1,k}+f^0_{i,k+1}-f^0_{i,k})=-\frac{qE}{3}\sqrt{\frac{2}{mU_{i+1/2}}}\cdot\frac{1}{4}(f^1_{i+1,k+1}+f^1_{i,k+1}+f^1_{i+1,k}+f^1_{i,k})$$

$$-\frac{qE}{3}\sqrt{\frac{2U_{i+1/2}}{m}}\cdot\frac{1}{2\Delta U}(f^1_{i+1,k+1}-f^1_{i,k+1}+f^1_{i+1,k}-f^1_{i,k})-\sum_l n\sqrt{\frac{2U_{i+1/2}}{m}}\sigma^l_{in}(U_{i+1/2})$$

$$\cdot\frac{1}{4}(f^0_{i+1,k+1}+f^0_{i,k+1}+f^0_{i+1,k}+f^0_{i,k})+\sum_l (U_{i+1/2}+U^l_{in})\cdot n\sqrt{\frac{2}{mU_{i+1/2}}}\cdot\sigma^l_{in}(U_{i+1/2}+U^l_{in}) \tag{3.82}$$

$$\cdot\frac{co^l_1\cdot f^0_{p^l_2,k+1}+co^l_2\cdot f^0_{p^l_1,k+1}+co^l_1\cdot f^0_{p^l_2,k}+co^l_2\cdot f^0_{p^l_1,k}}{2}+2n\cdot\frac{m}{M}\cdot\sqrt{\frac{2}{mU_{i+1/2}}}\cdot\frac{1}{2\Delta U}\cdot$$

$$(U^2\sigma_{el}(U)f_0(U)\big|_{i+1,k+1}-U^2\sigma_{el}(U)f_0(U)\big|_{i,k+1}+U^2\sigma_{el}(U)f_0(U)\big|_{i+1,k}-U^2\sigma_{el}(U)f_0(U)\big|_{i,k}),$$

$$\frac{1}{2\Delta t}(f^1_{i+1,k+1}-f^1_{i+1,k}+f^1_{i,k+1}-f^1_{i,k})=-qE\sqrt{\frac{2U_{i+1/2}}{m}}\cdot\frac{1}{2\Delta U}\cdot(f^0_{i+1,k+1}-f^0_{i,k+1}+f^0_{i+1,k}-f^0_{i,k})$$

$$-n\sqrt{\frac{2U_{i+1/2}}{m}}(\sigma_m(U_{i+1/2})+\sum_l \sigma^l_{in}(U_{i+1/2}))\cdot\frac{1}{4}(f^1_{i+1,k+1}+f^1_{i,k+1}+f^1_{i+1,k}+f^1_{i,k}). \tag{3.83}$$

Next we will rearrange the terms on both sides. We put all the $k+1$ terms on the left hand side and move all the k terms to the right hand side. Since k indicates time, that means all the items on the left hand side are items related with one more time step than the right hand side. Then we can obtain the updating equations related with time to be:

$$\frac{1}{2\Delta t}(f^0_{i+1,k+1}+f^0_{i,k+1})+\frac{qE}{3}\sqrt{\frac{2}{mU_{i+1/2}}}\cdot\frac{1}{4}f^1_{i+1,k+1}+\frac{qE}{3}\sqrt{\frac{2}{mU_{i+1/2}}}\cdot\frac{1}{4}f^1_{i,k+1}+\frac{qE}{3}\sqrt{\frac{2U_{i+1/2}}{m}}\cdot\frac{1}{2\Delta U}\cdot f^1_{i+1,k+1}$$
$$-\frac{qE}{3}\sqrt{\frac{2U_{i+1/2}}{m}}\cdot\frac{1}{2\Delta U}\cdot f^1_{i,k+1}+\sum_l n\cdot\sqrt{\frac{2U_{i+1/2}}{m}}\sigma^l_{in}(U_{i+1/2})\cdot\frac{1}{4}f^0_{i+1,k+1}+\sum_l n\cdot\sqrt{\frac{2U_{i+1/2}}{m}}\sigma^l_{in}(U_{i+1/2})\cdot$$
$$\frac{1}{4}f^0_{i,k+1}-\sum_l (U_{i+1/2}+U^l_{in})\cdot n\cdot\sqrt{\frac{2}{mU_{i+1/2}}}\cdot\sigma^l_{in}(U_{i+1/2}+U^l_{in})\cdot\frac{co^l_1}{2}\cdot f^0_{p^l_1+1,k+1}-\sum_l (U_{i+1/2}+U^l_{in})\cdot n\cdot$$
$$\sqrt{\frac{2}{mU_{i+1/2}}}\cdot\sigma^l_{in}(U_{i+1/2}+U^l_{in})\cdot\frac{co^l_2}{2}\cdot f^0_{p^l_2,k+1}-2n\cdot\frac{m}{M}\cdot\sqrt{\frac{2}{mU_{i+1/2}}}\cdot\frac{1}{2\Delta U}\cdot U^2_{i+1}\sigma_{el}(U_{i+1})\cdot f^0_{i+1,k+1}+2n\cdot\frac{m}{M}$$
$$\cdot\sqrt{\frac{2}{mU_{i+1/2}}}\cdot\frac{1}{2\Delta U}\cdot U^2_i\sigma_{el}(U_i)f^0_{i,k+1}=\frac{1}{2\Delta t}(f^0_{i+1,k}+f^0_{i,k})-\frac{qE}{3}\sqrt{\frac{2}{mU_{i+1/2}}}\cdot\frac{1}{4}(f^1_{i+1,k}+f^1_{i,k})-\frac{qE}{3}\sqrt{\frac{2U_{i+1/2}}{m}}$$
$$\cdot\frac{1}{2\Delta U}\cdot(f^1_{i+1,k}-f^1_{i,k})-\sum_l n\sqrt{\frac{2U_{i+1/2}}{m}}\sigma^l_{in}(U_{i+1/2})\cdot\frac{1}{4}(f^0_{i+1,k}+f^0_{i,k})+\sum_l (U_{i+1/2}+U^l_{in})\cdot n\cdot\sqrt{\frac{2}{mU_{i+1/2}}}$$
$$\sigma^l_{in}(U_{i+1/2}+U^l_{in})\cdot\frac{co^l_1\cdot f^0_{p^l_1+1,k}+co^l_2\cdot f^0_{p^l_2,k}}{2}+2n\cdot\frac{m}{M}\sqrt{\frac{2}{mU_{i+1/2}}}\frac{1}{2\Delta U}$$
$$\cdot(U^2_{i+1}\sigma_{el}(U_{i+1})f^0_{i+1,k}-U^2_i\sigma_{el}(U_i)f^0_{i,k}), \tag{3.84}$$

$$\frac{1}{2\Delta t}(f^1_{i+1,k+1}+f^1_{i,k+1})+qE\sqrt{\frac{2U_{i+1/2}}{m}}\cdot\frac{1}{2\Delta U}(f^0_{i+1,k+1}-f^0_{i,k+1})+n\sqrt{\frac{2U_{i+1/2}}{m}}(\sigma_{el}(U_{i+1/2})$$
$$+\sum_l \sigma^l_{in}(U_{i+1/2}))\cdot\frac{1}{4}(f^1_{i+1,k+1}+f^1_{i,k+1})=\frac{1}{2\Delta t}(f^1_{i+1,k}+f^1_{i,k})-qE\sqrt{\frac{2U_{i+1/2}}{m}}\cdot\frac{1}{2\Delta U}(f^0_{i+1,k}-f^0_{i,k})$$
$$-n\sqrt{\frac{2U_{i+1/2}}{m}}(\sigma_{el}(U_{i+1/2})+\sum_l \sigma^l_{in}(U_{i+1/2}))\cdot\frac{1}{4}(f^1_{i+1,k}+f^1_{i,k}). \tag{3.85}$$

Combining similar terms on the left hand side, we get 10 coefficients corresponding to the 10 different distribution function terms on the left hand side. For simplicity, these 10 coefficients are assigned the following notations:

$$T1=\frac{1}{2\Delta t}+\sum_l n\sqrt{\frac{2U_{i+1/2}}{m}}\sigma^l_{in}(U_{i+1/2})\cdot\frac{1}{4}+2n\cdot\frac{m}{M}\cdot\sqrt{\frac{2}{mU_{i+1/2}}}\frac{1}{2\Delta U}U^2_i\sigma_{el}(U_i), \tag{3.86}$$

$$T2=\frac{1}{2\Delta t}+\sum_l n\sqrt{\frac{2U_{i+1/2}}{m}}\sigma^l_{in}(U_{i+1/2})\cdot\frac{1}{4}-2n\cdot\frac{m}{M}\cdot\sqrt{\frac{2}{mU_{i+1/2}}}\frac{1}{2\Delta U}U^2_{i+1}\sigma_{el}(U_{i+1}), \tag{3.87}$$

$$T3=\frac{qE}{3}\sqrt{\frac{2}{mU_{i+1/2}}}\cdot\frac{1}{4}-\frac{qE}{3}\sqrt{\frac{2U_{i+1/2}}{m}}\cdot\frac{1}{2\Delta U}, \tag{3.88}$$

$$T4=\frac{qE}{3}\sqrt{\frac{2}{mU_{i+1/2}}}\cdot\frac{1}{4}+\frac{qE}{3}\sqrt{\frac{2U_{i+1/2}}{m}}\cdot\frac{1}{2\Delta U}, \tag{3.89}$$

$1\le l\le in\_num$:

$$T_5^l = -(U_{i+1/2} + U_{in}^l) \cdot n \cdot \sqrt{\frac{2}{mU_{i+1/2}}} \sigma_{in}^l (U_{i+1/2} + U_{in}^l) \cdot \frac{co_2^l}{2}, \tag{3.90}$$

$$T_6^l = -(U_{i+1/2} + U_{in}^l) \cdot n \cdot \sqrt{\frac{2}{mU_{i+1/2}}} \sigma_{in}^l (U_{i+1/2} + U_{in}^l) \cdot \frac{co_1^l}{2}, \tag{3.91}$$

$$T7 = -qE \sqrt{\frac{2U_{i+1/2}}{m}} \frac{1}{2\Delta U}, \tag{3.92}$$

$$T8 = qE \sqrt{\frac{2U_{i+1/2}}{m}} \frac{1}{2\Delta U}, \tag{3.93}$$

$$T9 = \frac{1}{2\Delta t} + n \sqrt{\frac{2U_{i+1/2}}{m}} (\sigma_{el}(U_{i+1/2}) + \sum_l \sigma_{in}^l (U_{i+1/2})) \cdot \frac{1}{4}, \tag{3.94}$$

and, $$T10 = \frac{1}{2\Delta t} + n \sqrt{\frac{2U_{i+1/2}}{m}} (\sigma_{el}(U_{i+1/2}) + \sum_l \sigma_{in}^l (U_{i+1/2})) \cdot \frac{1}{4} = T9. \tag{3.95}$$

Finally, denoting the right hand side of these equations to be "Equation (a)" and "Equation (b)", yields:

$$(a) = \frac{1}{2\Delta t}(f_{i+1,k}^0 + f_{i,k}^0) - \frac{qE}{3}\sqrt{\frac{2}{mU_{i+1/2}}} \cdot \frac{1}{4}(f_{i+1,k}^1 + f_{i,k}^1) - \frac{qE}{3}\sqrt{\frac{2U_{i+1/2}}{m}} \frac{1}{2\Delta U}(f_{i+1,k}^1 - f_{i,k}^1)$$
$$- \sum_l n \sqrt{\frac{2U_{i+1/2}}{m}} \sigma_{in}^l (U_{i+1/2}) \cdot \frac{1}{4}(f_{i+1,k}^0 + f_{i,k}^0) + \sum_l (U_{i+1/2} + U_{in}^l) \cdot n \cdot \sqrt{\frac{2}{mU_{i+1/2}}} \sigma_{in}^l (U_{i+1/2} + U_{in}^l)$$
$$\cdot \frac{co_1^l \cdot f_{p_1^l+1,k}^0 + co_2^l \cdot f_{p_1^l,k}^0}{2} + 2n \cdot \frac{m}{M} \cdot \sqrt{\frac{2}{mU_{i+1/2}}} \cdot \frac{1}{2\Delta U}(U_{i+1}^2 \sigma_{el}(U_{i+1}) f_{i+1,k}^0 - U_i^2 \sigma_{el}(U_i) f_{i,k}^0), \tag{3.96}$$

$$(b) = \frac{1}{2\Delta t}(f_{i+1,k}^1 + f_{i,k}^1) - qE\sqrt{\frac{2U_{i+1/2}}{m}} \cdot \frac{1}{2\Delta U}(f_{i+1,k}^0 - f_{i,k}^0) - n\sqrt{\frac{2U_{i+1/2}}{m}}(\sigma_{el}(U_{i+1/2}) + \sum_l \sigma_{in}^l (U_{i+1/2}))$$
$$\cdot \frac{1}{4}(f_{i+1,k}^1 + f_{i,k}^1). \tag{3.97}$$

Therefore, we can create a matrix multiplication as:

$$\begin{pmatrix} T1 & T2 & \cdots & T_5^l & T_6^l & \cdots & 0 & T3 & T4 & \cdots & & 0 \\ 0 & T1 & T2 & \cdots & T_5^l & T_6^l & \cdots & 0 & 0 & T3 & T4 & \cdots & 0 \\ & & & \vdots & & & & & & \vdots & & & \\ 0 & 0 & & \cdots & & \cdots & & 1 & 0 & 0 & \cdots & & 0 \\ 0 & 0 & \cdots & & & \cdots & & 0 & 1 & 0 & \cdots & \cdots & 0 \\ T7 & T8 & & \cdots & & & & 0 & T9 & T10 & & \cdots & 0 \\ 0 & T7 & T8 & & \cdots & & & 0 & 0 & T9 & T10 & \cdots & 0 \\ \vdots & & & \vdots & & \vdots & & & & \vdots & & \vdots & \vdots \end{pmatrix} \times \begin{pmatrix} f_{1,k+1}^0 \\ f_{2,k+1}^0 \\ f_{3,k+1}^0 \\ \vdots \\ f_{n,k+1}^0 \\ f_{1,k+1}^1 \\ f_{2,k+1}^1 \\ f_{3,k+1}^1 \\ \vdots \\ f_{n,k+1}^1 \end{pmatrix} = \begin{pmatrix} \vdots \\ Eq(a) \\ \vdots \\ 0 \\ 0 \\ \vdots \\ Eq(b) \\ \vdots \end{pmatrix}. \tag{3.98}$$

Using the following notation:

$$A = \begin{pmatrix} T1 & T2 & \cdots & T_5^l & T_6^l & \cdots & 0 \\ 0 & T1 & T2 & \cdots & T_5^l & T_6^l & \cdots & 0 \\ & & & \vdots & \vdots & & \\ 0 & 0 & & \cdots & \cdots & & 1 \end{pmatrix}_{num \times num}. \tag{3.99}$$

For $1 \le i \le num-1$, $1 \le l \le in\_num$, and $p_1^l + 1 \le num$,

$$A(i,i) = T1, \tag{3.100}$$

$$A(i,i+1) = T2, \tag{3.101}$$

$$A(i, p_1^l) = T_5^l, \tag{3.102}$$

$$A(i, p_1^l + 1) = T_6^l, \tag{3.103}$$

$$A(num, num) = 1, \quad \text{and} \tag{3.104}$$

$$B = \begin{pmatrix} T3 & T4 & \cdots & 0 \\ 0 & T3 & T4 & \cdots & 0 \\ & \vdots & & \vdots & \\ 0 & 0 & \cdots & & 0 \end{pmatrix}_{num \times num}. \tag{3.105}$$

For $1 \le i \le num-1$,

$$B(i,i) = T3, \tag{3.106}$$

$$B(i,i+1) = T4, \quad \text{and} \tag{3.107}$$

$$C = \begin{pmatrix} 0 & 0 & \cdots & \cdots & 0 \\ T7 & T8 & \cdots & \cdots & 0 \\ 0 & T7 & T8 & \cdots & 0 \\ \vdots & & & \vdots & \end{pmatrix}_{num \times num} . \tag{3.108}$$

For $2 \le i \le num$,

$$C(i,i-1) = T7, \tag{3.109}$$

$$C(i,i) = T8, \quad \text{and} \tag{3.110}$$

$$D = \begin{pmatrix} 1 & 0 & \cdots & \cdots & 0 \\ T9 & T10 & \cdots & \cdots & 0 \\ 0 & T9 & T10 & \cdots & 0 \\ \vdots & & \vdots & & \end{pmatrix}_{num \times num} . \tag{3.111}$$

For $2 \le i \le num$,

$$D(i,i-1) = T9, \tag{3.112}$$

$$D(i,i) = T10, \tag{3.113}$$

$$D(1,1) = 1. \tag{3.114}$$

We can rewrite the first matrix in the left hand side in Equation (3.98) as

$$G = \begin{pmatrix} A & B \\ C & D \end{pmatrix}_{2num \times 2num}, \tag{3.115}$$

$$X = \begin{pmatrix} f_{1,k+1}^0 \\ f_{2,k+1}^0 \\ f_{3,k+1}^0 \\ \vdots \\ f_{n,k+1}^0 \\ f_{1,k+1}^1 \\ f_{2,k+1}^1 \\ f_{3,k+1}^1 \\ \vdots \\ f_{n,k+1}^1 \end{pmatrix}_{2num \times 1}, \quad \text{and} \tag{3.116}$$

$$E=\begin{pmatrix} \vdots \\ Eq(a) \\ \vdots \\ 0 \\ 0 \\ \vdots \\ Eq(b) \\ \vdots \end{pmatrix}_{2num\times 1} . \tag{3.117}$$

The principle for matrix multiplication is still the same as the implicit time-independent method. Thus, in short:

$$G \times X = E, \tag{3.27}$$

$$P = inv(G), \tag{3.28}$$

and, $X = P \times E.$ (3.29)

Updated energy distribution functions f_0 and f_1 are stored in the array X. The updating process repeats until steady state is reached and drift velocity does not change with any of the time steps.

3.7.3 Method Analysis

This implicit time-dependent relaxation method is based upon generating 4-way grid to compute each term in the equation as the average value of four neighboring grid points in time and energy. This 4-way grid successfully overcomes the problem when $U_i = 0$ occurs at the denominator and applies the most accurate average value for each term in the equation. So this method prevents an error accumulation at the first energy point. Moreover, this method is fully implicit and updates f_0 and f_1 at the same time. Therefore, this method is stable, and can produce regular results with large electrical field values or a long period of time, particularly with higher order terms of distribution functions such as $f_2 \sim f_6$. Moreover, this method is the most accurate method among all the numerical methods discussed in this chapter. There is only one limitation for this method. Since this method is based upon matrix multiplication and was implemented in MATLAB, the program has a natural limit for the matrix size. This

will lead to the limit for U_{max} if we keep the energy step ΔU not changed. If we want to carry out simulation for large energy values U_{max}, then the energy step ΔU will also need to be large given the matrix size. This will cause the output curves for energy distribution functions to be less accurate and smooth. However, this is a practical difficulty, and not an inherent problem with the method.

3.8 Townsend's First Ionization Coefficient in Nitrogen

The ionization coefficient α is the mean number of ionizations per unit length (cm) in the direction of the field produced by electron collisions. The formula for computing the ionization coefficient α is:

$$\alpha = n \cdot \frac{\int \sigma_{ionization}(U) \cdot f(U) dU}{\int f(U) dU}. \tag{3.118}$$

n is the gas density and $\sigma_{ionization}(U)$ is the cross section for ionization scattering process. This coefficient is a measure of electrons that could be produced by an initial primary electron during its transit in a gas device. It is also a measure of the possibility for ionization and charge multiplication within the device at a given voltage. The ionization coefficient α is a function of reduced electric field strength and is expressed mathematically in the form:

$$\alpha / p = f(E / p), \tag{3.119}$$

where E is the electric field strength (usually measured in volts per cm) and p is the pressure (usually in mm of mercury) [32,33]. This coefficient is a very important parameter to be estimated in predicting the high-field physics and charge creation within the environment.

Let's compute Townsend's first ionization coefficient α in the form of α / p at different E / p values with the implicit time-dependent relaxation method and compare our results with published experimental results. The comparisons will further validate the simulation method as well as our code implementation.

CHAPTER 4

COMPUTATIONAL RESULTS AND DISCUSSION

4.1 Introduction

The numerical methods introduced in Chapter 3 are the implicit time-independent method, the time-dependent Euler method, the time-dependent Runge-Kutta method, and finally the implicit time-dependent relaxation method that involves generating the 4-way grid and solving a corresponding matrix equation.

The formulas described in Chapter 3 were strictly followed and numerical methods were implemented via the MATLAB software tool, with 29 inelastic scatterings included for nitrogen gas. Simulations for many different E/N values were carried out and the obtained drift velocity values were compared to the experimental results available in the published literature [34-36]. The energy distribution functions obtained are presented in both two-dimensional (2D) and three-dimensional (3D) formats. When presented as 2D plots, both normal and semi-logarithmic energy distribution functions are given at four different time instants as a function of electron energy. The 3D plots show the distribution as functions of both energy and time. Another important plot in this chapter shows the comparison of results between the steady-state drift velocity values obtained from the simulations, and the published experimental results for different E/N values. The numerical simulation results are observed to match a number of experimental data on electron drift velocity values in nitrogen. This provides an excellent validation of our method and its numerical implementation. Moreover, the Townsend Ionization Coefficient plot also shows our simulation results are in good agreement with published experimental results for nitrogen. This provides further validation of our method and its numerical implementation. The Townsend Ionization Coefficient is an important parameter for charge multiplication via electronic impact, and becomes important for practical predictions of plasma processing.

4.2 Simulation Results for Implicit Time-Independent Method

4.2.1 Parameter List of Simulation Control Variables

Table 4.1 gives the values of material parameters considered in the simulation. The pressure was fixed during the simulation process while the electrical field was changed to step through a set of 13 different E/N values. Since these sets of results being discussed first are for the implicit time-independent simulations, no time step and simulation time were considered here. The applied cross sections were elastic scattering and the 29 inelastic scatterings introduced in Chapter 2.

Table 4.1 Parameter List of Simulation Control Variables for the Implicit Time-Independent Method.

Parameter	Value (Units)
Temperature	300 K
Pressure	0.01 atmosphere
Electrical field	$0.12667\times10^{5}\sim1.22584\times10^{5}V/m$
Maximum energy	10^{4} eV
Number of energy intervals	10^{3}
Cross Sections	Elastic scattering plus 29 inelastic scatterings

4.2.2 Drift Velocity Values

The drift velocity values obtained with the implicit time-independent method corresponding to those 13 different E/N values are given in Table 4.2. These drift velocity values are compared to experimental and theoretical results reported in the literature by other investigators in the following Figure 4.1.

Table 4.2 Drift Velocity Values of Electrons in Nitrogen Gas as a Function of E/N Obtained with Implicit Time-Independent Method.

Number	E/N (Td)	Drift Velocity (W) in Nitrogen (10^5 m/s)
1	51.7561989	0.4931
2	103.512398	0.9939
3	155.268585	1.5102
4	177.449814	1.7381
5	200.346573	1.9786
6	238.874756	2.3971
7	270.032318	2.7502
8	310.537170	3.2321
9	354.899628	3.7936
10	378.703888	4.1108
11	443.624542	5.0366
12	465.805756	5.3733
13	500.866425	5.9243

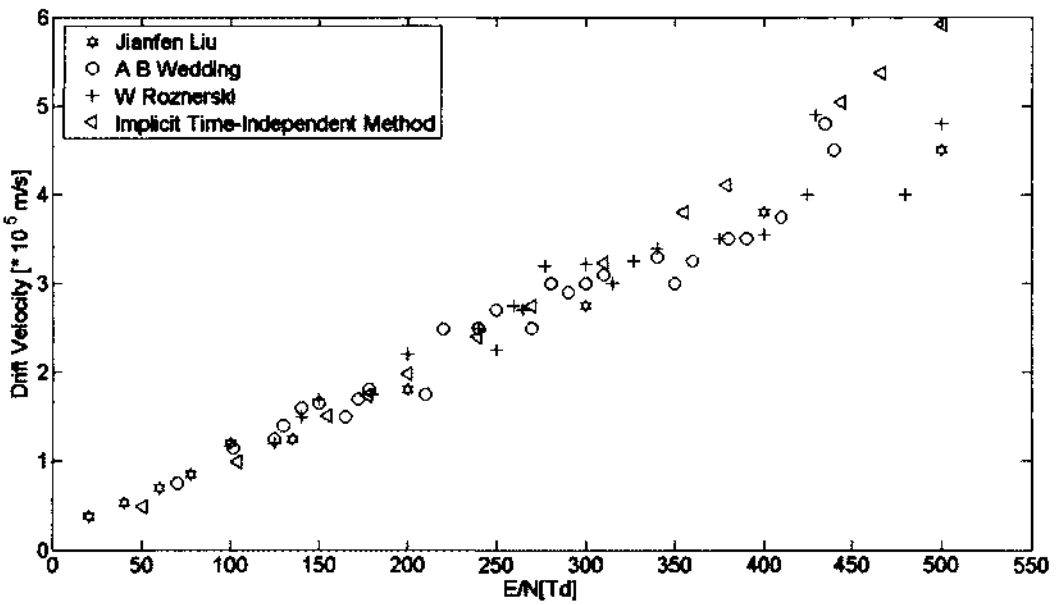

Figure 4.1 Comparison of Drift Velocities of Electrons in Nitrogen Gas Obtained at Different E/N Values with the Implicit Time-Independent Method and Experimental Data.

The drift velocity values obtained with implicit time-independent method are compared with the experimental and theoretical results reported in the literature by

other investigators such as A. B. Wedding [34], W. Roznerski [35] and Jianfen Liu [36]. Figure 4.1 shows that the drift velocity values of electrons in nitrogen obtained from implicit time-independent method are in excellent agreement with experimental results by other investigators when E/N<400 Td. However, when E/N>400 Td, the drift velocity values are quite different from the other investigators' results. Energy distribution functions will be examined in the next section to determine the potential reasons for this discrepancy.

4.2.3 Two-Dimensional Energy Distribution Functions

Next, four plots for the 2D energy distribution functions f_0 and f_1 evaluated under one low and one high E/N value are presented.

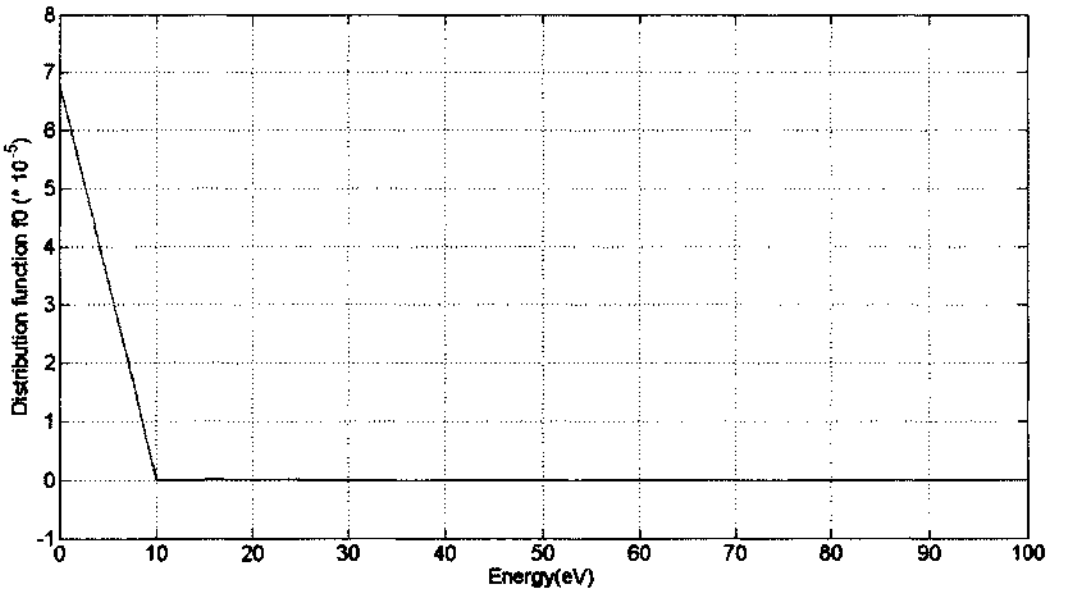

(a) Energy Distribution Function f_0 when E/N=51.7561989 Td.

Figure 4.2 Energy Distribution Functions Obtained with Implicit Time-Independent Method.

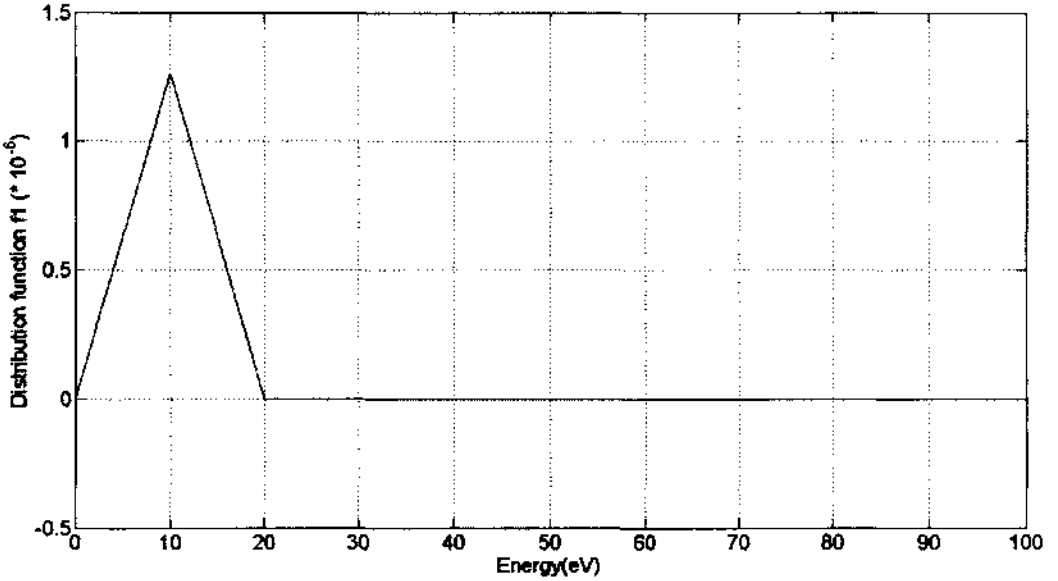

(b) Energy Distribution Function f_1 when E/N=51.7561989 Td.

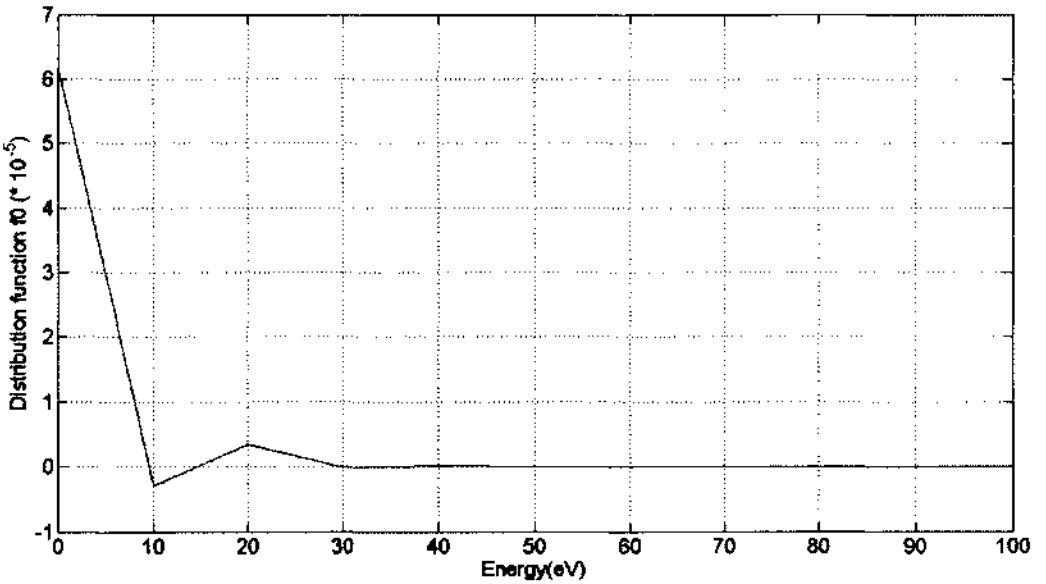

(c) Energy Distribution Function f_0 when E/N=500.866425 Td.

Figure 4.2 (Continued)

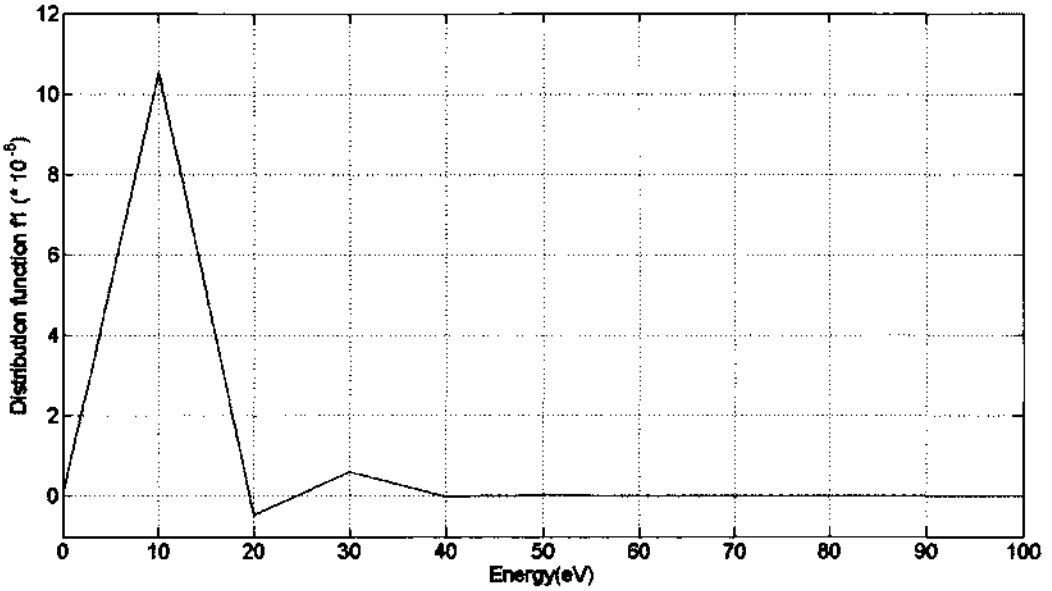

(d) Energy Distribution Function f_1 when E/N=500.866425 Td.

Figure 4.2 (Continued)

This implicit time-independent method estimates drift velocity as well as energy distribution functions without computing the updating values at each time step. Therefore, it is the fastest way to obtain those parameters. Since this is just an approximate estimate and only gives us a rough view for both drift velocity and energy distribution functions, one usually desires the fastest implementation possible. Therefore, one typically sets a large energy step for a fast numerical implementation. Hence, the obtained distribution functions are also with a large energy step as shown in Figure 4.2. As a result, the curves of f_0 and f_1 are not smooth and not very accurate either since it omits many intermediate energy values.

Furthermore, from Figure 4.1(a) and 4.1(b), we find that when E/N<400 Td, the curves for energy distribution functions are still regular and acceptable. However, when E/N>400 Td which are shown in Figure 4.1(c) and 4.1(d), there is an area where the curves for energy distribution functions become negative. At steady state (and when one computes the drift velocity), the distribution functions contained in (3.44) cannot be negative. That explains our reasoning behind the assessment that for

E/N>400 Td, the results are not very good and should not be matched to the experiment data.

Therefore, this method can serve at best, as a quick method for estimating drift velocity values and energy distribution functions, especially for low E/N values. If we want to proceed to obtain accurate drift velocity values and energy distribution functions, we need to follow the time-dependent methods discussed next.

4.3 Simulation Results for Time-Dependent Euler Method

4.3.1 Parameter List of Simulation Control Variables

Table 4.3 gives the values of material parameters considered in this simulation. The pressure was fixed during the simulation process while the electrical field was changed to attain eight different E/N values. Since this is a time-dependent method, different time steps are tested to produce reasonable results. Finally, based on the results obtained, it becomes evident that if and only if the time step is reduced down to $5\times10^{-7} ns$, with electrical fields below the E/N<270.0323 Td threshold, can acceptable and reasonable results be produced. Thus, in this case, two constraints are needed: (i) The E/N values have to be below a threshold level, and (ii) the time-step has to be sufficiently small. The applied cross sections are elastic scattering and 29 inelastic scatterings introduced in Chapter 2.

Table 4.3 Parameter List of Simulation Control Variables for the Time-Dependent Euler Method.

Parameter	Value(Units)
Temperature	300 K
Pressure	0.25 atmosphere
Electric field	$3.1668\times10^{5} \sim 3.0646\times10^{6} V/m$
Maximum energy	50 eV
Number of energy points	2000
Time Step	$5\times10^{-7} ns$
Total time of Simulation	$0.2ns$
Cross Sections	Elastic scattering plus 29 inelastic scatterings

4.3.2 Drift Velocity Values

Here the drift velocity values are obtained corresponding to the same eight E/N values that will be used for the time-dependent Runge-Kutta method. These drift velocity values are also compared to experimental and theoretical results reported in the literature by other investigators.

Table 4.4 Drift Velocity Values of Electrons in Nitrogen Gas as a Function of E/N Obtained with the Time-Dependent Euler Method.

Number	E/N(Td)	Drift Velocity(W) in Nitrogen (10^5 m/s)
1	51.7561989	0.32967
2	103.512398	0.46836
3	155.268585	0.84625
4	200.346573	2.7601
5	270.032318	NaN
6	354.899628	NaN
7	443.624542	NaN
8	500.866425	NaN

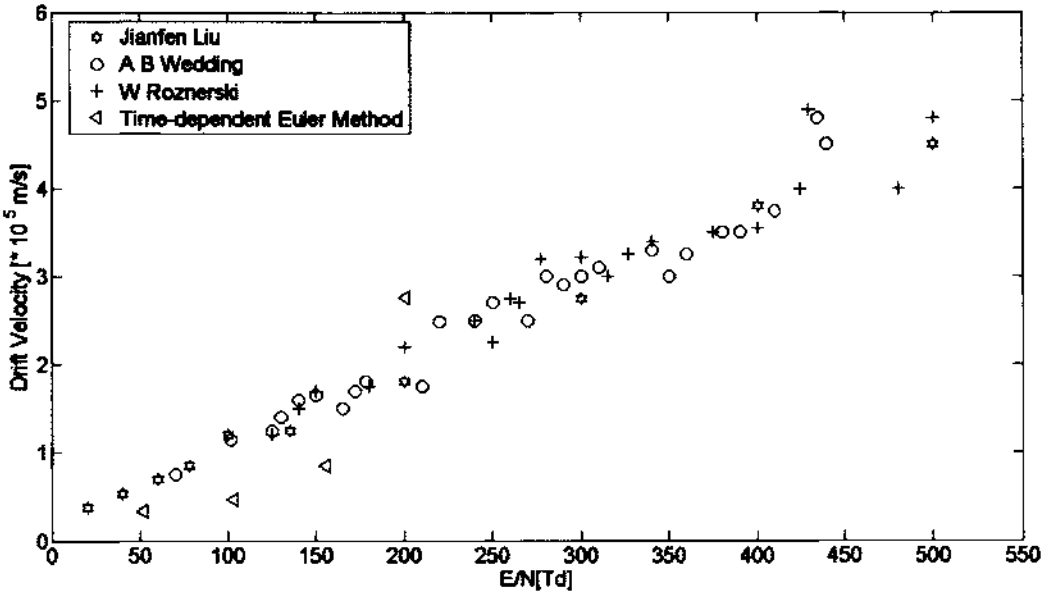

Figure 4.3 Comparison of Drift Velocities of Electrons in Nitrogen Gas Obtained at Different E/N Values with the Time-Dependent Euler Method and Experimental Data.

As can be seen from Table 4.4, when E/N<200 Td, time-dependent Euler method will generally produce results which are not quite different from those obtained by other investigators. This shows that this time-dependent method is still an effective time-dependent method to solve the partial differential equations (PDEs) when E/N is quite small. These results are also not quite different from those obtained by time-dependent Runge-Kutta method either which are shown later in Table 4.5. Thus this shows that in some sense the time-dependent Euler and time-dependent Runge-Kutta method have some features and characteristics that are similar. However, as analyzed in Chapter 3, since this method updates f_1 and f_0 in sequential order rather than simultaneously and is a fully explicit numerical method, the primary feature for this method is still the instability issue. When it comes to large E/N values, results cannot be obtained by this method, and unpredictable values are produced as listed in Table 4.4.

4.4 Simulation Results for Time-Dependent Runge-Kutta Method

4.4.1 Parameter List of Simulation Control Variables

Table 4.5 gives the values of material parameters considered in this simulation. The pressure was fixed during the simulation process while the electrical field was changed to take on eight different E/N values. Since this is time-dependent method, different time steps are tested to produce reasonable results. The final result was that only when the time step was reduced below $10^{-6} ns$ did the code under all the different E/N values produce acceptable and reasonable results. The applied cross sections are elastic scattering and 29 inelastic scatterings given in Chapter 2.

Table 4.5 Parameter List of Simulation Control Variables for the Time-dependent Runge-Kutta method.

Parameter	Value(Units)
Temperature	300 K
Pressure	0.25 atmosphere
Electric field	$3.1668\times10^{5} \sim 3.0646\times10^{6} V/m$
Maximum energy	50 eV
Number of energy gaps	2000
Time Step	$10^{-6} ns$
Time of Simulation	$0.2ns$
Cross Sections	Elastic scattering plus 29 inelastic scatterings

4.4.2 Drift Velocity Values

The drift velocity values obtained corresponding to eight different E/N values with the time-dependent Runge-Kutta method are given in Figure 4.4. These can be compared to the drift velocity values obtained experimentally and from other theoretical simulations reported in the literature by other investigators.

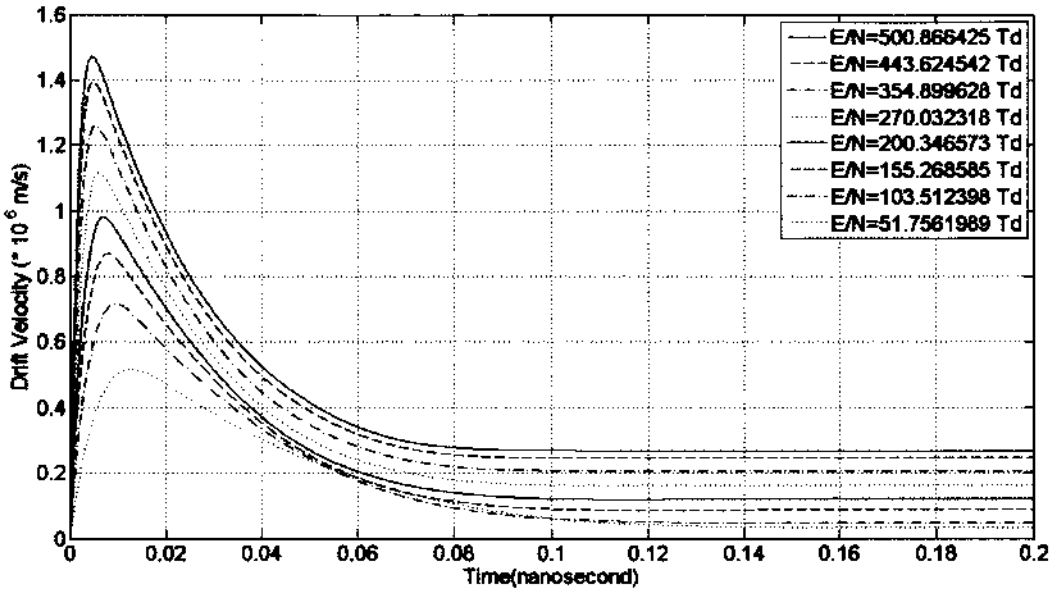

Figure 4.4 Drift Velocities of Electrons in Nitrogen Gas Obtained at Different E/N Values with the Time-Dependent Runge-Kutta Method.

Figure 4.4 combines all the drift velocity curves corresponding to different E/N values. The curves from the highest to lowest correspond to the E/N values from the highest to lowest listed in the upper right corner of the plot. The drift velocity data in Table 4.6 was obtained from Figure 4.4. This drift velocity figure shows that the program runs to steady state under each E/N value which proves that the energy distribution functions obtained are those under steady state and the time-dependent Runge-Kutta method is an effective numerical method in solving the PDEs.

Table 4.6 Drift Velocity Values of Electrons in Nitrogen Gas as a Function of E/N Obtained with the Time-Dependent Runge-Kutta Method.

Number	E/N (Td)	Drift Velocity(W) in Nitrogen (10^5 m/s)
1	51.7561989	0.33746
2	103.512398	0.49003
3	155.268585	0.90049
4	200.346573	1.2148
5	270.032318	1.6331
6	354.899628	2.0665
7	443.624542	2.4592
8	500.866425	2.6871

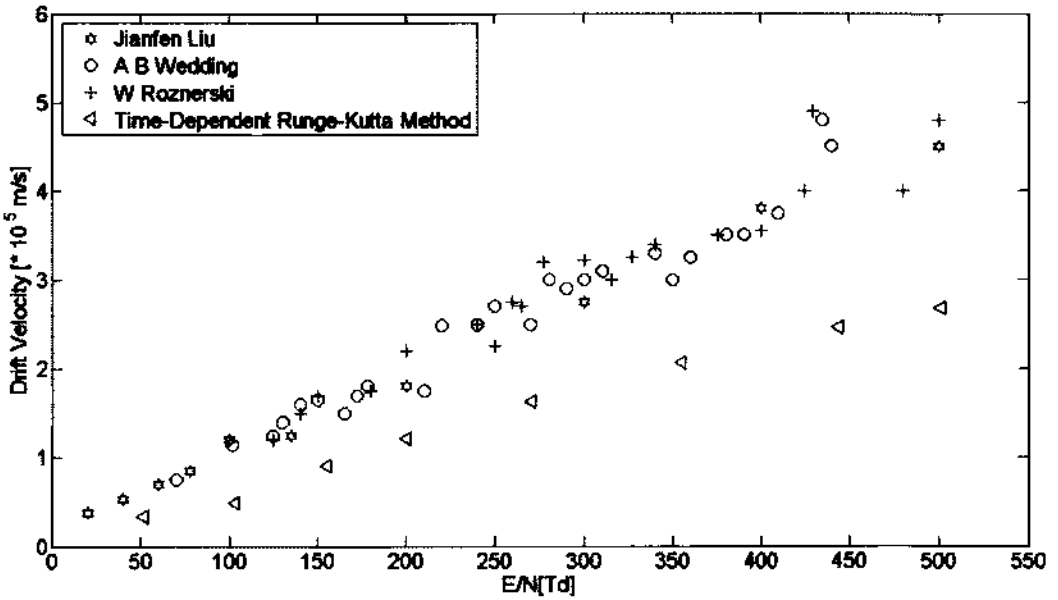

Figure 4.5 Comparison of Drift Velocities of Electrons in Nitrogen Gas Obtained at Different E/N Values with the Time-Dependent Runge-Kutta Method and Experimental Data.

The drift velocity values obtained with the implicit time-dependent Runge-Kutta method were compared to the experimental and theoretical results reported in the literature by other investigators such as A. B. Wedding [34], W. Roznerski [35] and Jianfen Liu [36]. Figure 4.5 shows that the obtained drift velocity values of electrons in nitrogen gas with time-dependent Runge-Kutta method has the same general trend and is not much different from the published experimental results.

As analyzed in Chapter 3, time-dependent Runge-Kutta method updates with much smaller time steps and more importantly, updates both f_1 and f_0 simultaneously. As a result, the Runge-Kutta method improves both the accuracy and stability considerably as compared to the time-dependent Euler method. Therefore, time-dependent Runge-Kutta method works for all the E/N values and is never seen to overflow before it reaches steady state. The drift velocity values obtained have the same general trend as that of the experimental data. This essentially validates the implementation of this time-dependent Runge-Kutta method. Since it is not a fully implicit method and always has a small step accumulation error, the results are not

perfectly matched with the results of the other investigators, and still show some minor differences with most of the experiment data. In order to improve these differences, we need to proceed to a fully implicit method such as the implicit time-dependent relaxation method.

4.4.3 Two-Dimensional and Three-Dimensional Energy Distribution Functions

Since all the simulations under different E/N values run to steady state, we can present 2D normal and semi-logarithmic energy distribution functions at four different time instants, as well as 3D distribution functions with an additional time axis for each E/N value. Because of the space, only two groups of figures under one low and one high E/N value are shown to verify the ability of this time-dependent Runge-Kutta method to produce regular distribution functions with all ranges of E/N values.

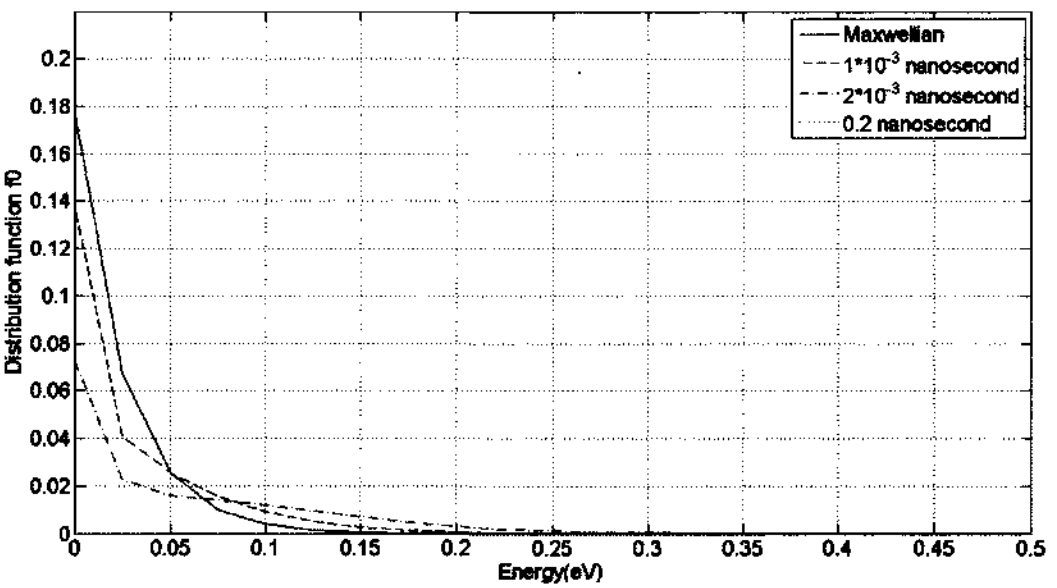

(a) 2D Normal Energy Distribution Function f_0.

Figure 4.6 Two-Dimensional (2D) and Three-Dimensional (3D) Energy Distribution Function Plots Obtained with Time-Dependent Runge-Kutta Method when E/N=103.5123 Td.

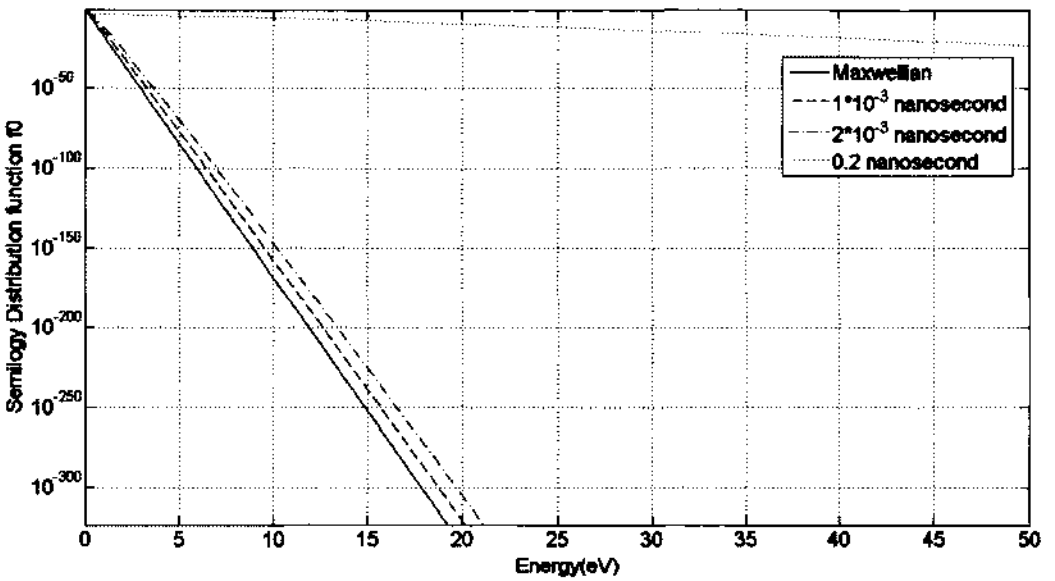

(b) 2D Semi-Logarithmic Energy Distribution Function f_0.

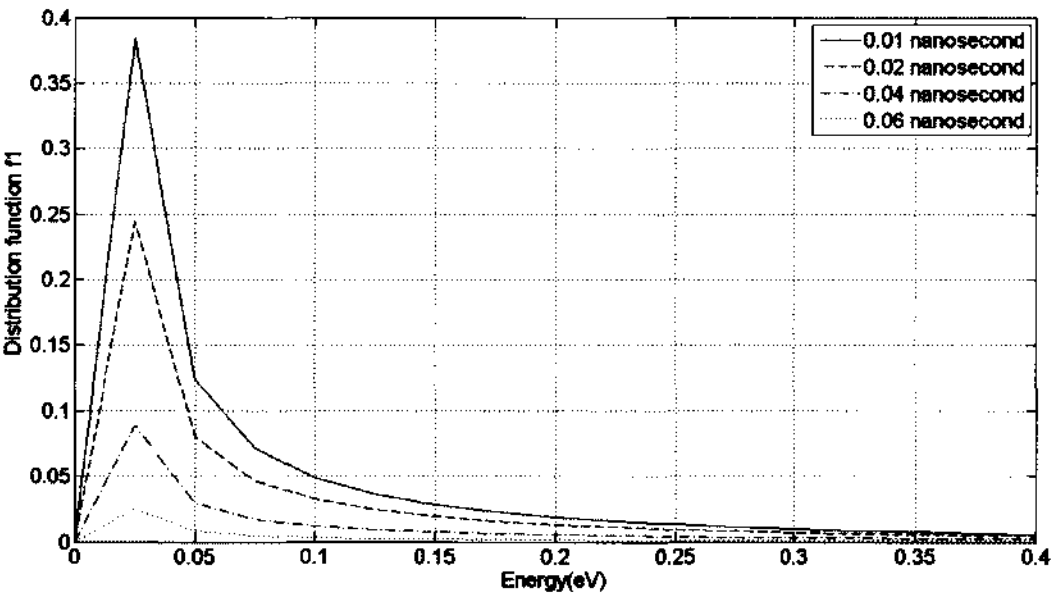

(c) 2D Normal Energy Distribution Function f_1.

Figure 4.6 (Continued)

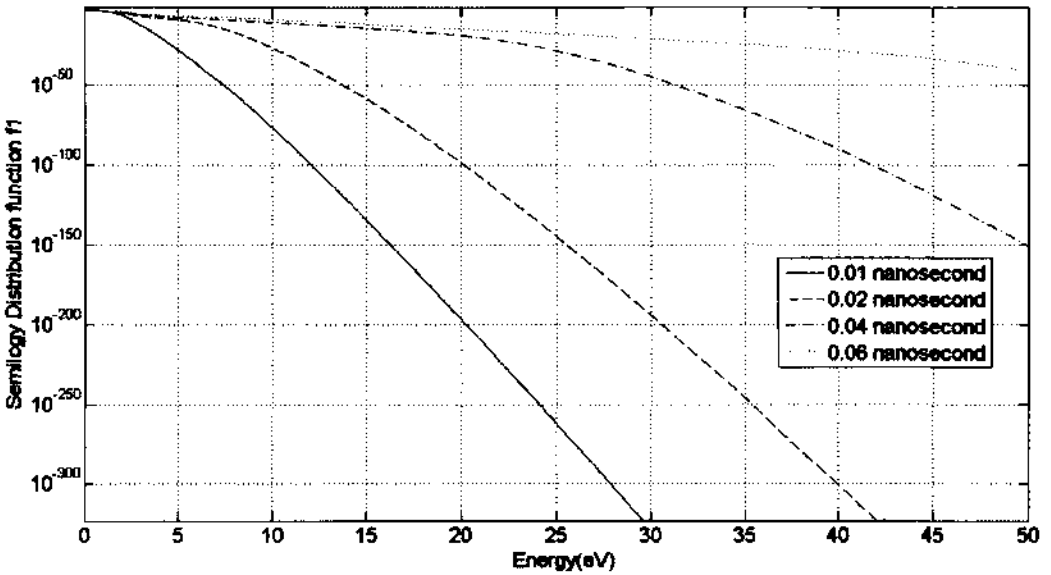

(d) 2D Semi-Logarithmic Energy Distribution Function f_1.

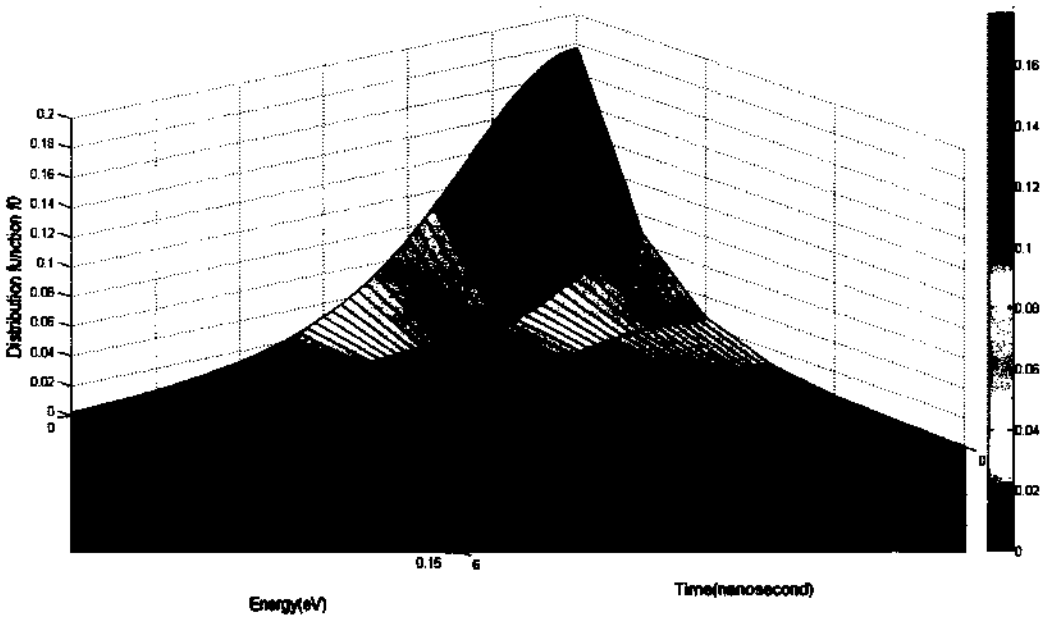

(e) 3D Energy Distribution Function f_0 at the 1st angle.

Figure 4.6 (Continued)

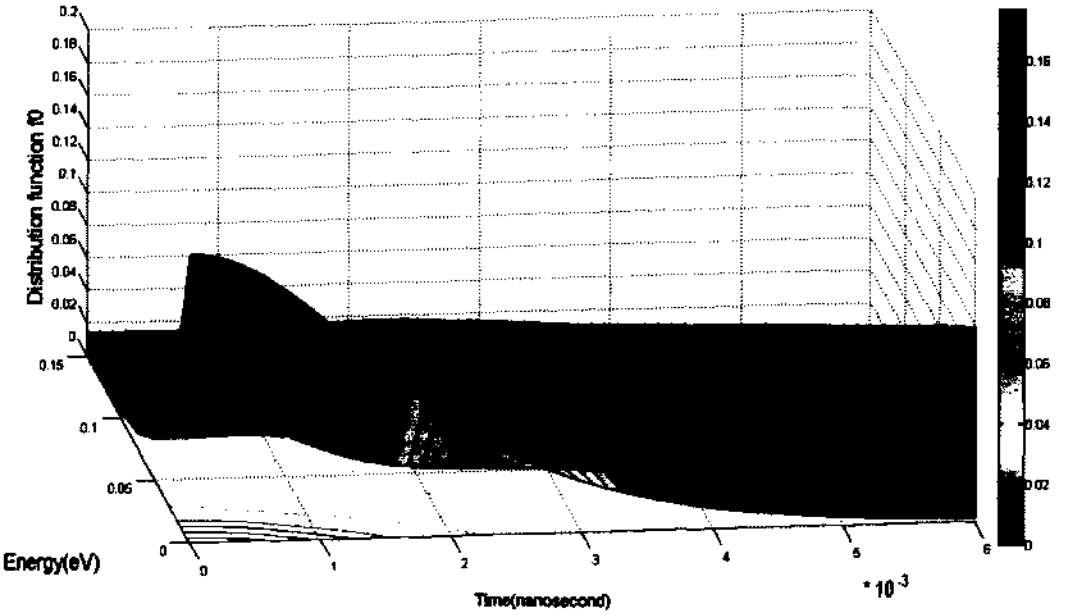

(f) 3D Energy Distribution Function f_0 at the 2nd angle.

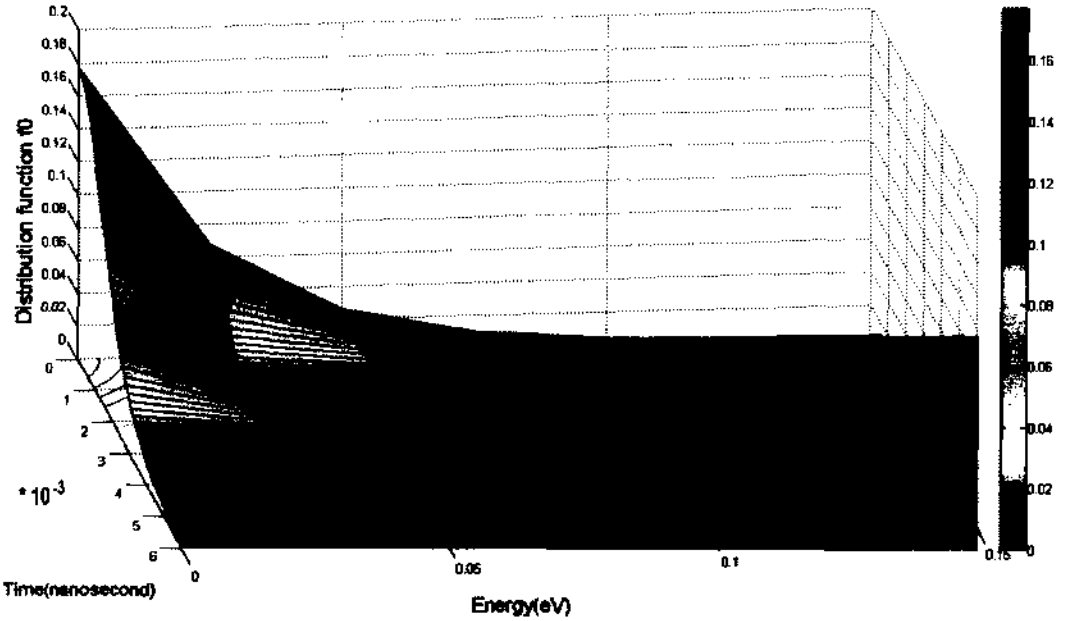

(g) 3D Energy Distribution Function f_0 at the 3rd angle.

Figure 4.6 (Continued)

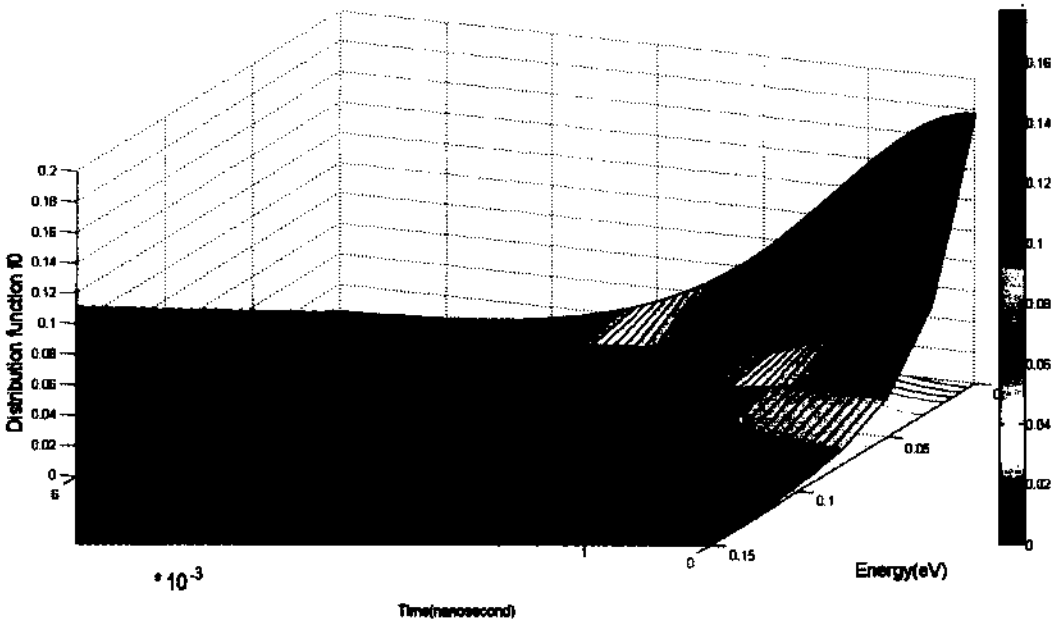

(h) 3D Energy Distribution Function f_0 at the 4th angle.

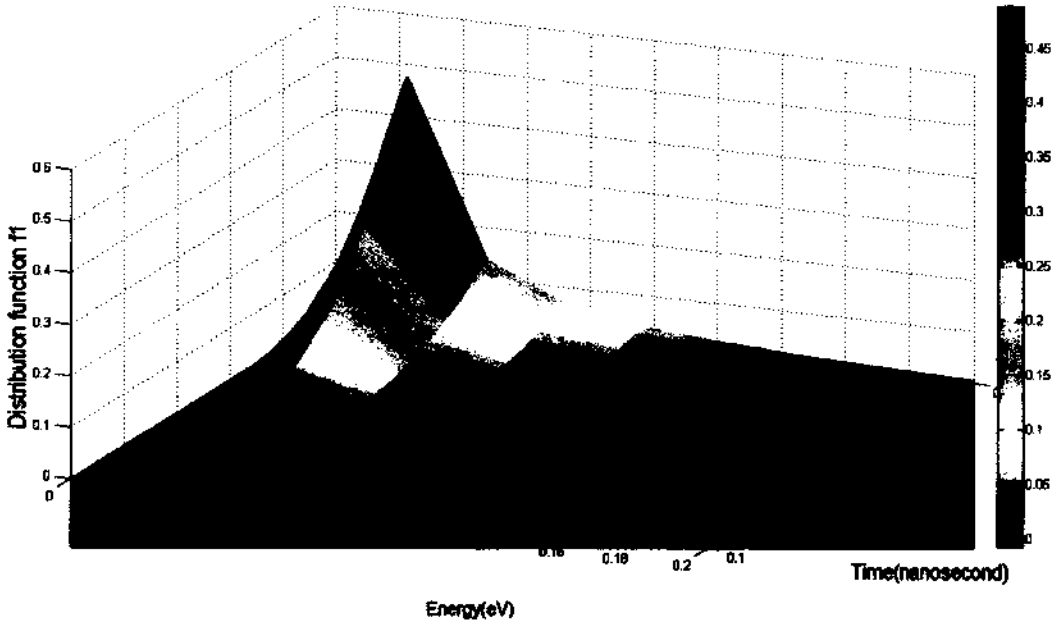

(i) 3D Energy Distribution Function f_1 at the 1st angle.

Figure 4.6 (Continued)

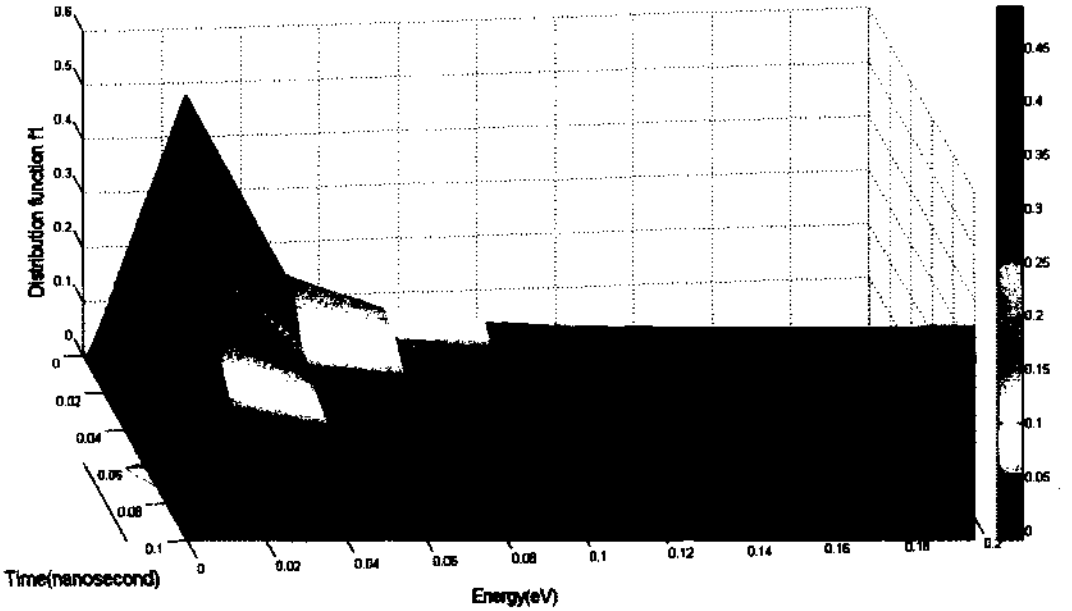

(j) 3D Energy Distribution Function f_1 at the 2nd angle.

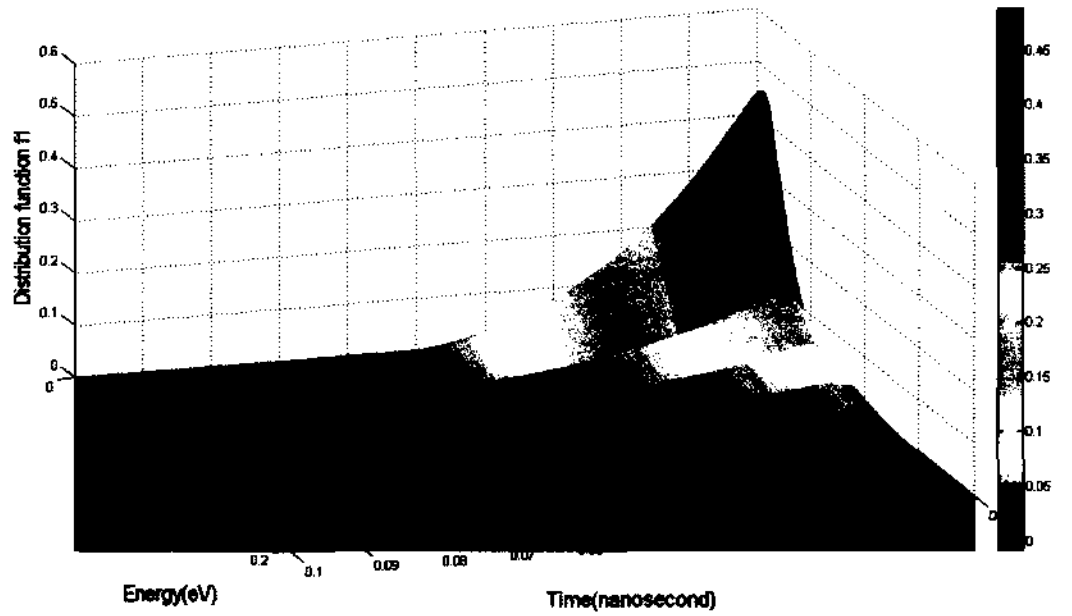

(k) 3D Energy Distribution Function f_1 at the 3rd angle.

Figure 4.6 (Continued)

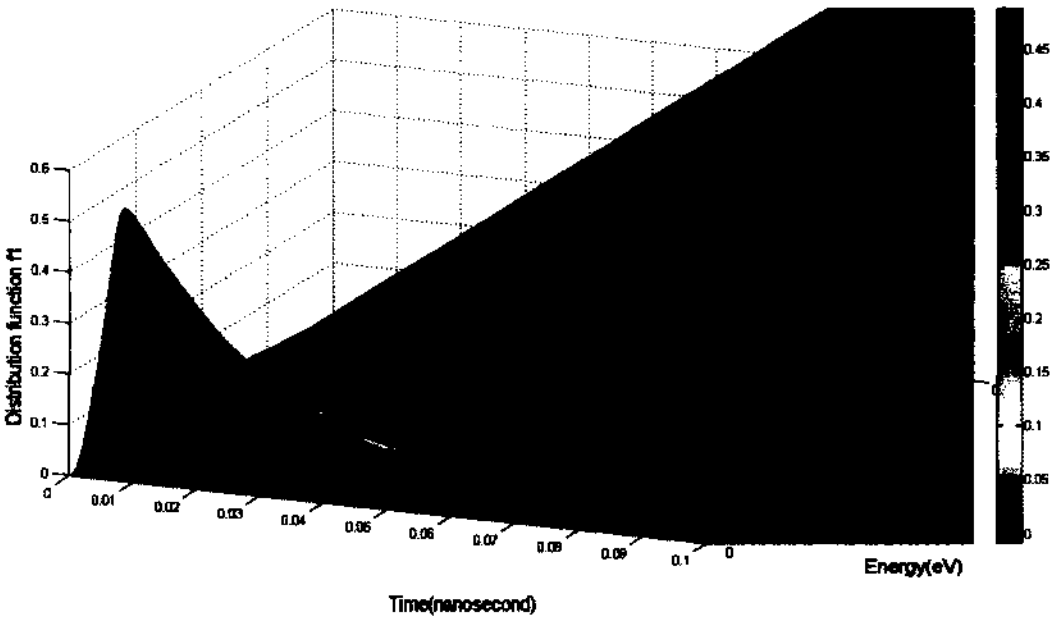

(l) 3D Energy Distribution Function f_1 at the 4th angle.

Figure 4.6 (Continued)

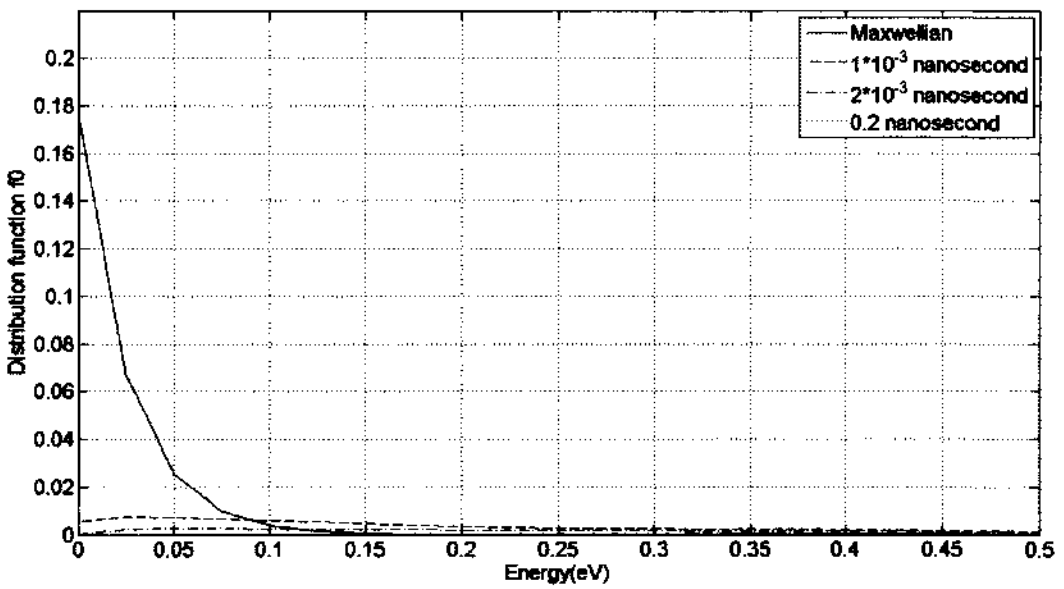

(a) 2D Normal Energy Distribution Function f_0.

Figure 4.7 Two-Dimensional (2D) and Three-Dimensional (3D) Energy Distribution Function Plots Obtained with Time-Dependent Runge-Kutta Method when E/N=500.8613 Td.

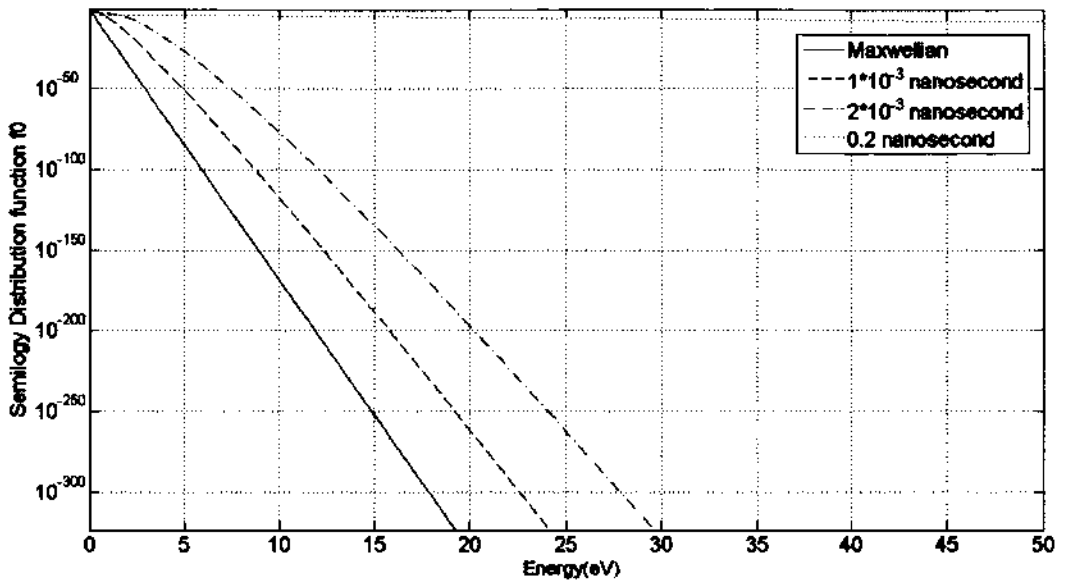

(b) 2D Semi-Logarithmic Energy Distribution Function f_0.

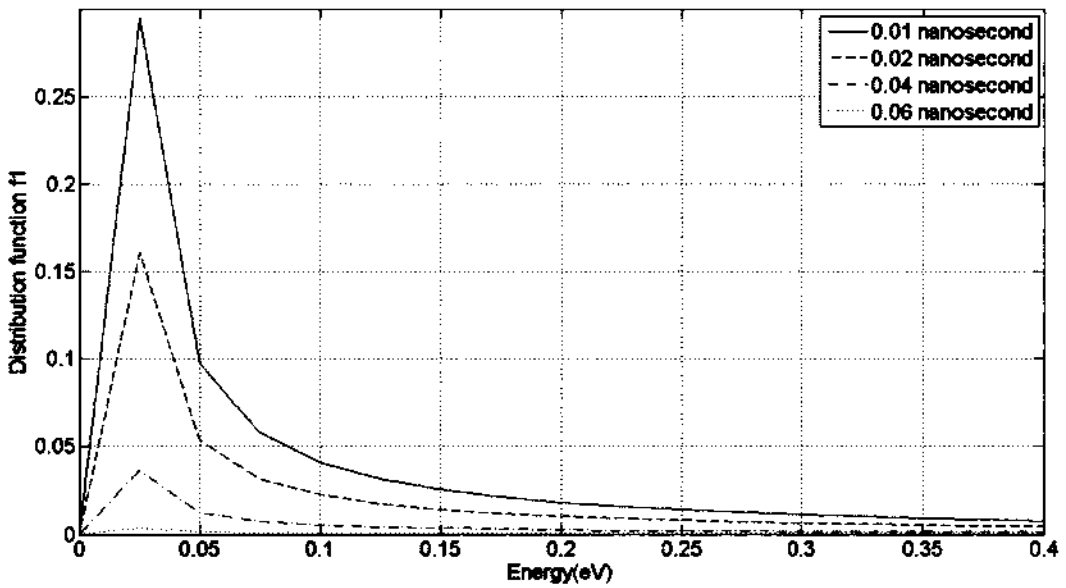

(c) 2D Normal Energy Distribution Function f_1.

Figure 4.7 (Continued)

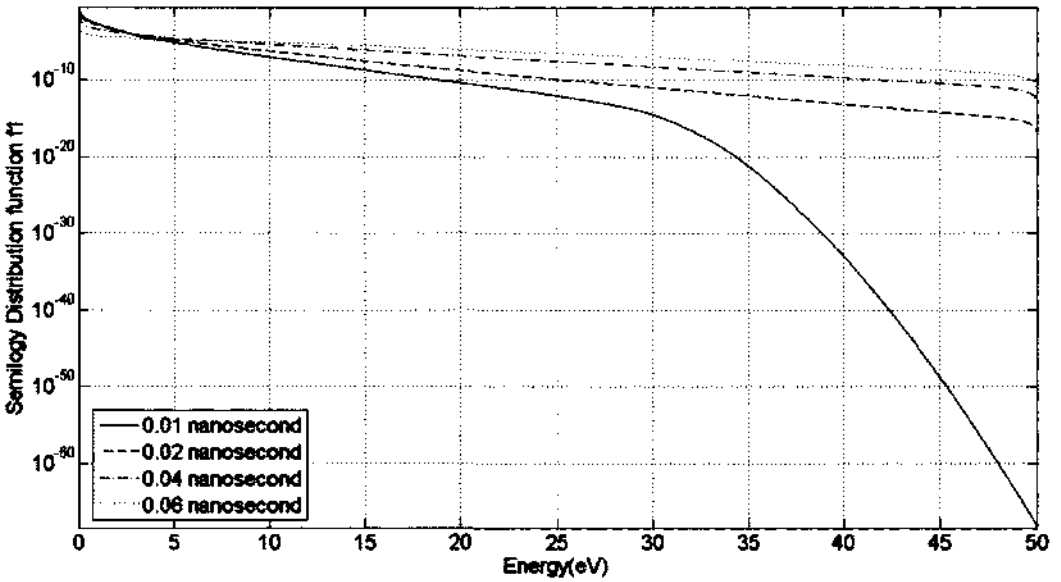

(d) 2D Semi-Logarithmic Energy Distribution Function f_1.

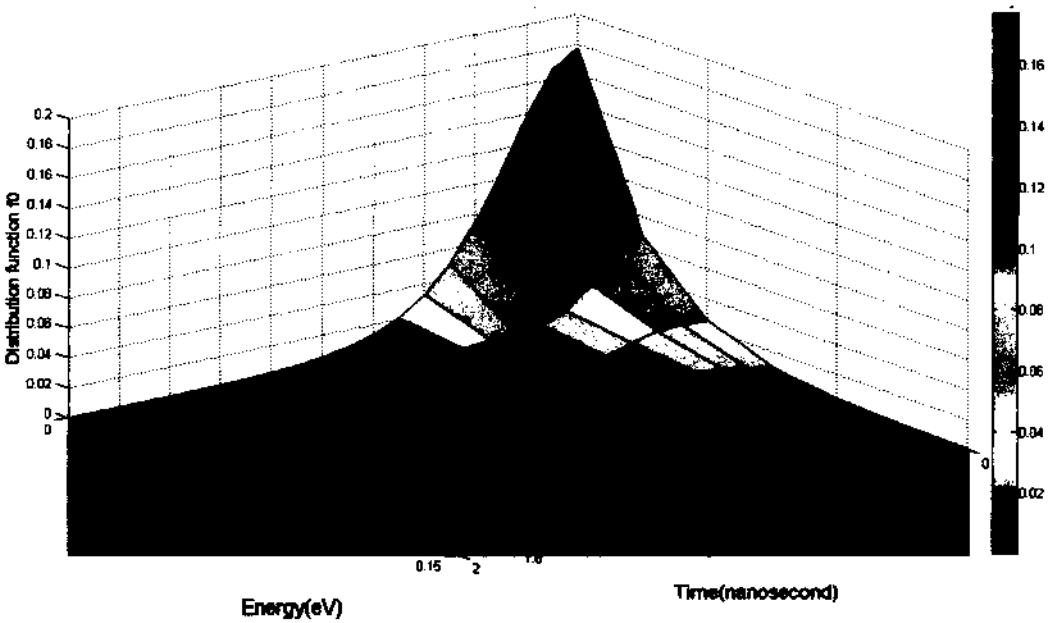

(e) 3D Energy Distribution Function f_0 at the 1st angle.

Figure 4.7 (Continued)

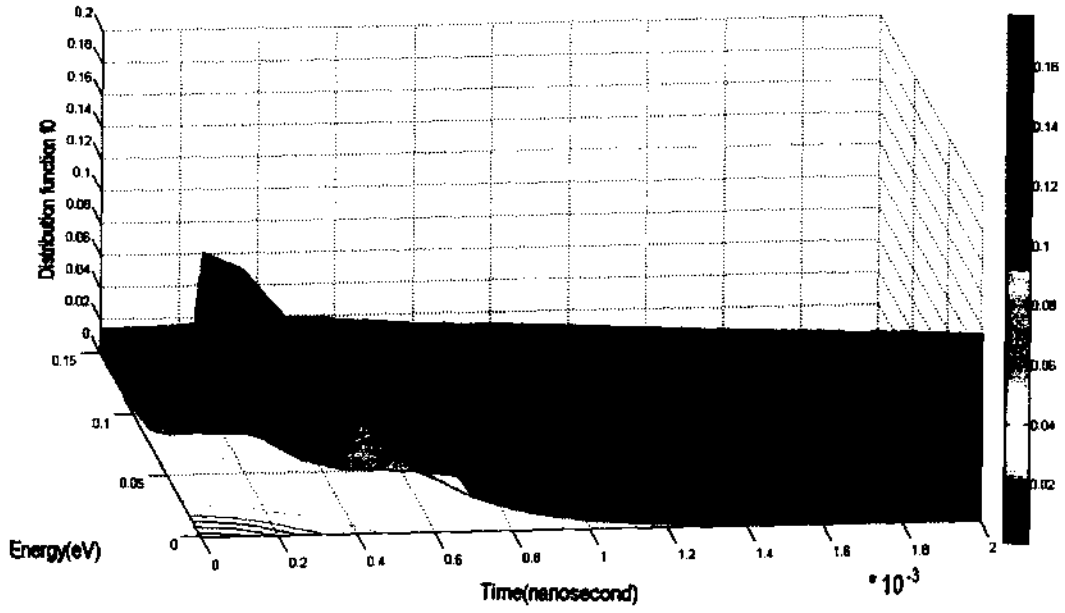

(f) 3D Energy Distribution Function f_0 at the 2nd angle.

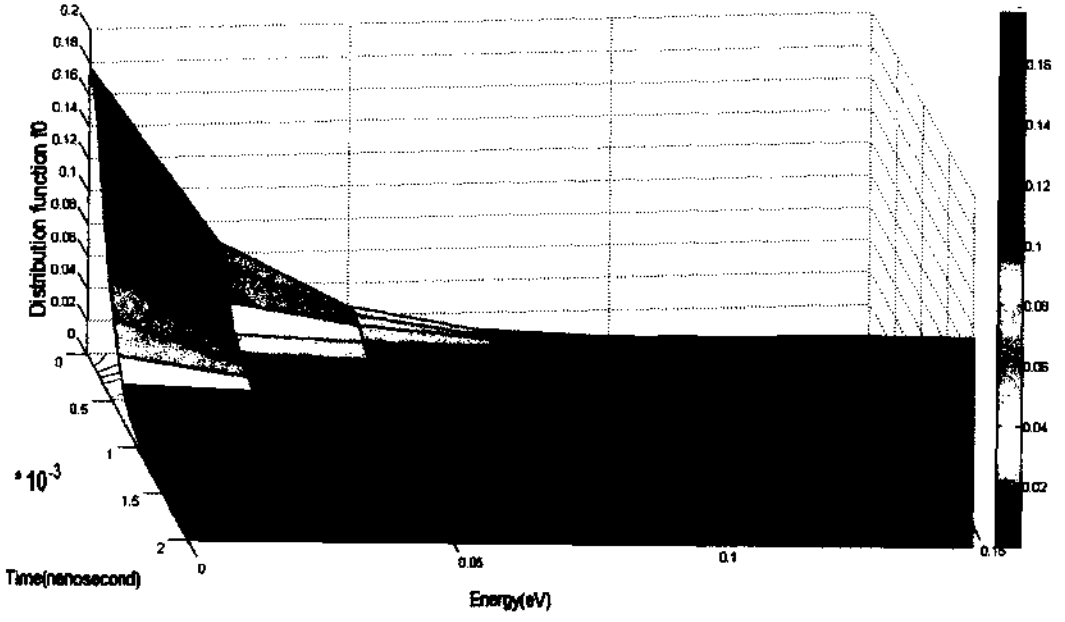

(g) 3D Energy Distribution Function f_0 at the 3rd angle.

Figure 4.7 (Continued)

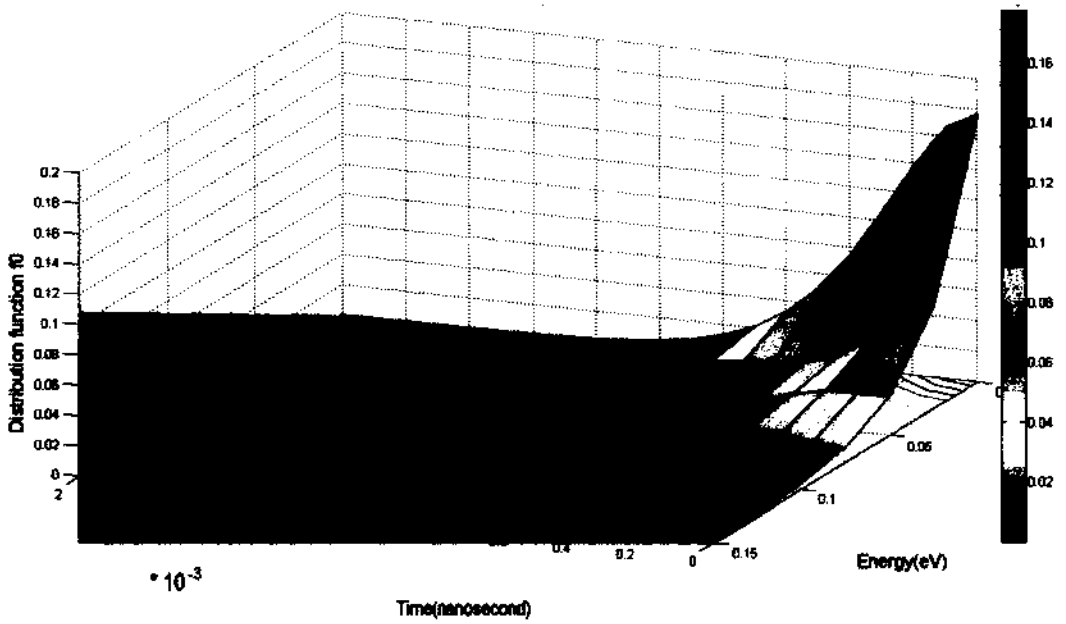

(h) 3D Energy Distribution Function f_0 at the 4th angle.

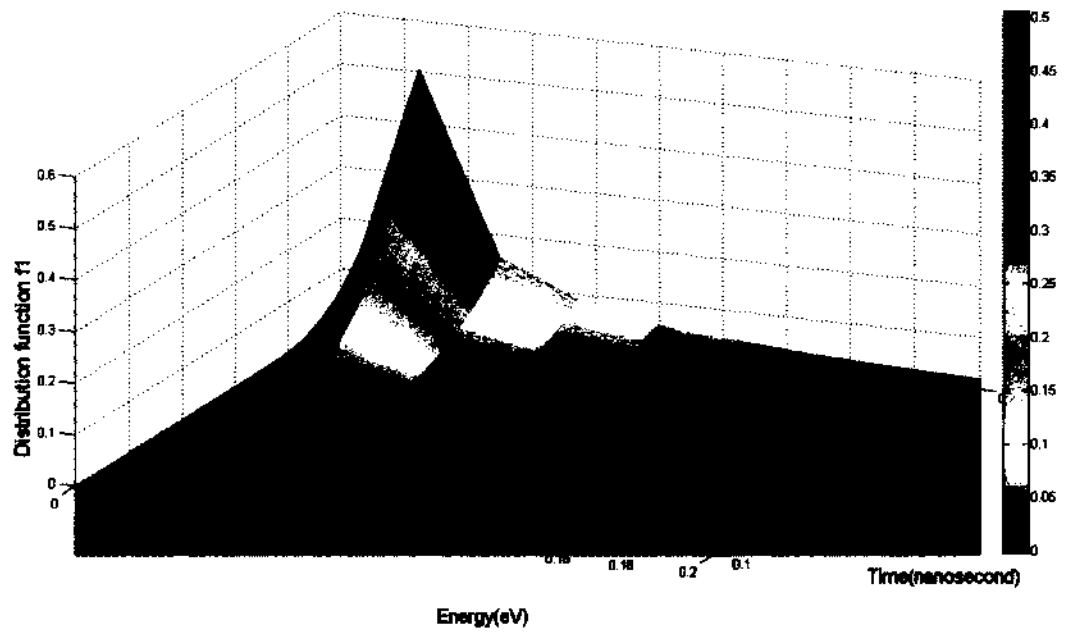

(i) 3D Energy Distribution Function f_1 at the 1st angle.

Figure 4.7 (Continued)

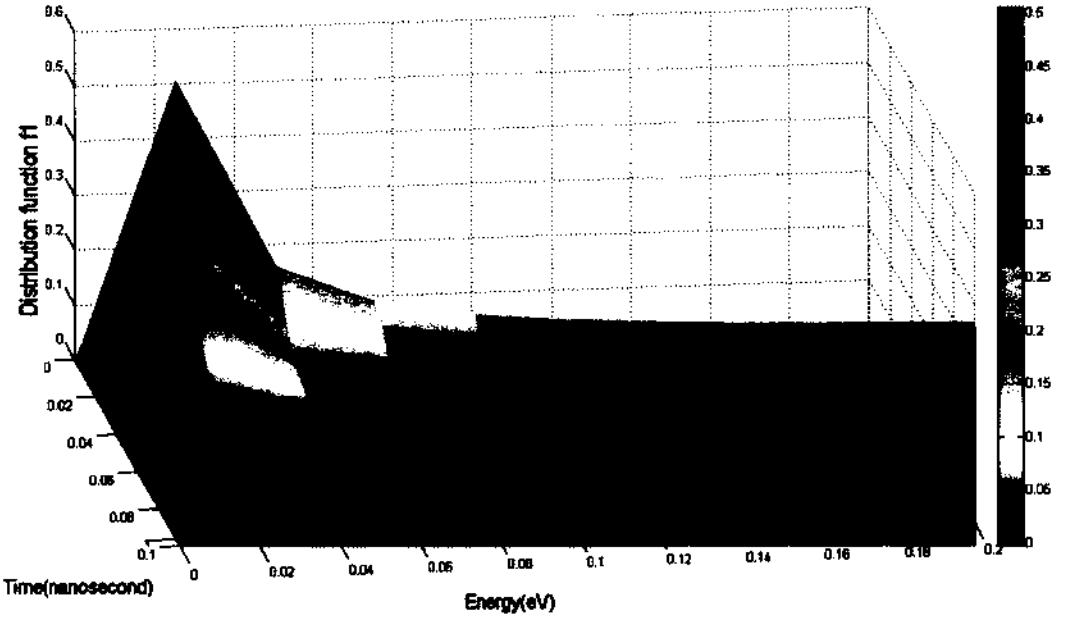

(j) 3D Energy Distribution Function f_1 at the 2nd angle.

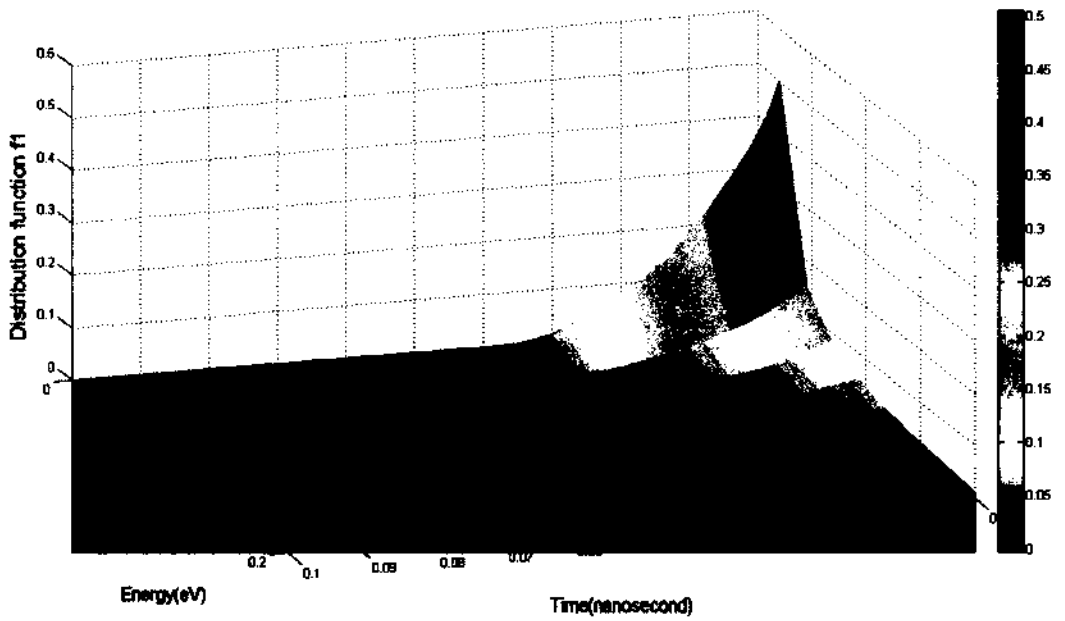

(k) 3D Energy Distribution Function f_1 at the 3rd angle.

Figure 4.7 (Continued)

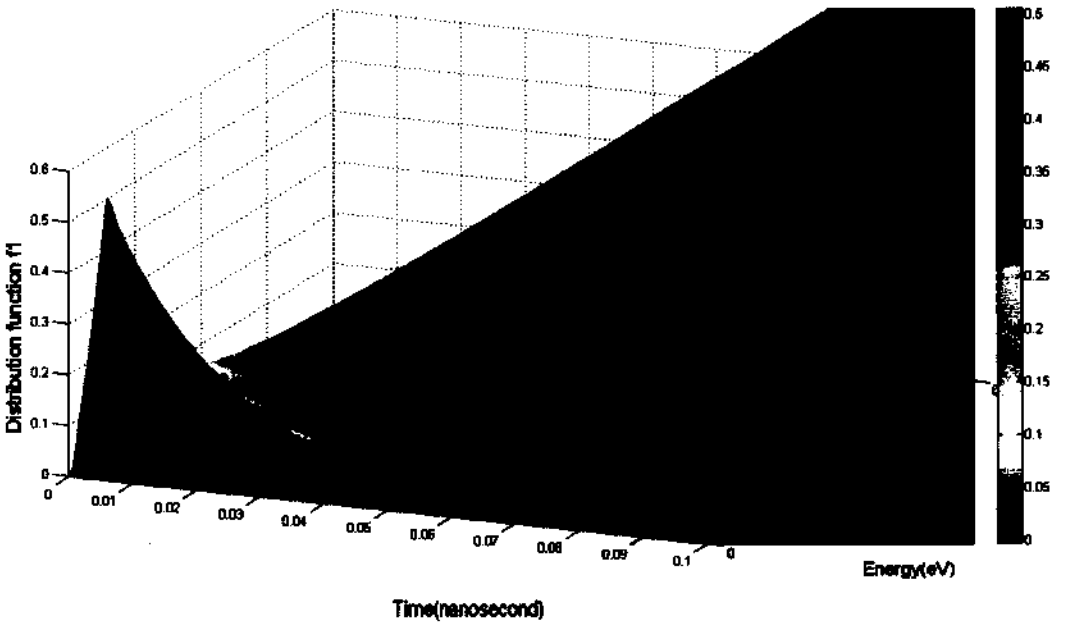

(l) 3D Energy Distribution Function f_1 at the 4th angle.

Figure 4.7 (Continued)

These two groups of figure contain 2D energy distribution function plots on both normal and semi-logarithmic scale. The 2D semi-logarithmic figures for energy distribution functions show the values for energy distribution function f_0 and f_1 at the end of simulation time more clearly, since these values are too small to read from the 2D normal figures.

First, we look carefully into the plots of the 2D distribution function f_0 in Figures 4.6(a-b) and Figures 4.7(a-b). Since distribution function f_0 is the main part of the total distribution function f, it dominates the total distribution function f. The original Maxwellian distribution at time $t = 0$, corresponds to the lowest energy state, and hence, it is a "bottom-heavy" distribution. All the electrons generally occupy the low velocity (i.e., low energy) regime. With time, the particles gain energy from the electrical field and the particle ensemble moves towards larger velocities. This is shown from the curves at the four different time instants. Hence, one finds the curve moving towards right starting from the original Maxwellian curve as time changes. At the end of simulation time, all the particles are almost uniformly distributed in every

energy interval as can be clearly seen from the semi-logarithmic plots of Figures 4.6(b) and 4.7(b). The curve is predicted to finally exhibit a shape that is very close to and parallel with the X-axis at the later time instant with a value of 10^{-5}. Figure 4.6(b) and 4.7(b) are in agreement with the above physical analysis.

Next, we analyze the 2D plots for f_1 as shown in figures 4.6(c-d) and figures 4.7(c-d). The distribution function f_1 is also part of the total distribution function f and will show the change of total distribution function f along the direction parallel to the applied electric field. As opposed to f_0, the distribution function f_1 is zero at the initial time $t = 0$. As time goes by and the particles acquire energy from the external electrical field, the distribution function f_1 dramatically increases to exhibit a peak value. At later times, more particles accelerate into higher energies and the curve drops down quite close to the X-axis at the end of simulation time. Only a small value for distribution function in every energy interval can be seen from Figures 4.6(d) and 4.7(d).

As explained for the 2D distribution function plots, the 3D distribution function plots present the changes in the 2D curve over time and make the results more intuitive to read. From the 3D plots, one can select a slice to represent the energy axis and the distribution function. These 2D curves thus cut-out correspond to the 2D energy distribution function curve at a particular time. If we choose to make an intersection parallel to the time axis, then the distribution function represents a temporal evolution of a particular energy value.

These two groups of figure are shown under one low E/N value (103.5123 Td) and one high E/N value (500.8613 Td). This verifies that time-dependent Runge-Kutta method can produce regular distribution functions with all ranges of E/N values. These results do not show much difference in the shapes. The only difference is that the larger E/N value is, the quicker distribution function f_0 reduces to its final saturated value which is quite small and close to zero.

Compared to the implicit time-independent method discussed earlier, this time-dependent Runge-Kutta method has more points within any energy interval. Hence, the curves for energy distribution functions are much smoother and more accurate than those obtained with the implicit time-independent method. This method produces results even when E/N values are very large. This therefore demonstrates that both the stability and accuracy are greatly improved as compared to time-dependent Euler method. In order to obtain better results perfectly matching the published experimental data, we will need to proceed to a fully implicit method called implicit time-dependent relaxation method as detailed below.

4.5 Simulation Results for Implicit Time-Dependent Relaxation Method

As analyzed in Chapter 3, to overcome the problem of evaluating the equations at the $U_i = 0$ singularity, and to obtain the fully implicit and stable numerical solution, we implemented the implicit time-dependent relaxation method by generating the 4-way grid. The implementation involves solving a matrix equation.

4.5.1 Parameter List of Simulation Control Variables

Table 4.7 gives the values of material parameters considered in this simulation. The pressure was fixed during the simulation process while the electrical field was changed to cover 13 different E/N values. Since this is a time-dependent method, different time steps were tested to produce reasonable results. It turned out that time steps below $10^{-5} ns$ could produce acceptable and reasonable results under the different E/N values. As with the previous simulations, the cross sections involving one elastic scattering and 29 inelastic scattering process as discussed in Chapter 2 were used.

Table 4.7 Parameter List of Simulation Control Variables for the Implicit Time-Dependent Relaxation Method.

Parameter	Value(Units)
Temperature	300 K
Pressure	0.25 atmosphere
Electric field	$3.1668\times10^{5}\sim3.0646\times10^{6}V/m$
Maximum energy	10 eV
Number of energy gaps	1000
Time Step	$10^{-5}ns$
Time of Simulation	$0.03\sim0.1ns$
Cross Sections	Elastic scattering plus 29 inelastic scattering processes

4.5.2 Drift Velocity Results

In this section, the drift velocity plots corresponding to 13 different E/N values obtained with the implicit time-dependent relaxation method are shown.

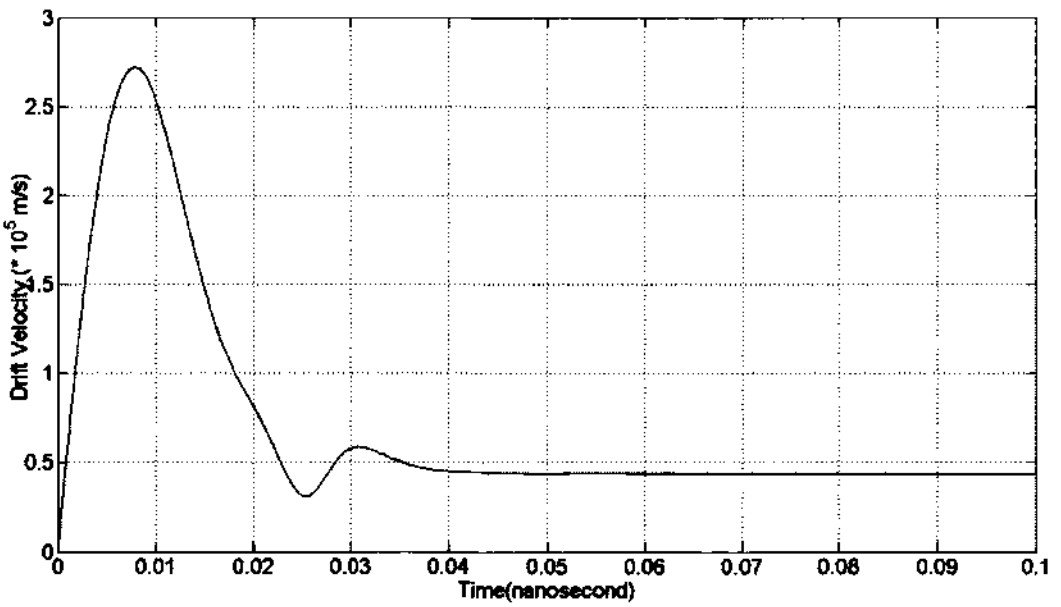

(a) E/N=51.7561989 Td.

Figure 4.8 Drift Velocities of Electrons in Nitrogen Gas Obtained at Different E/N Values with the Implicit Time-Dependent Relaxation Method.

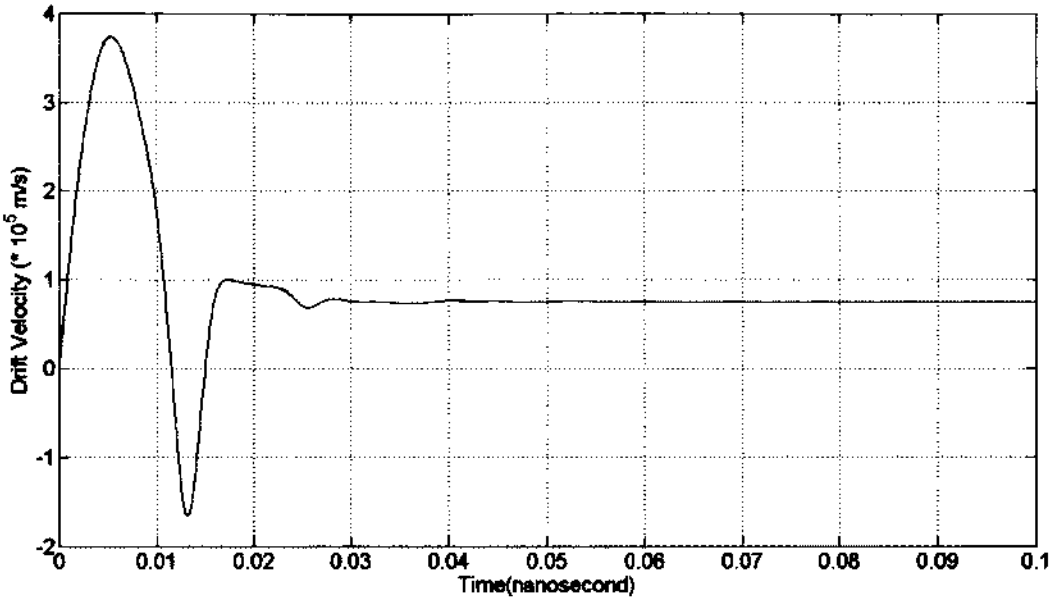

(b) E/N=103.512398 Td.

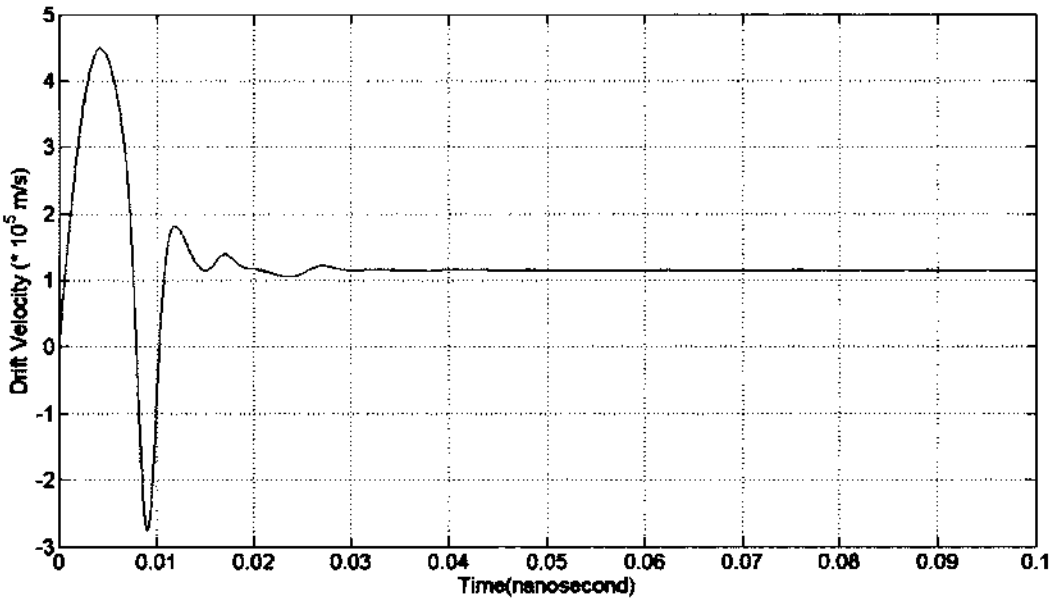

(c) E/N=155.268585 Td.

Figure 4.8 (Continued)

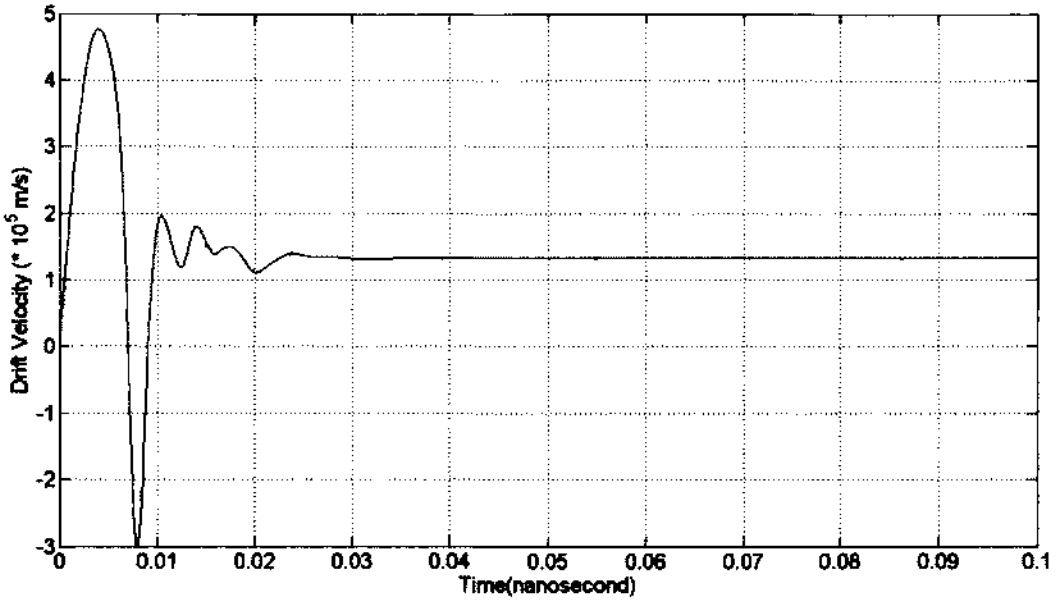

(d) E/N=177.449814 Td.

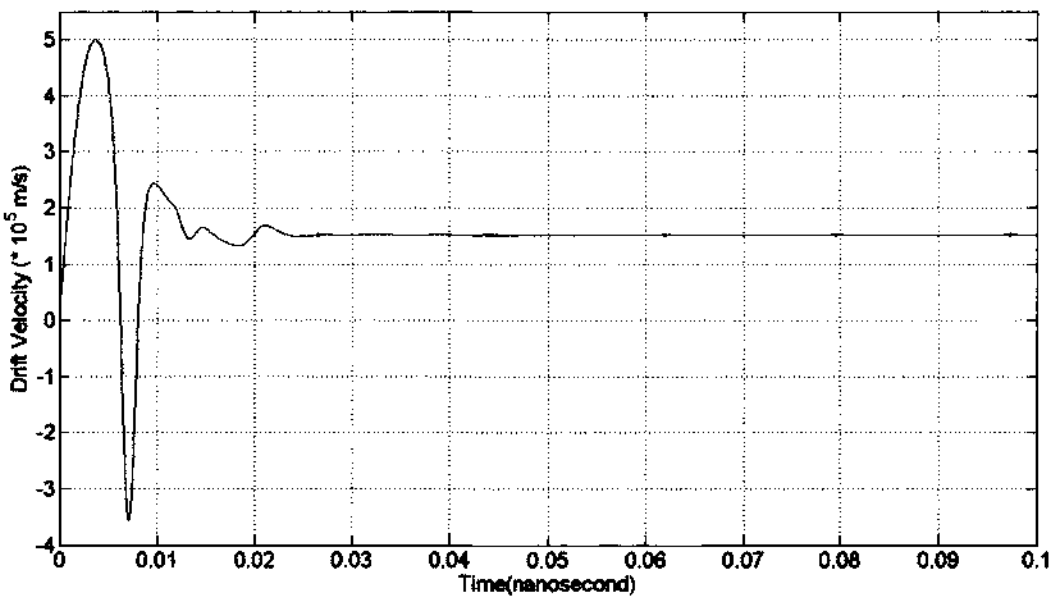

(e) E/N=200.346573 Td.

Figure 4.8 (Continued)

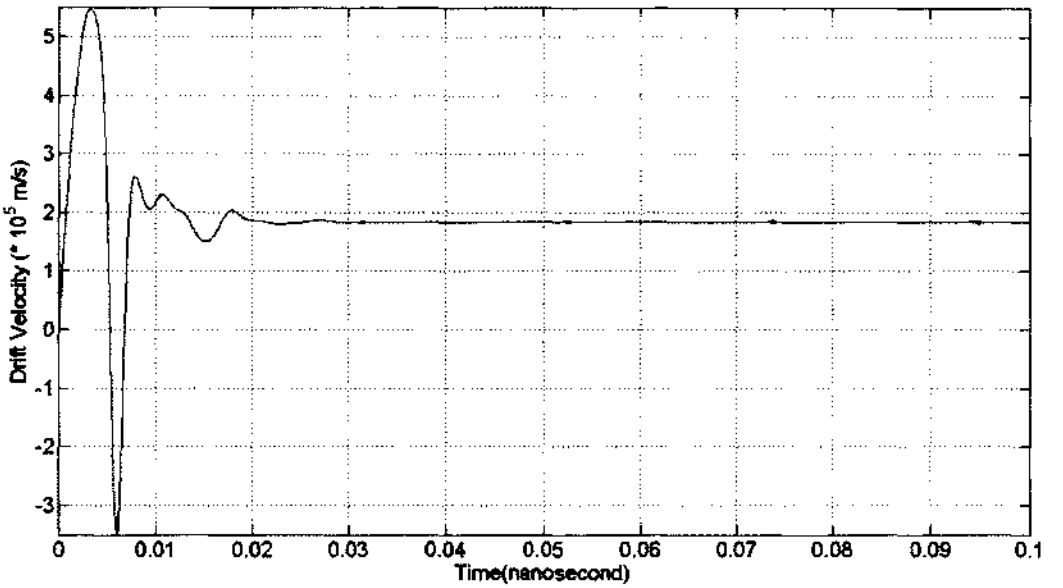

(f) E/N=238.874756 Td.

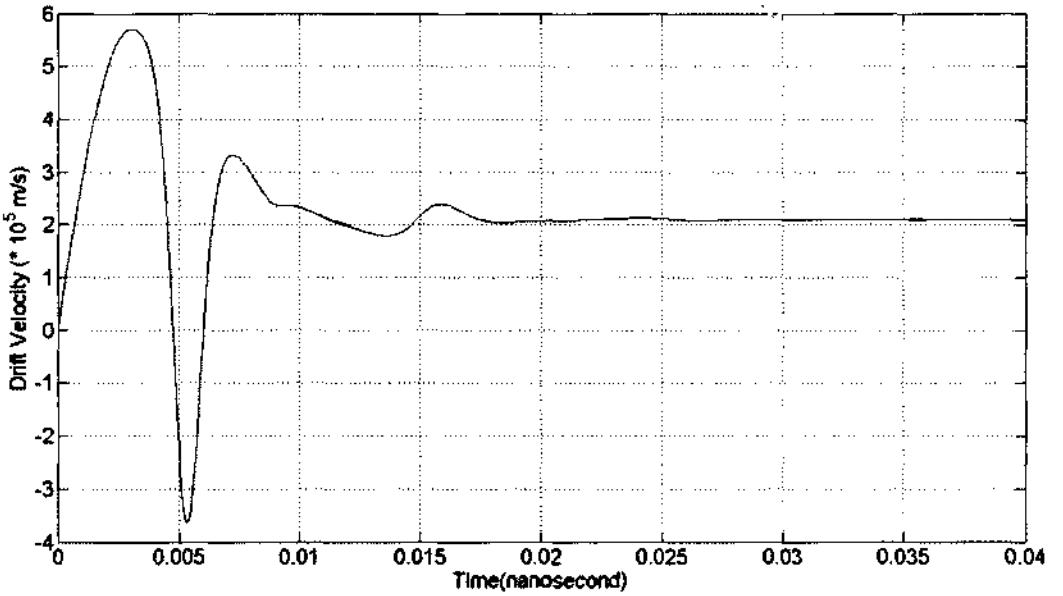

(g) E/N=270.032318 Td.

Figure 4.8 (Continued)

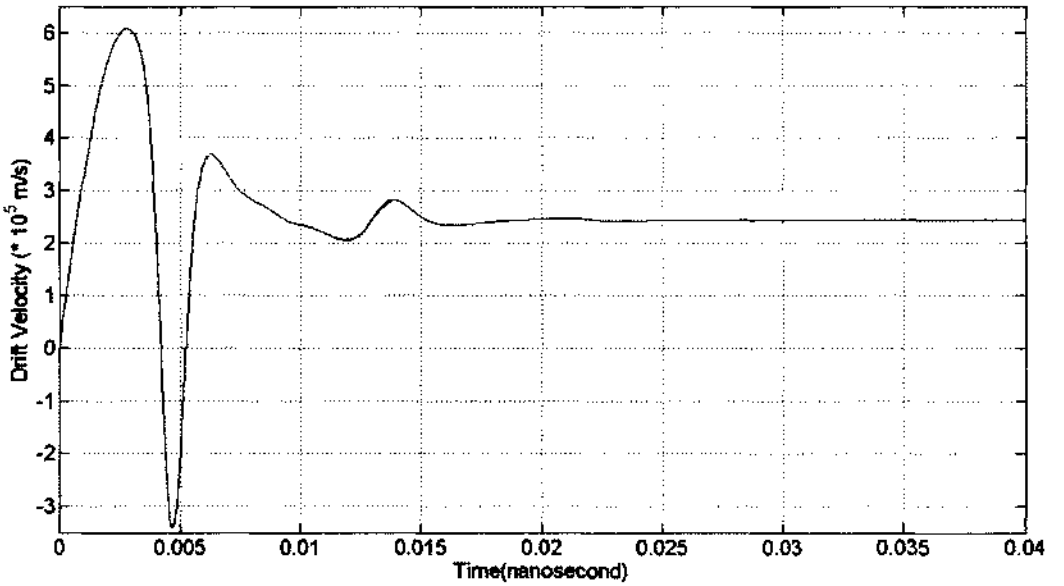

(h) E/N=310.537170 Td.

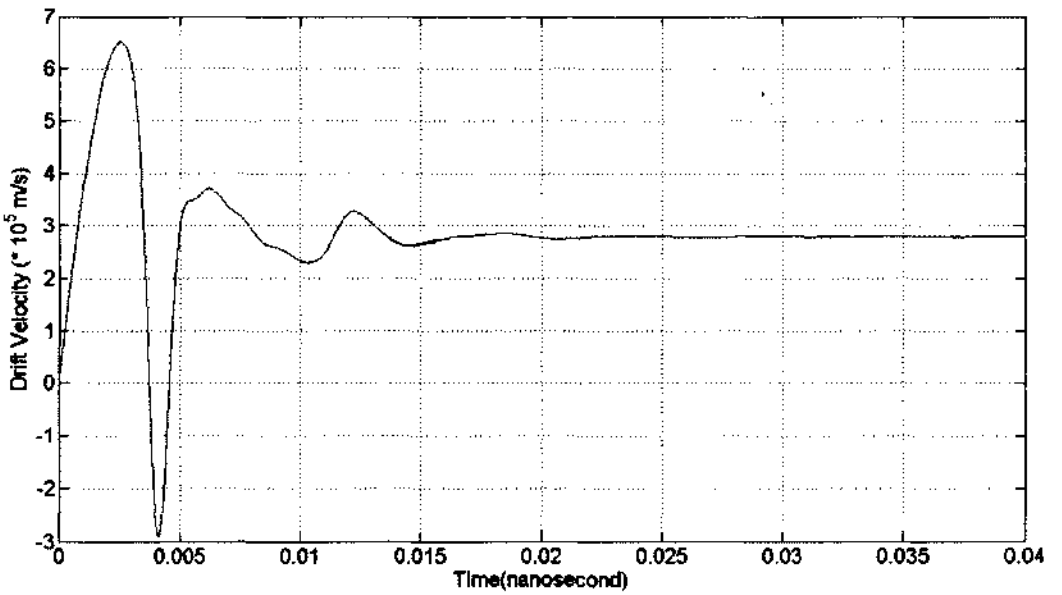

(i) E/N=354.899628 Td.

Figure 4.8 (Continued)

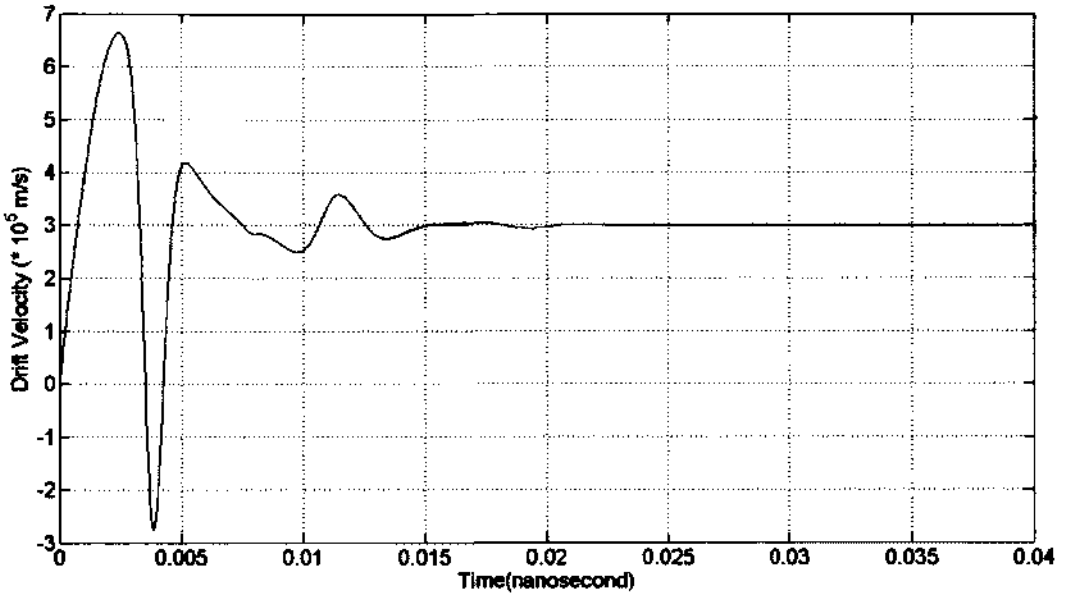

(j) E/N=378.703888 Td.

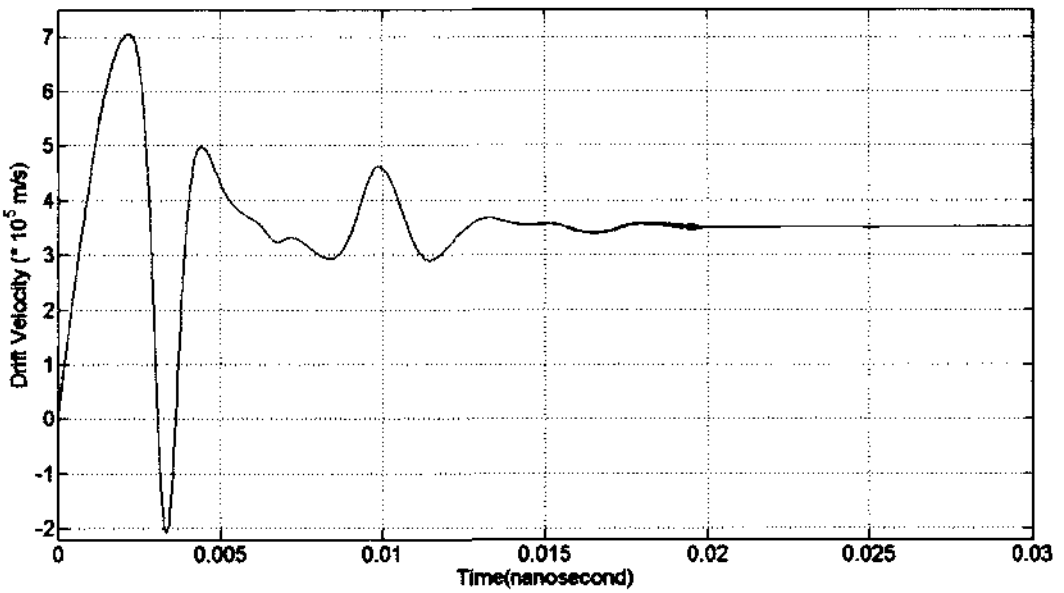

(k) E/N=443.624542 Td.

Figure 4.8 (Continued)

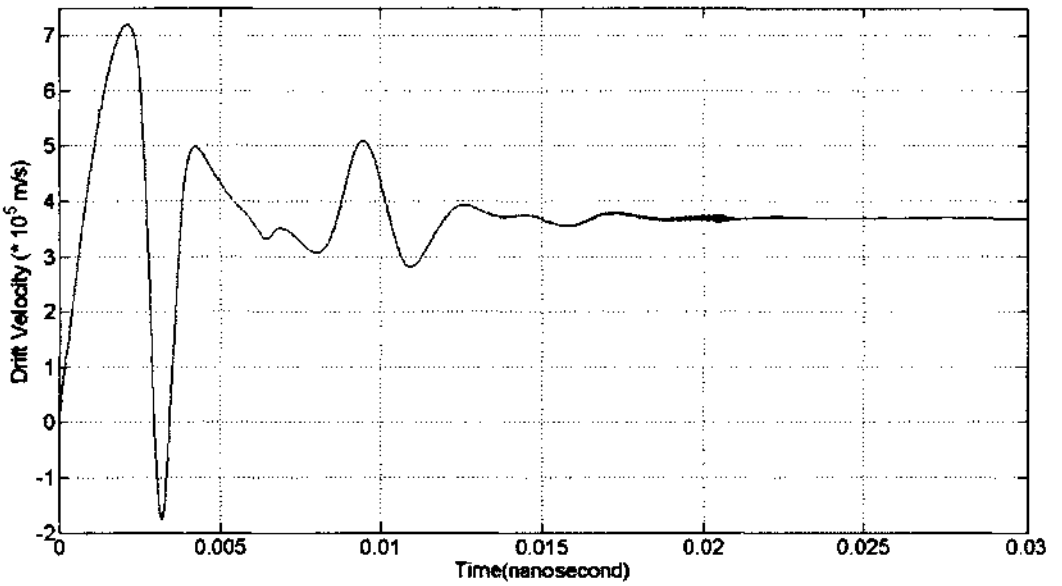

(l) E/N=465.805756 Td.

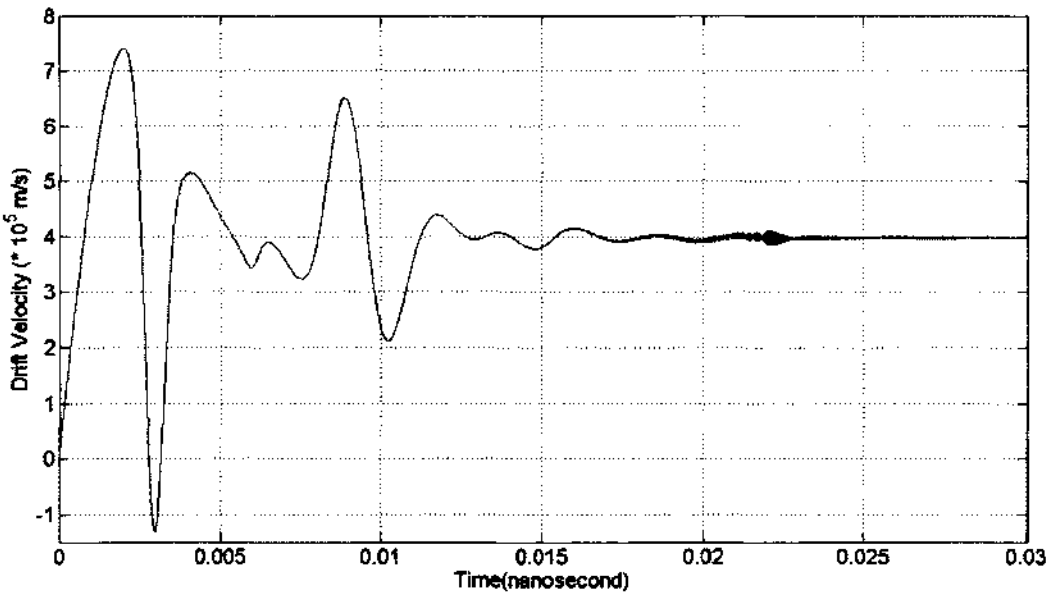

(m) E/N=500.866425 Td.

Figure 4.8 (Continued)

All 13 plots in Figure 4.8 show the program reaches steady state in the end which proves that the energy distribution functions obtained (and shown later) are those under steady state. It also demonstrates that the implicit time-dependent relaxation method is an effective numerical method in solving the PDEs.

4.5.3 Drift Velocity Values

Here we obtain the drift velocity values corresponding to 13 different E/N values with the implicit time-dependent relaxation method. We will compare these drift velocity values to the experimental and theoretical results reported in the literature by other investigators.

Table 4.8 Drift Velocity Values of Electrons in Nitrogen Gas as a Function of E/N Obtained with the Implicit Time-Dependent Relaxation Method.

Number	E/N(Td)	Drift Velocity(W) in Nitrogen (10^5 m/s)
1	51.7561989	0.4377
2	103.512398	0.7523
3	155.268585	1.1522
4	177.449814	1.3332
5	200.346573	1.5218
6	238.874756	1.8422
7	270.032318	2.0993
8	310.537170	2.4321
9	354.899628	2.7944
10	378.703888	2.9891
11	443.624542	3.5149
12	465.805756	3.6921
13	500.866425	3.9761

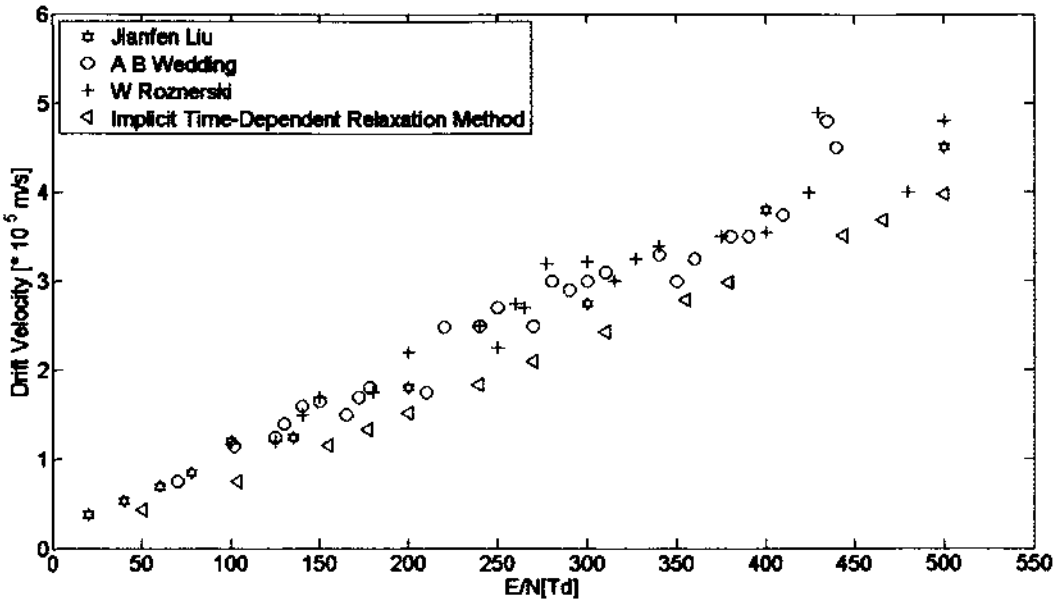

Figure 4.9 Comparison of Drift Velocities of Electrons in Nitrogen Gas Obtained at Different E/N Values with the Implicit Time-Dependent Relaxation Method and Experimental Data.

Figure 4.9 shows excellent agreement between our drift velocity values under 13 different E/N values and other investigators' published results. These include the publications by A. B. Wedding [34], W. Roznerski [35], and Jianfen Liu [36] that are available over a high E/N range. This is a great improvement over both the implicit time-independent method and the time-dependent Runge-Kutta method. It may be recalled that the implicit time-independent method could not obtain results in good agreement with published data for high E/N values. Also, the time-dependent Runge-Kutta method could not obtain results in close match to the published experiment data due to its non-implicit and non-stable characteristic. Figure 4.9 conclusively proves that the implicit time-dependent relaxation method is the most accurate and stable numerical method among all the numerical methods discussed in this dissertation. The correctness and accuracy of the implementation is validated as well.

4.5.4 Three-Dimensional Energy Distribution Functions

Since all the simulations under different E/N values run to steady state, we can present 3D energy distribution function for each E/N value here. Because of space limitations, only two groups of figures – one under low and the other under high E/N value – are shown.

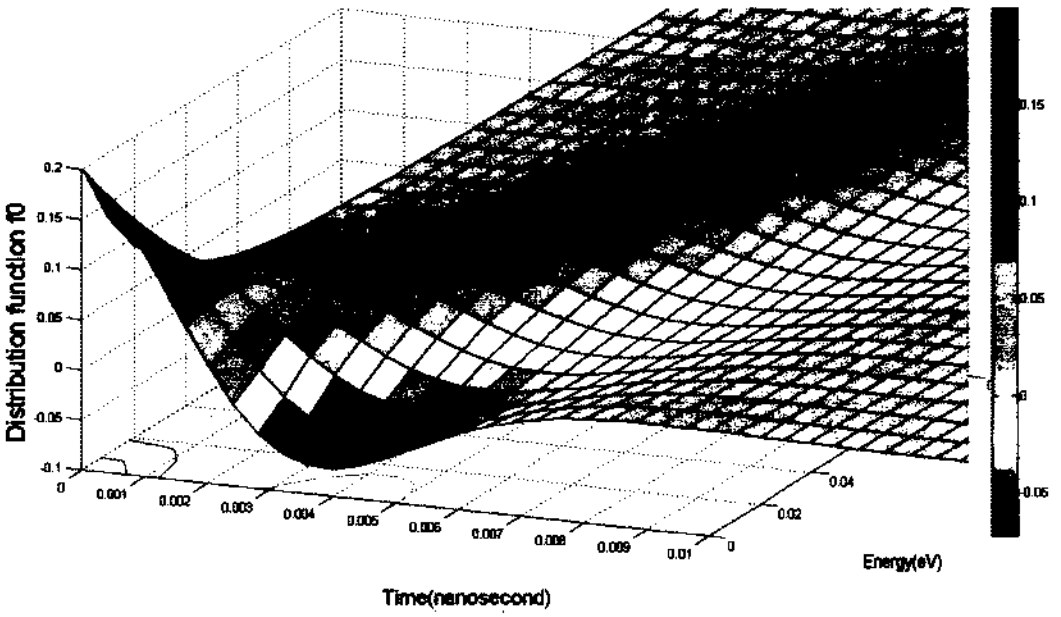

(a) 3D Energy Distribution Function f_0 at the 1st angle.

Figure 4.10 Three-Dimensional (3D) Energy Distribution Function Plots with Implicit Time-Dependent Relaxation Method when E/N=51.7561 Td.

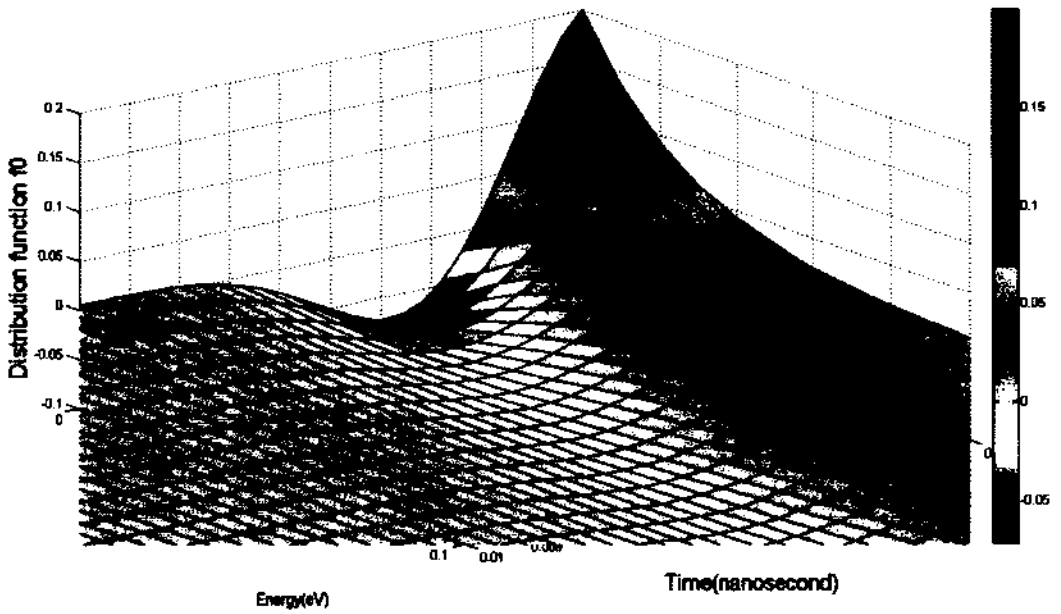

(b) 3D Energy Distribution Function f_0 at the 2nd angle.

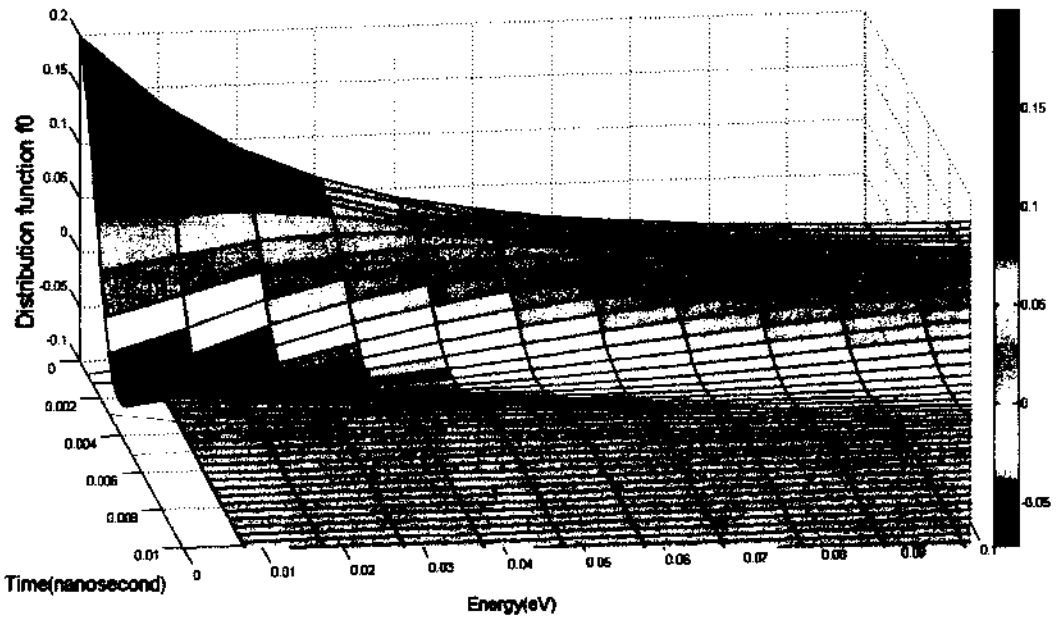

(c) 3D Energy Distribution Function f_0 at the 3rd angle.

Figure 4.10 (Continued)

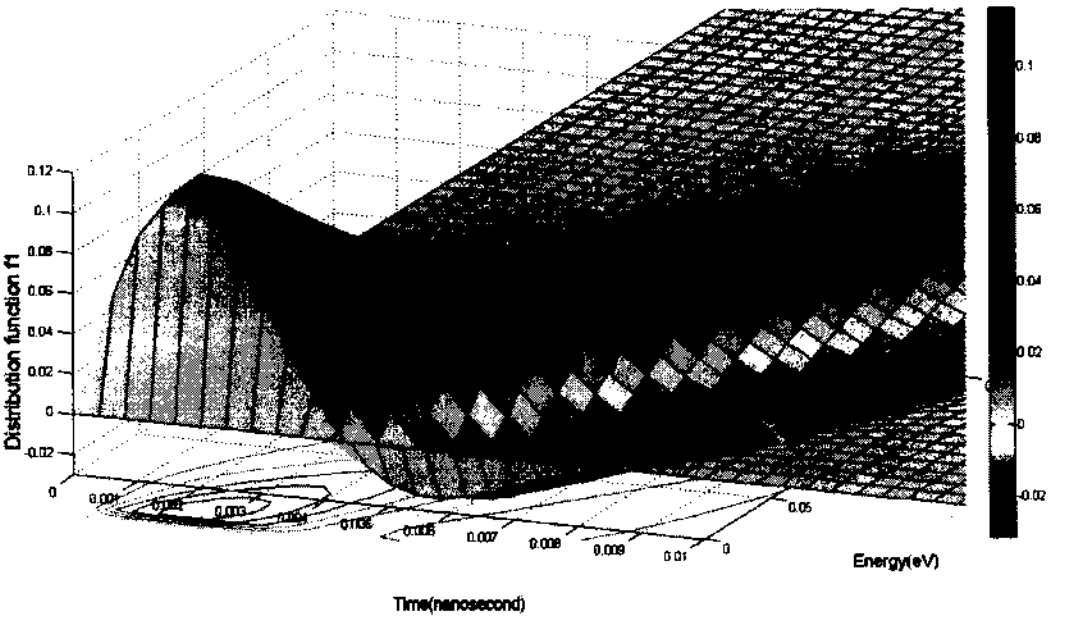

(d) 3D Energy Distribution Function f_1 at the 1st angle.

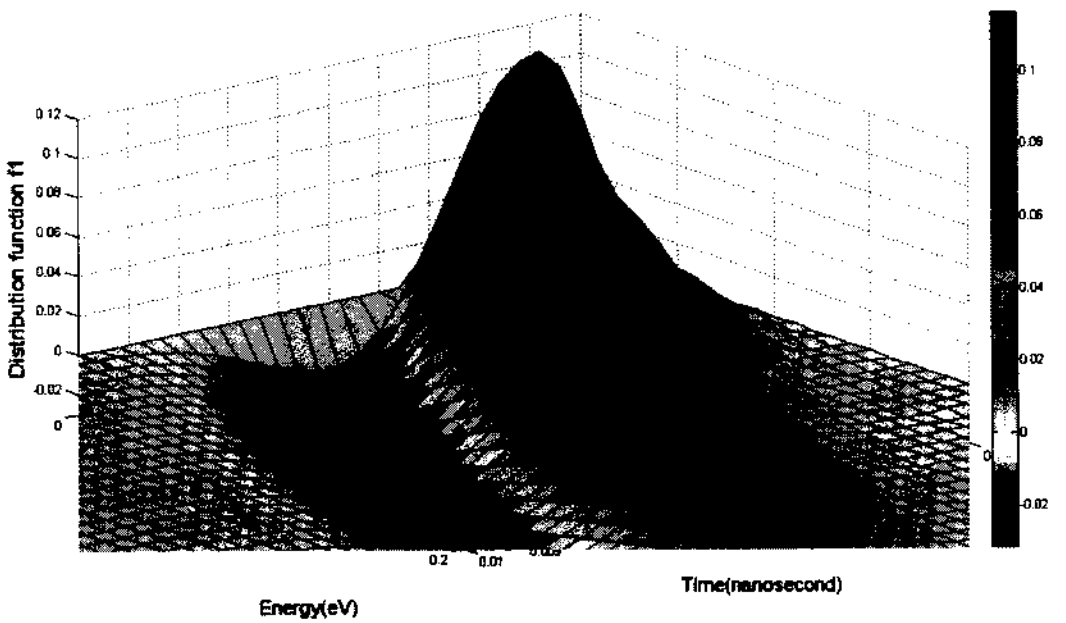

(e) 3D Energy Distribution Function f_1 at the 2nd angle.

Figure 4.10 (Continued)

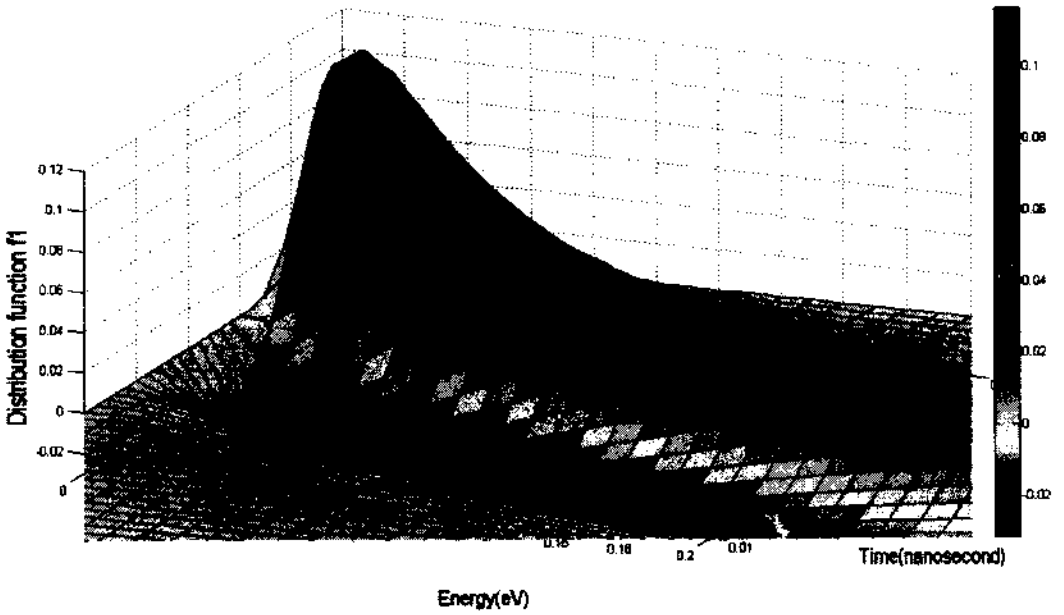

(f) 3D Energy Distribution Function f_1 at the 3rd angle.

Figure 4.10 (Continued)

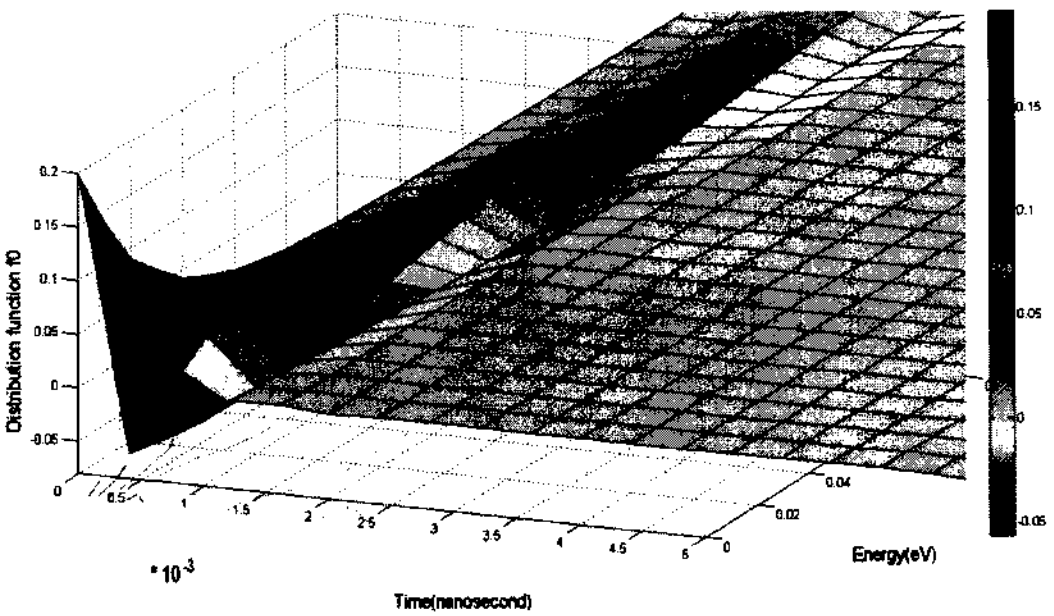

(a) 3D Energy Distribution Function f_0 at the 1st angle.

Figure 4.11 Three-Dimensional (3D) Energy Distribution Function Plots with Implicit Time-Dependent Relaxation Method when E/N=378.7038 Td.

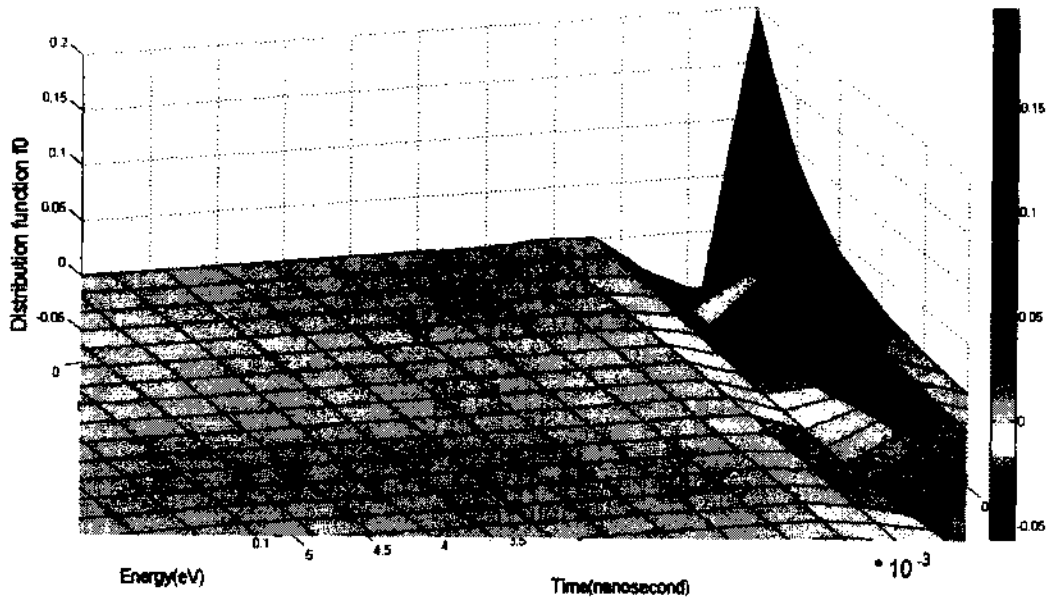

(b) 3D Energy Distribution Function f_0 at the 2nd angle.

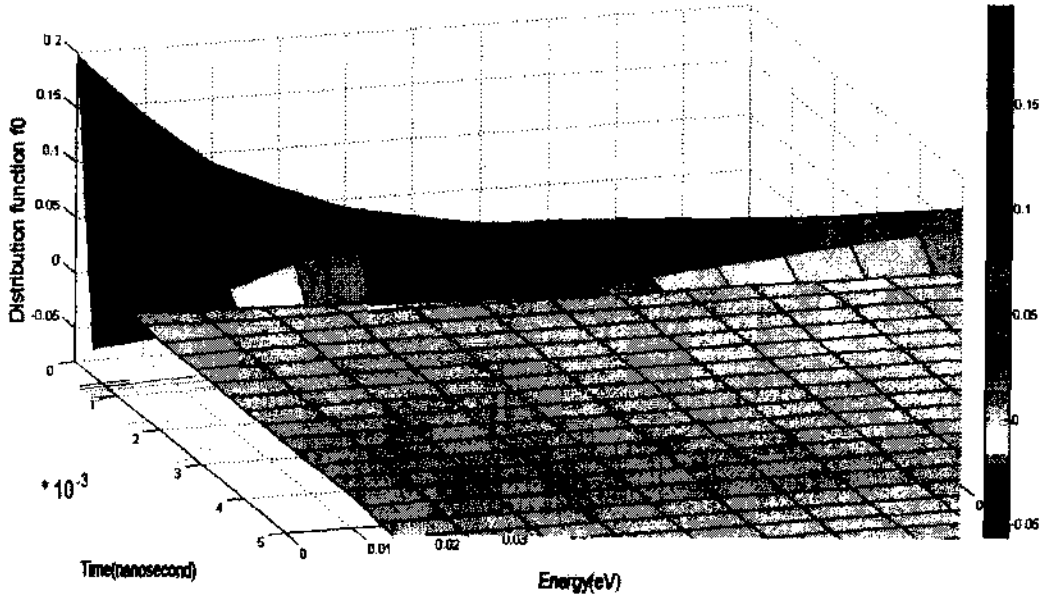

(c) 3D Energy Distribution Function f_0 at the 3rd angle.

Figure 4.11 (Continued)

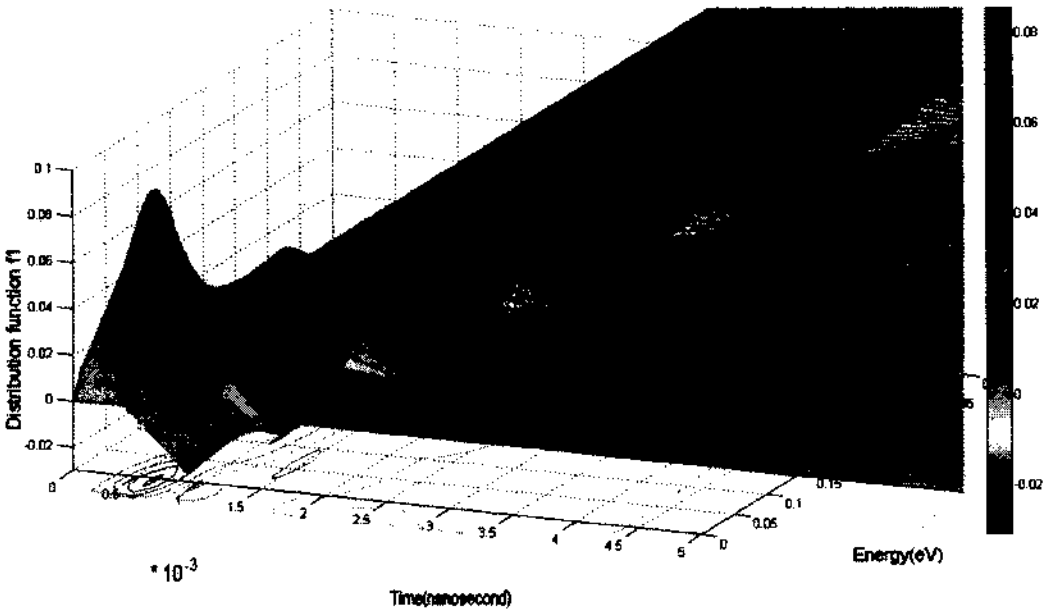

(d) 3D Energy Distribution Function f_1 at the 1st angle.

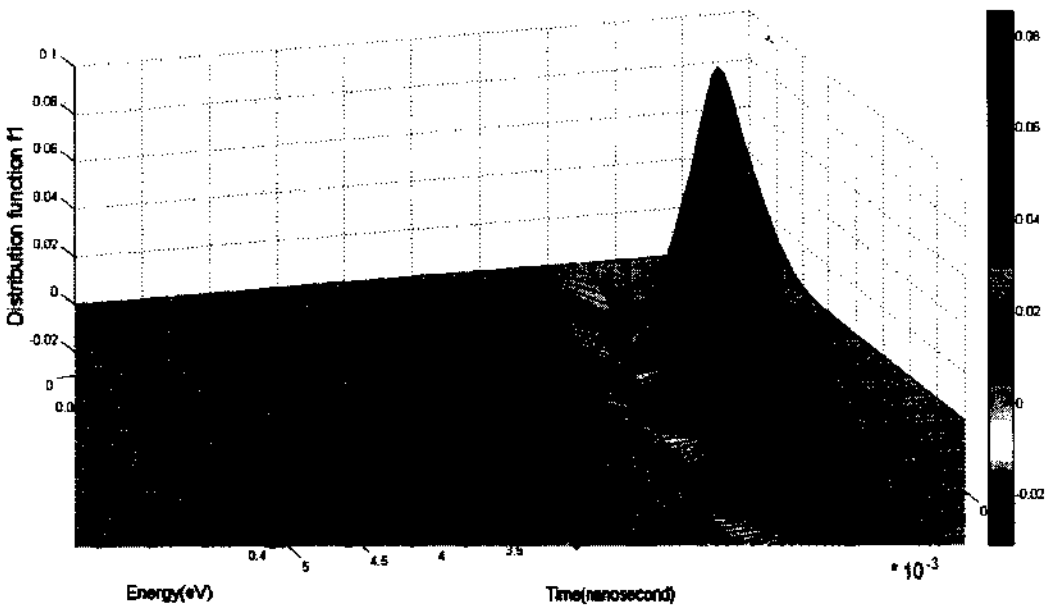

(e) 3D Energy Distribution Function f_1 at the 2nd angle.

Figure 4.11 (Continued)

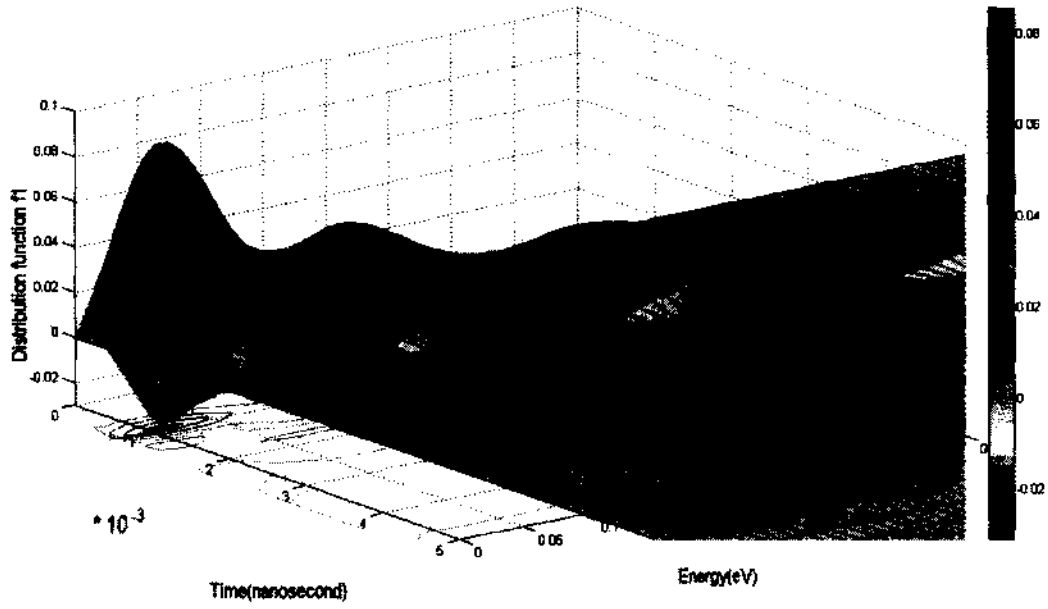

(f) 3D Energy Distribution Function f_1 at the 3rd angle.

Figure 4.11 (Continued)

These two groups of figures are shown under a low E/N value of 51.7561 Td and another relatively high E/N value of 378.7038 Td. This verifies that this implicit time-dependent relaxation method is an accurate and stable method. Furthermore, it can produce acceptable distribution functions with all ranges of E/N values, without any numerical instabilities or problems. The simulations also showed that the larger E/N value was, the quicker distribution function f_0 reached its final saturated value. This is expected since the higher driving force (i.e., higher E/N) would quicken the system response.

As analyzed with the time-dependent Runge-Kutta method, these two groups of 3D plots still show the distribution function f_0 changing from an initial Maxwellian curve to final saturated curve that is very small in magnitude, but has a much longer energy span. Distribution function f_1 increases to the peak value after a short time and drops down gradually until steady state. Overall its value was observed to remain relatively small close to the steady-state saturation regime.

4.6 Simulation Results for Calculation of Townsend's First Ionization Coefficient

Since the implicit time-dependent relaxation method is the most accurate and stable numerical method among all the numerical methods discussed in this dissertation, we follow this method and apply Equation (3.118) to compute Townsend's first ionization coefficient at different E/p values. The values of α/p in Nitrogen gas obtained at different E/p values from the simulation are recorded in Table 4.9 below. These can be compared to the published experimental results with nitrogen gas.

Table 4.9 Values of α/p in Nitrogen Gas as a Function of E/p Obtained with the Implicit Time-Dependent Relaxation Method.

Number	E/p (Volts/cm/mm)	α/p (1/cm/mm)
1	22	0.0024
2	25	0.0049
3	30	0.0079
4	31	0.0098
5	33	0.009
6	34	0.013
7	36	0.02
8	38	0.024
9	39	0.033
10	40	0.035
11	42	0.046
12	44	0.056
13	48	0.062
14	50	0.079

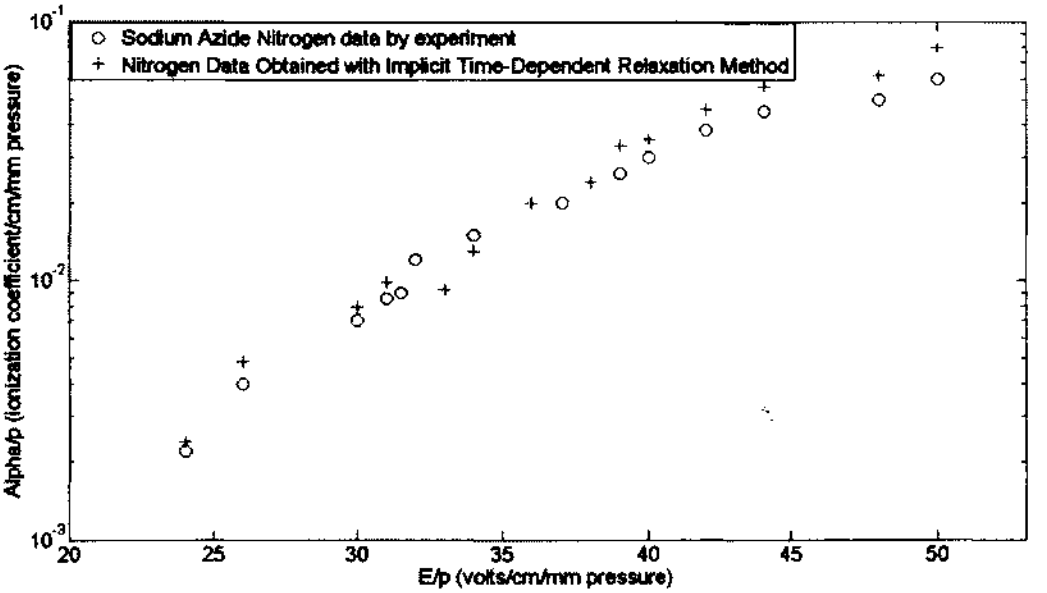

Figure 4.12 Comparison of α / p in Nitrogen Gas Obtained as a Function of E / p with the Implicit Time-Dependent Relaxation Method and Experimental Data.

The results obtained with the implicit time-dependent relaxation method are compared with the experimental results reported in the literature by Melvin A. Harrison [37]. We can see that the results are in good agreement with the published data. This further validates the ability of implicit time-dependent relaxation method and the correctness of our code implementation.

CHAPTER 5

CONCLUSIONS AND FUTURE WORK

5.1 Summarizing Conclusions

In this dissertation research a multi-term approximation for Boltzmann Transport Equation was proposed. The multi-term approximation was based on using an expansion of the electron velocity distribution function in Legendre polynomials. This is valid in situations of axial symmetry, for example, when one has only one electric field oriented along a fixed direction. Using the multi-term approximation, the Boltzmann Transport Equation was transformed essentially into a system of partial differential equations. Four different numerical methods were proposed to solve the PDEs. These were: the implicit time-independent relaxation method, a time-dependent Euler method, the time-dependent Runge-Kutta method, and finally the implicit time-dependent relaxation method by generating the 4-way grid that also involved solving a matrix equation.

As part of the work, the simulations were run until steady state and the distribution functions as well as drift velocity values were obtained under steady state for electrons in nitrogen gas. One elastic scattering and 29 inelastic scattering cross-sections were included, with their values taken from the published literature. The results shown in Chapter 3 indicate the following: (i) The implicit time-independent method was not quite accurate in estimating energy distribution functions, but it was still a fast way to estimate the drift velocity with reasonable accuracy. (ii) Although time-dependent Runge-Kutta method improved a lot compared to time-dependent Euler method and largely reduces the error, it was still not a fully implicit method and could be unstable under "severe" conditions. Therefore, although the drift velocities obtained with this method have the same general trend as the experimental data, the results still show minor differences with most of the experimental values. (iii) The implicit time-dependent relaxation method obtained the drift velocity values under 13 different E/N values. The results were

shown to be in excellent agreement with the published results of other investigators, including the high E/N range. Implicit time-dependent relaxation method is an accurate as well as most stable numerical method, among all the numerical methods discussed in this dissertation. It presents great improvement over both the implicit time-independent and the time-dependent Runge-Kutta method. (iv) In addition to drift velocity values, results were also obtained for the impact ionization coefficient, i.e., the Townsend First Ionization Coefficient. These were again observed to be in good agreement with the published experimental data for nitrogen. Since the results obtained were in good agreement with published data, our numerical methods and program implementations prove to be correct, valid and acceptable. This sets a benchmark for future simulation, including extensions to other gases such as oxygen, atmospheric air, as well as realistic inclusions of constraining geometries and different excitation waveforms.

5.2 Future Work

Although the drift velocity values were successfully obtained with 13 different E/N values that are in good agreement with published results which verify the availability of our method and program, there is still ample scope for future work and to enhance the capabilities of the program for more general and realistic simulations. Some of the possible extensions are as given below:

(1) Stable results for those higher order terms f_2 to f_6 could be obtained in the multi-term expansion of the distribution function f_0 to f_6 and beyond. As we know, one of the key points for the multi-term approach is to analyze the impact of the higher order terms on both of the electron velocity distribution function and the relevant macroscopic quantities of the electrons. These higher order terms still influence the overall accuracy of the final distribution function and need to be estimated carefully.

(2) In the simulation the only focus is in changing E/N values, that is, only two physical factors were taken into account–the electrical field and the gas pressure. However, there are many other physical factors, such as gas flow rate, discharge tube length,

discharge gap space, dielectric thickness and so on that all influence the distribution functions. Appropriate models can be created for these physical elements to see how these factors influence the distribution functions. In particular, including a realistic constraining geometry with appropriate boundary conditions could be a useful extension.

(3) In the current program, a constant electrical field is applied. However, in most of realistic situations, electrical field is changing with time. The program may need to be developed by treating these non-constant electrical field situations and an array of different voltage waveforms.

(4) Given the Boltzmann Transport Equation's flexibility with respect to collision cross sections, the collision cross-sections for nitrogen can be replaced by those for oxygen. Then by putting in the cross-sections for both nitrogen and oxygen, a complete analysis for air-plasmas can be carried out. It should also be possible to expand to other commonly used gases, such as argon, hydrogen, carbon dioxide and etc. Therefore, this will bring more wide applications from the simulations.

REFERENCES

[1] P. M. Bellan, Fundamentals of Plasma Physics, Cambridge University Press, 2006.

[2] D. A. Gurnett and A. Bhattacharjee, Introduction to Plasma Physics, Cambridge University Press, 2005.

[3] J. M. Meek and J. D. Craggs, Electrical Breakdown of Gases, John Wiley and Sons, 1978.

[4] S. Liu and M. Neiger, "Excitation of dielectric barrier discharge by unipolar submicrosecond square pulses," J. Phys. D, Appl. Phys., vol. 34, pp. 1632-1638, June 2001.

[5] Y. Itikawa, "Cross sections for electron collisions with oxygen molecules," Institute of Space and Astronautical Science, Japan, 2008.

[6] U. Kogelschatz, "Dielectric-barrier discharges: Their history, discharge physics, and industrial applications," Plasma Chemistry and Plasma Processing, vol. 23, no. 1, pp. 1-45, March 2003.

[7] A. A. Garamoon, F. F. Elakshar, A. M. Nossair and E. F. Kotp, "Experimental study of ozone synthesis," Plasma Sources Sci. Technol. vol. 11, pp. 254-259, May 2002.

[8] B. S. Rajanikanth and D. Sinha, "Achieving better NO_x removal in discharge plasma reactor by field enhancement," Plasma Sci. and Technol. vol. 10, no. 2, pp. 198-202, Apr. 2008.

[9] X. Zhuang, Q. Han, H. Zhang, X. Feng, M. Roth, O. Rosier, S. Zhu and S. Zhang, "The efficiency of coaxial $KrCl^*$ excilamps," J. Phys. D, Appl. Phys., vol. 43, no. 20, pp. 205202-205210, May 2010.

[10] J. P. Boeuf, "Plasma display panels: physics, recent developments and key issues," J. Phys. D, Appl. Phys., vol. 36, pp. R53-R79, March 2003.

[11] E. M. Lifshitz and L. P. Pitaevskii, Physical Kinetics, Pergamon Press, 1981.

[12] R. D. White, R. E. Robson, S. Dujko, P. Nicoletopoulos and B. Li, "Recent advances in the application of Boltzmann equation and fluid equation methods to charged particle transport in non-equilibrium plasmas," J. Phys. D, Appl. Phys., vol. 42, pp. 194001-194019, Sep. 2009.

[13] R. E. Robson, P. Nicoletopoulos, B. Li and R. D. White, "Kinetic theoretical and fluid modeling of plasmas and swarms: the big picture," Plasma Sources Sci. Technol., vol. 17, pp. 024020-024026, May 2008.

[14] R. D. White, K. F. Ness and R. E. Robson, "Development of swarm transport theory in radio-frequency electric and crossed electric and magnetic fields," Applied Surface Science, vol. 192, pp. 26-49, Feb. 2002.

[15] Z. Lj. Petrovic, Z. M. Raspopovic, S. Dujko and T. Makabe, "Kinetic phenomena in electron transport in radio-frequency fields," Applied Surface Science, vol. 192, pp. 1-25, Feb. 2002.

[16] V. R. Guggilam, "Monte Carlo simulation for electron swarm parameters in atmospheric nitrogen, oxygen, and air," Old Dominion University Master thesis, pp. 21-33, 2008

[17] M. J. Kushner, "Distribution of ion energies incident on electrodes in capacitively coupled RF discharges," J. Appl. Phys., vol. 58, no. 11, pp. 4024-4031, Dec. 1985.

[18] B. E. Thompson, H. H. Sawin, and D. A. Fisher, "Monte Carlo simulation of ion transport through RF glow discharge sheaths," J. Appl. Phys., vol. 63, no. 7, pp. 2241-2251, Apr. 1988.

[19] V. A. Feoktistov, A. V. Mukhovatova, A. M. Popov, and T. V. Rakhimova, "Self-consistent modeling of low-pressure RF discharges in oxygen plasma," J. Phys. D: Appl. Phys., vol. 28, pp. 1346-1353, July 1995.

[20] A. Bogaerts and R. Gijbels, "Monte Carlo model for the argon ions and fast argon Atoms in a radio-frequency discharge," IEEE Transactions on Plasma Science, vol. 27, pp. 1406-1415, Oct. 1999.

[21] M. J. Brennan, "Optimization of Monte Carlo codes using null collision techniques for experimental simulation at low E/N," IEEE Transactions on Plasma Science, vol. 19, no. 2, pp. 256-261, Apr. 1991.

[22] H. R. Skullerud, "The stochastic computer simulation of ion motion in a gas subjected to a constant electric field," Brit. J. appl. Phys., vol. 1, pp. 1567-1568, Jul. 1968.

[23] S. L. Lin and J. N. Bardsley, "Monte Carlo Simulation of ion motion in drift tubes," The Journal of Chemical Physics, vol. 66, no. 2, pp. 435-445, Aug. 1976.

[24] T. Tabata, T. Shirai, M. Sataka and H. Kubo, "Analytic cross sections for electron impact collisions with nitrogen molecules," Atomic Data and Nuclear Data Tables, vol. 92, pp. 375-406, Feb. 2006.

[25] K. F. Ness, "Multi-term solution of the Boltzmann equation of electron swarms in crossed electric and magnetic fields," J. Phys. D, Appl. Phys., vol. 27, pp. 1848-1861, May 1994.

[26] R. D. White, K. F. Ness, R. E. Robson and B. Li, "Charged-particle transport in gases in electric and magnetic fields crossed at arbitrary angles: Multi-term solution of Boltzmann's equation," Physical Review E., vol. 60, no. 2, pp. 2231-2249, Aug. 1999.

[27] B. Li, R. E. Robson and R. D. White, "Magnetic field effects on spatial relaxation of swarm particles in the idealized steady-state Townsend experiment," Physical Review E., vol. 74, pp. 026405 1-13, Aug. 2006.

[28] B. Li, R. D. White and R. E. Robson, "Spatially periodic structures in electron swarms: ionization, NDC effects and multi-term analysis," J. Phys. D, Appl. Phys., vol. 35, pp. 2914-2924, Nov. 2002.

[29] S. Yachi, Y. Kitamura, K. Kitamori and H. Tagashira, "A multi-term Boltzmann equation analysis of electron swarms in gases," J. Phys. D, Appl. Phys., vol. 21, pp. 914-921, June 1988.

[30] D. Loffhagen and R. Winkler, "Time-dependent multi-term approximation of the velocity distribution in the temporal relaxation of plasma electrons," J. Phys. D, Appl. Phys., vol. 29, pp. 618-627, March 1996.

[31] D. Loffhagen and R. Winkler, "Temporal relaxation of plasma electrons acted upon by direct current electric and magnetic fields," IEEE Transactions on Plasma Science, vol. 27, no. 5, pp. 1262-1270, Oct. 1999.

[32] G. R. Govinda Raju and S. Rajapandian, "Townsend's first ionization coefficients in crossed electric and magnetic fields in nitrogen," Int. J. Electronics, vol. 40, no. 1, pp. 65-79, Sep. 1975.

[33] M. P. Watts and A. E. D. Heylen, "Positive-ion drift and Townsend primary ionization coefficient in hydrogen and nitrogen," Int. J. Electronics, vol. 67, no. 4, pp. 661-668, Feb. 1989.

[34] A. B. Wedding, H. A. Blevin and J. Fletcher, "The transport of electrons through nitrogen gas," J. Phys. D, Appl. Phys., vol. 18, pp. 2361-2373, March 1985.

[35] W. Roznerski, "Transport parameters of electron swarms in nitrogen at moderate and elevated E/N," J. Phys. D, Appl. Phys., vol. 29, pp. 614-617, Oct. 1995.

[36] J. Liu and G. R. Govinda Raju, "Electron swarm parameters in nitrogen, oxygen and air," IEEE transactions on Electrical Insulation, vol. 28, no.1, pp. 154-156, Feb. 1993.

[37] M. A. Harrison, "Townsend's first ionization coefficient in nitrogen," Physical Review, vol. 105, no. 2, pp. 366-368, Jan. 1957.

CURRICULUM VITA

for

YUE FENG

E-MAIL:yfeng003@odu.edu
1304 W 38th street, Norfolk, VA, 23508
Phone: (757)277-1296

EDUCATION

• Doctor of Philosophy in Electrical and Computer Engineering, Old Dominion University, Norfolk, Virginia, May 2012.

• Master of Science in Computer Science, Huazhong University of Science and Technology, Wuhan, Hubei, China, June 2007.

• Bachelor of Science in Computer Science, Jiangxi Normal University, Nanchang, Jiangxi, China, June 2005.

INTERESTS

• Modeling and Simulation, Data Mining, Machine Learning, Pattern Recognition, Image Processing, Computer Graphics.

TECHNICAL SKILLS

• Programming: C/C++, Java, MATLAB

• Operating systems: Windows NT/2000/XP/Vista

• Tools: Visual Studio, Microsoft Office, Photoshop, Visio

WORK EXPERIENCE

• Graduate Research Assistant, Department of Electrical and Computer Engineering, Old Dominion University (August 2007-December 2011)

• Graduate Teaching Assistant, Department of Electrical and Computer Engineering, Old Dominion University (August 2007-December 2011)